UNIVERSITY OF TWENTE.

Nelen & Schuurmans

Catching the details of mangrove dynamics:
A case study in Lac Bay, Bonaire

Berend te Booij, s2057905

Master Thesis

October 28, 2024

(Daily) Supervisors:
Dr. Ir. P.C. Roos
Dr. Ir. E.M. Horstman
Ir. M. Siemerink
Ir. R. van Zee
Dr. N.D. Volp

Civil Engineering & Management
Faculty of Engineering Technology
University of Twente
7522 NB Enschede

1 Preface

This master's thesis marks the completion of my Master's degree in Water Engineering and Management, specialising in River and Coastal Engineering at the University of Twente. I had the privilege of doing this research during an internship at Nelen & Schuurmans, where I was provided with a workspace at their Utrecht office.

I would like to express my gratitude to my daily supervisors, Rob van Zee, Martijn Siemerink, and Nicolette Volp, from Nelen & Schuurmans. I truly appreciated their constant availability and support, even when I interrupted them with daily questions. I also extend my thanks to my other colleagues at Nelen & Schuurmans for their time and for making my stay both enjoyable and memorable.

Additionally, I am grateful to my university supervisors, Erik Horstman and Pieter Roos, for their support throughout this project. I would also like to thank Matthijs van de Geest and Gema Casal for providing essential information on the two mangrove species in Lac Bay.

Lastly, I thank my friends and family for their continuous support, especially my father, Pieter, for repeatedly proofreading this document.

I hope you enjoy reading my thesis and that it broadens your understanding of mangroves.

Berend te Booij,

Utrecht, 28-10-2024

2 Abstract

Lac Bay is a mangrove ecosystem located in Bonaire, Carribbean Netherlands. The mangrove vegetation has a large influence on the tidal dynamics in the Lac Bay system. Field measurements of flow velocities within the creeks, water levels around the mangrove forest, and mangrove vegetation characteristics were mapped in previous research. No flow measurements inside the mangrove forest were available, leaving uncertainties regarding the hydrodynamics through the mangrove forest itself. This study investigates the vegetation influences on the tidal dynamics and how to model these vegetation influences. Using 3Di software, a subgrid-based model was developed to complement these measurements and enhance understanding of the system dynamics. The subgrid method allows the use of high-resolution data while computing hydrodynamics on a coarser computational grid. To capture the dynamics and establish an appropriate method for representing vegetation effects, three methods were evaluated: i) increasing bed roughness, ii) the Baptist drag formulation, and iii) porous layer methods. The methods were primarily assessed based on their ability to reproduce the measured tidal range and tidal asymmetry, while also considering flow patterns and water level variations.

Calibrating the individual vegetation representations revealed their limitations: The use of an increased bottom roughness required unrealistically low Chézy values, while the Baptist approach primarily improved the tidal exchange between the bay and Awa di Lodo, improving the simulated tidal range. The porous layer method showed very good results in modelling the tidal duration asymmetry, without accurately simulating the tidal range. To optimise simulation accuracy, a hybrid model was created. The Baptist method is more suitable for vertical and well-structured roots such as pneumatophores of black mangroves, whereas the porous layer better represents the dense root networks of red mangroves. The use of a hybrid model, along with species-specific calibrations, enhances the model's accuracy significantly, especially the tidal exchange between the bay and Awa di Lodo.

Results highlight vegetation's critical role in modifying tidal hydrodynamics, particularly in dense root areas. Discrepancies between predicted and observed results, especially during neap tides, suggest some physical processes may not be fully accounted for in the model. The study area is known for hypersaline conditions, typically caused by strong evaporation. An exploratory test indicated that incorporating evaporation effects could improve model performance during neap tide conditions. By combining field measurements with advanced numerical modelling, this study provided new insights into the system's dynamics as well as the different vegetation schematisations in numerical modelling. The results demonstrate the effectiveness of a species-specific, hybrid model approach in understanding mangrove hydrodynamics, particularly for complex environments where different mangrove species coexist and interact, such as Lac Bay.

Contents

List of Figures

List of Tables

List of Parameters

a = Frontal area density $[/m]$
A = Cross-sectional area $[m^2]$
C = Chézy coefficient $[m^{1/2}/s]$
C_b = Chézy coefficient of the bed $[m^{1/2}/s]$
C_D = Bulk drag coefficient $[-]$
C_k = Representative Chézy value for non-submerged vegetation $[m^{1/2}/s]$
C_r = Representative Chézy value for vegetation $[m^{1/2}/s]$
D = Stem diameter $[m]$
H = Water depth $[m]$
h = Vegetation height $[m]$
h_p = Porous layer height $[m]$
K = Hydraulic conductivity $[m/s]$
k_N = Nikuradse roughness height $[m]$
N = Number of roots per square meter $[/m^2]$
Q = Discharge $[m^3/s]$
u_c = Uniform flow velocity through fully submerged vegetation $[m/s]$
u_u = Velocity above the vegetation layer [including slip velocity] $[m/s]$
z_0 = Roughness height in the logarithmic velocity profile for a fully rough bed $[m]$
z_{creek} = Creek delineation height $[mLVD]$
Δx = Computational grid cell edge $[m]$
κ = Von Kármán constant
ϕ = Porosity $[-]$
φ = Solid volume fraction $[m]$

3 Introduction

Mangrove forests are complex and dynamic ecosystems. They play a crucial role in providing habitats for various species and protect inland areas from floods (Asari et al., 2021; Kandasamy, 2021). They are recognised as a cost-effective and sustainable option for coastal protection (Gijsman et al., 2021). Their natural abilities to attenuate wind waves and reduce surge levels contribute significantly to coastal protection (Horstman et al., 2013; Mazda et al., 2006). Furthermore, mangroves help to trap sediments and reduce erosion and naturally elevate their surroundings, a process that allows them to keep pace with moderate sea level rise and continue protecting low-lying coastal areas from its impacts (Gijsman et al., 2023; Krauss et al., 2003).

Despite the natural ability of mangroves to adapt to rising sea levels, they are increasingly threatened by the accelerating pace of climate change, including faster rates of sea level rise and higher temperatures (Barnes, 2022; Merzdorf, 2020). When the rate of sea level rise exceeds their ability to trap sediment and grow vertically, mangroves may struggle to keep pace. This imbalance can lead to prolonged inundation, potentially drowning mangrove ecosystems (Larsen, 2019). Additionally, climate change exacerbates salinity issues through higher temperatures and increased wind. These conditions enhance evaporation rates, concentrating salt in the water and further stressing the mangroves. Other threats, such as erosion and changes in sediment fluxes, directly contribute to the degradation of mangrove forests by disrupting their natural processes of sediment accumulation and water flow (Jennerjahn et al., 2017; Lucas et al., 2017). These disruptions can have severe impacts on the health and resilience of mangrove ecosystems. Furthermore, the conversion of mangrove forests into agriculture and aquaculture land has led to a significant reduction in their total area (Adame et al., 2021; Lee, 2009). In the past 30 years, the total area has been reduced by 5%, of which human actions caused more than 60% (Cooper, 2022).

One site facing significant challenges is the mangrove forest in Lac Bay, Bonaire (Figure 3.1), where environmental stressors exacerbate the threats to the ecosystem. Despite the mangrove's natural capacity to trap sediment, the excessive accumulation in Lac Bay has led to problems of its own. Creek clogging, along with creek overgrowth, has reduced tidal exchange in parts of the forest (van der Meulen, 2023; van Zee, 2022). This limited exchange has resulted in hypersaline conditions in the back of the forest, which threaten both the health of the mangroves and the biodiversity they support (Debrot et al., 2010; Van Moorsel & Meijer, 1993). Conservation efforts in the area focus on mitigating these stress factors by improving water circulation and managing salinity through creek restoration. These efforts aim to restore ecological balance and safeguard the long-term resilience of the forest. However, ensuring the resilience of Lac Bay's mangroves will require adaptive management strategies that can address the ongoing environmental challenges while enhancing the ecosystem's natural processes of sediment accumulation and tidal flow.

Figure 3.1: A front view on the Lac Bay mangrove forest from the bay (left photo) and a view on the creek system within Lac Bay mangrove forest (right photo) (van Zee, 2022)

To address these challenges, there is an increasing focus on modelling these complex intertidal systems to understand and predict their future dynamics under varying and changing environmental conditions. Hydrodynamic models can be used to predict tidal dynamics in mangroves and improve understanding of the effects of human-induced changes in these ecosystems (Horstman et al., 2015). The complex dynamics of mangrove ecosystems, influenced by the interplay of tidal creeks and mangroves, pose a unique challenge

to hydrodynamic modelling. Given the typically low water depths in mangrove ecosystems, factors such as bathymetry, bottom friction, and vegetation drag critically influence water flow. These factors are interdependent and affect both field measurements and model outcomes, creating a complex system that challenges accurate representation in hydrodynamic models (Furukawa & Wolanski, 1996; Mazda et al., 1997; Van Santen et al., 2007). The high spatial variability of bathymetry and vegetation within mangroves, especially near creeks, further complicates modelling efforts. While shallow flows do not necessarily require greater detail, traditional numerical models that attempt to capture such variability tend to increase computational time exponentially (Popescu, 2014; Versteeg & Malalasekera, 2007). Thus, it is crucial to develop precise models that can capture this complexity while keeping computational time low.

Traditionally, in such models, bottom friction and vegetation drag, both critical factors influencing water flow in mangrove ecosystems, have been represented by the same parameter (Hanipah et al., 2018). This simplification overlooks the distinct roles and impacts of bottom topography and mangrove vegetation on ecosystem dynamics, potentially limiting the accuracy of predictions. Recognizing these limitations is crucial to develop precise models that better capture the complexity of mangrove systems.

3.1 Background Information

3.1.1 Mangrove ecosystems

Mangrove forests are coastal intertidal wetlands found in tropical and subtropical regions, shown in Figure 3.2. They are characterised by their ability to thrive in saline environments, subject to tidal fluctuations. The mangrove forest of Lac Bay, Bonaire, is located in the Caribbean Sea, north of the Venezuelan coast, indicated with the arrow in Figure 3.2.

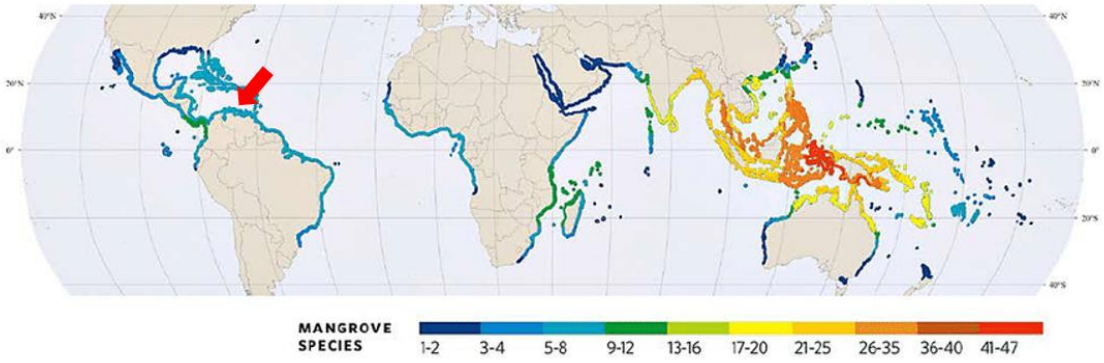

Figure 3.2: The map shows the global distribution of mangrove forests, with the mangrove forest of Lac Bay in Bonaire indicated by a red arrow (Hoff et al., 2010)

Mangroves are adapted to their challenging environment with specialised aerial roots that cope with waterlogged, oxygen-poor soils and provide physical support for the trees (Cheng et al., 2015). The three main types of aerial roots found in mangrove forests are pneumatophores, knee roots and stilt roots, as shown in Figure 3.3. These root types vary in their prevalence depending on factors such as inundation time, depth, and salt concentration. The forest of Lac Bay consists of pneumatophores and stilt roots.

The root systems of mangroves are dense and complex and contribute to complex interactions between hydrodynamic, morphological and ecological processes within the ecosystem (Gijsman et al., 2021). They serve as natural barriers that protect the coast and increase wave attenuation by absorbing and dissipating wave energy (Tusinski & Verhagen, 2014). These root systems also enhance sediment deposition within the forest (Gijsman et al., 2023). Sediment accumulation is crucial for the mangrove ecosystem's flood protection service and its ability to adapt to sea level rise due to climate change.

The impact of mangrove ecosystems on flood risk reduction depends on various hydrodynamic and biophysical factors. These include inundation depth, wave characteristics, flow velocity, intertidal topography, presence of creeks, forest dimensions, and tree properties such as species, density, stem diameter, and height (Baltus, 2022). Understanding these intricate processes and their interactions is essential for assessing and maintaining the long-term effectiveness of mangrove ecosystems in coastal protection.

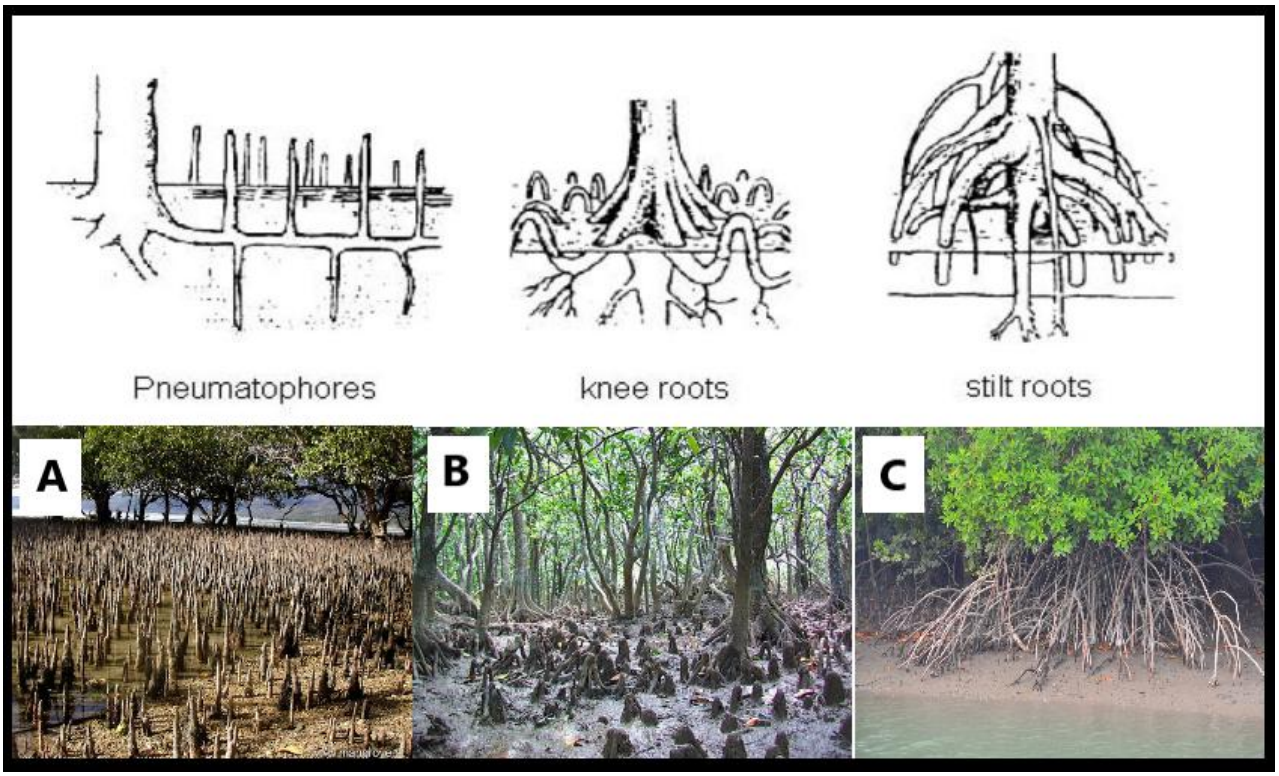

Figure 3.3: A schematisation of root types (de Vos, 2004), [A] Pneumatophores roots by (Marek, 2024), [B] Knee roots by (Andersson, 2007), [C] stilt roots by (Stevens, 2019)

The survival and persistence of mangrove forests over time is governed by changes in these same factors, which affect forest composition and the hydrodynamic forcings they experience (Alongi, 2015). This dynamic interplay between environmental conditions and mangrove ecology is crucial for the ecosystem's ability to adapt to environmental changes. In Lac Bay, this balance is currently challenged by the reduction of creek networks due to siltation processes and the expansion of mangroves into existing creeks. These changes not only increase the forest area but also compromise the tidal exchange between the bay and back of the forest, potentially affecting the long-term stability and functionality of the ecosystem.

3.1.2 Effect of vegetation on Hydrodynamics

Mangrove forest ecosystems impact the hydrodynamics in intertidal regions through their complex vegetation structure. The intricate root systems, stems, and branches of mangroves act as natural obstructions, creating drag and resistance to water flow when submerged during high tides. The presence of roots modifies the flow patterns within the forest. The effect of mangrove vegetation on hydrodynamics is largely influenced by its geometry, which can vary significantly between species and within areas (Mullarney & Henderson, 2018). A key characteristic describing vegetation geometry is the solid volume fraction, $\varphi[-]$, calculated as:

$$\varphi = \frac{N\pi D^2}{4} \tag{3.1}$$

where N is the number of stems per square meter and D is the stem diameter $[m]$. Observed solid volume fractions for different mangrove types range from 0.0003 to 0.13, depending on whether they are trunks, prop roots, or pneumatophores (Krauss et al., 2003; Mazda et al., 1997; Norris et al., 2017).

A crucial aspect of mangrove vegetation is its ability to dissipate energy of water flow. The complex structure of mangrove forests acts as a natural buffer, dissipating wave and current energy as water flows through the vegetation. This energy reduction occurs through several mechanisms, such as friction and drag as water flows through the dense network of roots, trunks, and branches, wave attenuation (particularly during storm surges or high tides), and flow redirection. The energy-reduction function of mangroves is vital for coastal protection,

as they protect inland areas from high-energy wave action, reducing the impact of storm surges and help to mitigate erosion (Alongi, 2008; Zhang et al., 2012).

The presence of mangroves introduces spatial variation in flow at multiple scales, which can be characterised by the vegetation height and the frontal area density ($a = ND$). At the individual root scale, flow resistance in low-density vegetation is dominated by turbulence through vortex shedding and wake generation, see Figure 3.4a (Mullarney & Henderson, 2018). As vegetation density increases, flow resistance is primarily caused by the blockage of flow, resulting in reduced velocities through the vegetation (Figure 3.4b) (Nepf, 2012). At the canopy scale, dense, uniform-height canopies can create strong shear layers at the top of the vegetation, leading to canopy-scale turbulence (Figure 3.4c). This can also dampen larger-scale motion due to increased drag force and eddy viscosity (Mazda et al., 2005; Nepf, 2012). The mangrove forest in Lac Bay exhibits characteristics of increased vegetation density, with flow dynamics predominantly governed by vegetation blockage, suggesting a system where reduced velocities through the dense vegetation play a crucial role in the local hydrodynamics.

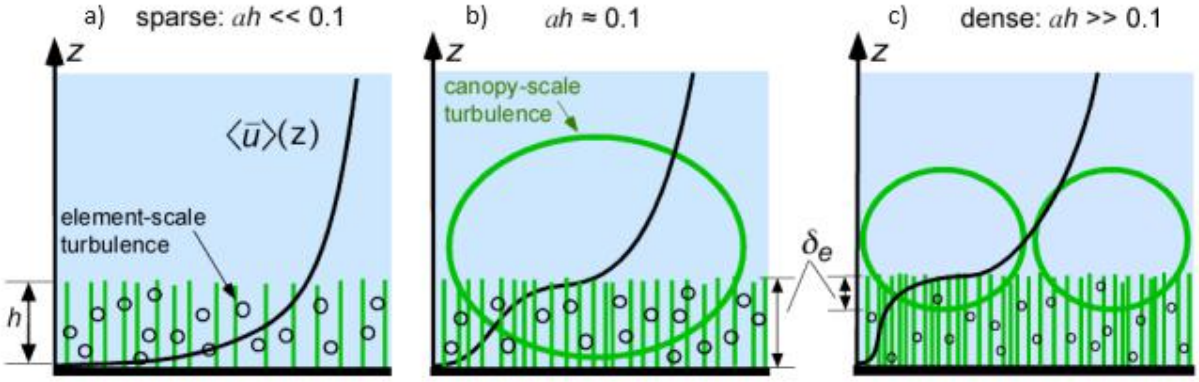

Figure 3.4: Vertical profiles of longitudinal velocity and dominant turbulence scales for [a] sparse canopy, [b] transitional canopy and [c] dense canopy, h is the submerged canopy height and a is the frontal area density (Nepf, 2012)

These spatial variations and energy-reduction properties of mangroves lead to several significant hydrodynamic effects. One of the key effects, which this section focuses on, is tidal asymmetry, where vegetation significantly alters tidal dynamics. The vegetation's friction affects the momentum equation by introducing an additional drag term, which varies spatially and temporally with water depth and flow velocity (Horstman et al., 2015).

In mangrove forests, water levels rise faster in creeks than in the forest during flood tides due to the obstructive nature of the vegetation. Conversely, during ebb tides, the vegetation slows down the outflow, causing water levels to drop more quickly in creeks than in the forest interior. This results in longer falling tides than rising tides (flood dominant), particularly towards the back of the forest (Mazda et al., 1995). Flow velocity variations also arise, but these differ between the creeks and the forest interior. In the creeks, flood tides typically have higher velocities as water is pushed toward the back of the forest, while ebb tides experience lower velocities due to their extended duration. However, within the forest itself, the opposite pattern often occurs, with ebb flows showing higher velocities than flood flows (Mazda et al., 2005). Notably, the flood/ebb dominance differs between the creeks and the forest—while the forest is ebb-dominant, the creeks exhibit flood-dominance, illustrating the contrasting tidal behaviors in these interconnected areas.

3.1.3 Vegetation representations in hydrodynamic models

Vegetation effect is incorporated into numerical models through various methods, primarily by modifying the hydrodynamic equations to account for the presence of vegetation (Mazda et al., 2005). While many approaches involve adjusting friction terms in equations such as the shallow-water equations derived from the Navier-Stokes equations (Bosboom & Stive, 2021), some methods take a different approach. In 2DH numerical models, several techniques can be used for the representation of vegetation. These methods aim to capture the influence of vegetation on water flow in different ways. The following sections will explore three approaches for representing vegetation in 2DH numerical models.

Increasing bed roughness

A common method to account for vegetation drag in hydrodynamic models is by increasing the bed roughness with the friction coefficient. This approach uses the existing friction formulation by the Chézy equation to reflect the additional drag exerted by vegetation on water flow.

The implementation typically involves adjusting the friction coefficient based on empirical relationships derived from field measurements or laboratory experiments (Hanipah et al., 2018). For the Chézy friction coefficient (C), vegetation presence is represented by decreasing its value. This modification can be applied by increasing the bed roughness uniformly across the entire vegetated area, as done by Menéndez et al. (2018), or by implementing a spatially varying raster that adjusts the roughness for each grid cell where vegetation is present, as demonstrated by Breda et al. (2021).

The magnitude of roughness adjustment varies depending on the type and density of vegetation. For mangrove ecosystems, studies have reported Chézy friction values as low as $1.0 - 5.0 m^{1/2}/s$ for forest platforms (Horstman et al., 2021; Mazda et al., 1995; Stark et al., 2015). In contrast, creek channels through these ecosystems typically have higher Chézy friction values, ranging from $55 - 75 m^{1/2}/s$ (Mazda et al., 1995).

Increasing the bed roughness to represent vegetation has several effects on model outcomes. It simulates the larger drag force exerted by vegetation on water flow, resulting in reduced flow velocities within vegetated areas. The increased resistance can lead to steeper water surface slopes in vegetated regions. It can affect the timing and extent of flooding in coastal areas during storm surge events (Wamsley et al., 2010).

One of the key advantages of using the roughness friction coefficient is its ease of implementation in hydrodynamic models. It simplifies the representation of complex surfaces like vegetated areas without requiring detailed, site-specific measurements of vegetation characteristics (Chow, 1959). This makes it particularly useful when vegetation data is unavailable or incomplete, allowing modelers to estimate flow resistance based on general empirical relationships. Additionally, the roughness coefficient is generally applicable across different ecosystems, making it a versatile tool for simulating the effects of vegetation or surface roughness in a wide variety of environments (Järvelä, 2002).

While widely used, this method has several limitations. The roughness coefficient derived from specific settings may not be easily transferable to different ecological or geographical conditions, limiting the model's adaptability. Model outputs are highly sensitive to the combined effects of bottom friction and vegetation drag, which are integrated into a single roughness value (Nepf, 2012). This integration can increase overall uncertainty in the model. It's important to note that in a 2DH model, the roughness value represents a depth-averaged horizontal shear stress. This approach simplifies the flow by assuming a uniform velocity profile across the water column, which means it does not account for vertical variations in vegetation drag and resistance. This simplification overlooks how vegetation influences flow at different depths, which can lead to inaccuracies in predicting flow structures within and around vegetation.

The relationship between water level and vegetation height is particularly significant. As water levels fluctuate, the proportion of submerged vegetation changes, altering the effective drag and flow patterns. Since the roughness coefficient remains constant regardless of water depth, it fails to capture this dynamic interaction. Recognizing this relationship is crucial for accurate modelling of flow and resistance, as the interaction between water levels and vegetation height plays a vital role in determining flow behaviour.

The method does not capture the dynamic nature of vegetation-flow interactions, such as the flexibility of plants or changes in drag coefficients with flow conditions. The exact roughness values often require calibration against field observations, which can be time-consuming and may not always be feasible for all modelled scenarios.

Baptist approach

The Baptist approach is a method for representing vegetation in numerical models that refines vegetation drag modelling by differentiating between submerged and emergent vegetation (Baptist et al., 2007; Gijsman et al., 2023; Haughey, 2017; Hu et al., 2018). This method adjusts bed roughness and resistance calculations based on vegetation characteristics and water depth, enhancing model accuracy by incorporating vegetation-induced resistance and bed roughness adjustment (Horstman et al., 2015).

The core of the Baptist approach lies in its detailed consideration of how different types of vegetation (non-submerged and emerged) affect water flow. The computation of bed roughness and flow resistance is based on the vegetation equations of Baptist et al. (2007), which are split into equations for emerged and submerged vegetation.

For emergent vegetation, the equation calculates a representative roughness that does not directly scale with water depth. Instead, it accounts for the interaction between the vegetation and the flow. The representative Chézy coefficient for emergent vegetation is given by:

$$C_k = \sqrt{\frac{1}{1/C_b^2 + (C_D N D h)/(2g)}} \tag{3.2}$$

Where C_k is the representative Chézy coefficient for emergent vegetation $[m^{1/2}/s]$, C_b is the Chézy friction coefficient for the bed $[m^{1/2}/s]$ and C_D is the drag coefficient effected by the vegetation. Therefore, the uniform flow velocity (u_c) through emerged vegetation $[m/s]$ follows from the momentum balance and is give by:

$$u_c = \sqrt{\frac{hi}{1/C_b^2 + (C_D N D h)/(2g)}} \tag{3.3}$$

Where i is the water level slope. The Chézy friction coefficient used here is the same parameter applied in the previous method, where all relevant information was already incorporated.

For submerged vegetation, Baptist et al. (2007) proposed the "method of effective water depth." This method is based on the assumption that there are two flow zones:

1. A vegetation zone, where a uniform flow velocity (u_c) is present

2. A layer above the vegetation, where the flow velocity (u_u) is assumed to vary in height with a logarithmic profile.

At the top of the vegetation (h), u_u has the same flow velocity as within the vegetation. This creates a dual-zone model that reflects the stratified nature of flow within and above the vegetation layer, shown in Figure 3.5.

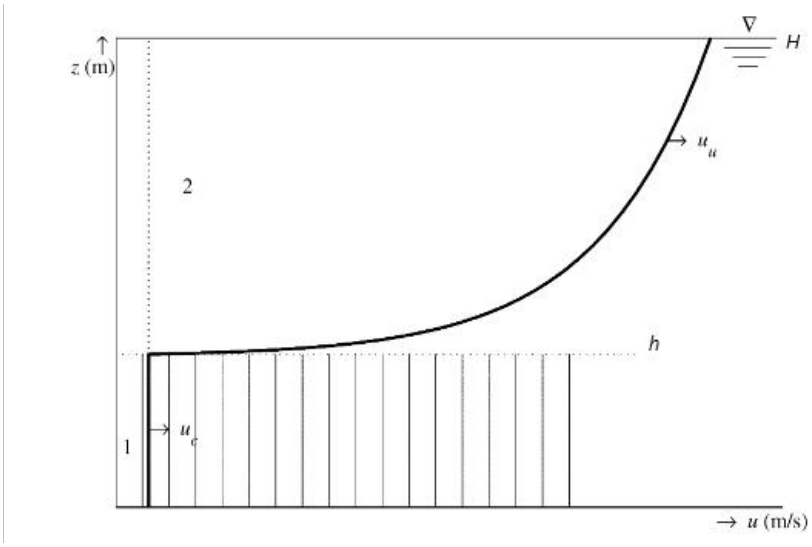

Figure 3.5: Representation of the vertical velocity profile in two zones for the submerged vegetation representation by Baptist et al. (2007)

In the layer above the vegetation, the flow velocity u_u is assumed to vary in height with a logarithmic profile. To match the two velocity profiles at the top of the vegetation (h), u_u has the same flow velocity as within the vegetation at the top of the vegetation. When combining the two velocities, a representative Chézy roughness value, where the first term on the right being equal with the emergent vegetation, follows as:

$$C_r = \sqrt{\frac{1}{1/C_b^2 + (C_D N D h)/(2g)}} + \frac{(H-h)^{3/2}(\sqrt{g}/\kappa)\ln((H-h)/ez_0)}{H^{3/2}} \tag{3.4}$$

where C_r is the representative Chézy value for vegetation $[m^{1/2}/s]$, κ is the Karman constant, H is the water depth $[m]$, and z_0 is the roughness height $[m]$ in the logarithmic velocity profile for a fully rough bed .

By differentiating between submerged and emerged vegetation and adjusting calculations based on vegetation characteristics and water depth, the Baptist approach provides a more nuanced representation of vegetation-induced drag in numerical models (Gijsman et al., 2023). This method enhances model accuracy by incorporating vegetation-induced resistance and bed roughness adjustment, accounting for the complex interactions between vegetation and water flow in both submerged and non-submerged conditions.

A key limitation of the Baptist model is its assumption that vegetation stems are straight, vertical columns, which is not applicable to some mangrove types. Certain mangrove types have complex stilt root systems that grow in multiple directions, forming irregular and three-dimensional networks. This intricate structure creates significantly different flow dynamics and drag effects compared to the simplified vertical stems the model is designed for. As a result, applying the Baptist model to environments with complex root systems can lead to inaccuracies in estimating flow resistance and velocity, requiring alternative models to account for such complexities.

Porous layer

The porous layer is an innovative approach to represent dense vegetation in numerical models, particularly for simulating the interaction between water flow and vegetation structures such as mangroves. This method introduces a permeable layer within the model domain that mimics the physical barrier created by vegetation, allowing for a more nuanced representation of water movement through and around densely vegetated areas.

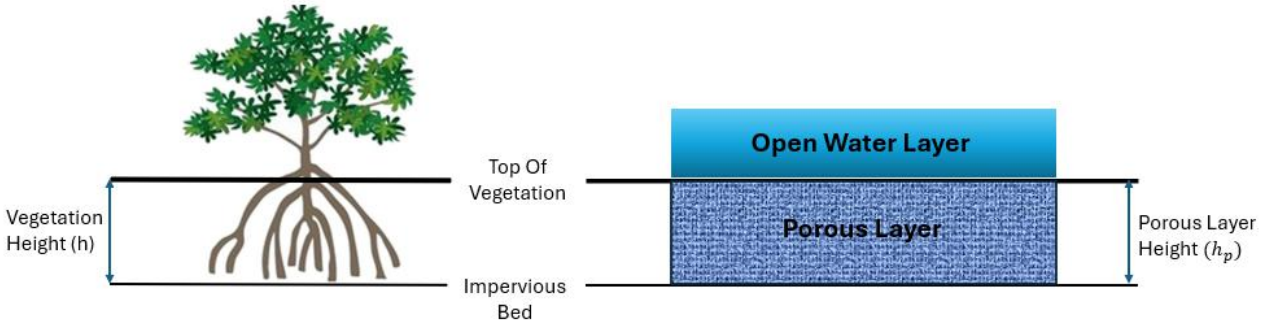

Figure 3.6: A schematisation of the porous layer, where the left side resemble the mangrove forest with a side view and the right side the implementation of the porous layer in a model environment.

Figure 3.6 shows the porous layer, which is defined from the bed up to the top of the vegetation structure, such as the roots in mangrove systems. This approach distinguishes two different types of flow. Above the vegetation, open water flow is simulated using depth-averaged shallow water equations. Within the vegetation, in the porous layer, diffusive flow is simulated using Darcy's law.

The porous layer is characterised by three main parameters: porosity (ϕ) $[-]$, which is the ratio of void space (between roots and stems) to the total volume of the layer; porous layer height (h_p) $[m]$, which is the vertical extent of the vegetation structure; and hydraulic conductivity (K) $[m/s]$, which represents the ease with which water can move through the porous medium.

The flow through the porous layer is described by Darcy's equations for diffusive flow:

$$Q_x = -KA_x \frac{\delta \zeta}{\delta x} \tag{3.5}$$

$$Q_y = -KA_y \frac{\delta \zeta}{\delta y} \tag{3.6}$$

In these equations, Q_x and Q_y represent the discharge $[m^3/s]$ in the x and y directions, respectively. A_x and A_y are the cross-sectional areas $[m^2]$ in the x and y directions, respectively, calculated as the product of the vegetation height and the width over which Q is calculated. $\frac{\delta \zeta}{\delta x}$ and $\frac{\delta \zeta}{\delta y}$ are water level gradients $[-]$ in the x and y directions, respectively.

This approach is hypothesised to be particularly effective for modelling dense vegetation structures such as mangrove roots because it captures the combined effects of vegetation density and surface roughness (Baltus, 2022). The hydraulic conductivity incorporates both the resistance due to the density of vegetation elements and the skin friction caused by their surface texture. This allows for a more comprehensive representation of the flow resistance in densely vegetated areas, accounting for both the obstruction created by the vegetation structure and the frictional effects at the vegetation-water interface. The porous layer affects the water surface slope and flow velocity. As water levels rise above the vegetation, the flow transitions from purely diffusive within the porous layer to a combination of diffusive and open channel flow.

The porous layer method offers a novel approach to representing dense vegetation in hydrodynamic models, particularly for environments with complex root systems such as mangrove forests. Unlike simple drag force approaches, this method simulates the flow through vegetation as diffusive flow in a porous medium, potentially providing a more accurate representation of the hydrodynamics in these environments.

3.1.4 3Di modelling software

Traditional hydrodynamic models often face challenges in balancing computational efficiency with the need for high-resolution data representation, especially in complex environments such as urban areas, coastal regions, and ecosystems like mangrove forests. The 3Di modelling software offers a solution to these challenges through its subgrid-based modelling approach (Casulli, 2009; Casulli & Stelling, 2011).

The subgrid-based modelling approach allows for the integration of high-resolution spatial data without significantly increasing computational costs, making it particularly valuable for modelling complex aquatic environments like mangrove forests (Volp et al., 2013). This approach is especially beneficial when dealing with vegetation, which is often highly spatially variable. By utilising subgrid modelling, more detailed information about vegetation distribution and characteristics can be incorporated, leading to more accurate modelling results. The subgrid method in 3Di operates on a dual-grid system: a high-resolution grid captures detailed bathymetry, vegetation patterns, and other small-scale variations in forcings, such as roughness and initial water level, while a coarser computational grid handles the main calculations efficiently. This dual approach allows for a more precise representation of the spatially variable vegetation while maintaining computational efficiency.

One of the key strengths of the subgrid approach is its ability to represent varying bathymetry within a single computational cell while assuming an uniform water level across that cell. It acknowledges that water levels typically vary more gradually compared to the underlying topography. By leveraging this principle, 3Di can provide more accurate simulations of water flow patterns without sacrificing computational efficiency. This distinction is crucial for employing the wetting and drying algorithm (Casulli, 2009) to handle the non-linear relationship between water volume and level, ensuring precise calculations even in dynamically changing conditions. This capability allows the model to seamlessly simulate scenarios where grid cells may be partially wet, fully submerged, or completely dry, reflecting the dynamic nature of water movement in real-world environments. This is particularly valuable in tidal coastal areas or floodplains.

3.2 Knowledge gap

The complex hydrodynamics of Lac Bay's mangrove ecosystem in Bonaire presents a unique modelling challenge. While the general understanding of mangrove hydrodynamics exists, the specific dynamics of this system, including the interactions between tidal flows, diverse vegetation types, and complex topography, are not fully clear. Current modelling approaches struggle to capture these intricate relationships effectively.

Traditional hydrodynamic models, using spatially averaged data, oversimplify the geometry of tidal creeks, vegetation distribution, and elevation variations in shallow water environments. This simplification leads to unrealistic predictions of flow patterns and water levels, which are crucial for ecosystem health. Subgrid-based models show promise in handling high-resolution spatial data and representing vegetation effects, but their application to mangrove ecosystems requires further development and validation.

Specifically, these models need refinement to accurately capture the multifaceted impacts of mangrove vegetation on water flow, including altered flow paths, local turbulence, and water storage capacity. The challenge lies in determining how to optimally implement subgrid models in Lac Bay, considering the intricate interplay

between high-resolution topography, diverse vegetation characteristics (such as root density, diameter, and height of different mangrove species), and varying hydrodynamic conditions.

It remains unclear how to efficiently integrate detailed Digital Elevation Models (DEM) with specific vegetation characteristics while maintaining feasible computational times. Such improvements would enhance our capacity to study the hydrodynamics in Lac Bay under changing field conditions, informing comprehensive ecosystem management strategies for this vital coastal habitat.

3.3 Research objective

This research aims to develop and assess a subgrid-based hydrodynamic model for simulating flow dynamics within Lac Bay's mangrove forest by applying the increased bed roughness approach, the Baptist method, and the porous layer method to model vegetation resistance, while also evaluating whether combining these approaches can improve model performance for different mangrove species.

3.4 Research questions

In order to fulfill the objective, four research questions were formulated.

Q1 What are the hydrodynamic forcings, spatial extent, and flow characteristics both within the tidal creeks and mangrove forest of Lac Bay and in the surrounding area?

Q2 What computational grid resolution is necessary to adequately represent the bathymetry and vegetation variations in Lac Bay's mangrove forest to achieve an optimal balance between computational efficiency and accuracy in modelling the hydrodynamics?

Q3 How do the increase in bed roughness, the Baptist approach, and a porous layer differ in their ability to accurately capture the effects of vegetation resistance on flow velocities and water levels within the forest and creeks, and which method performs best in simulating these effects?

Q4 How can a combination of vegetation modelling approaches (Baptist method and porous layer) be optimised to accurately represent the hydrodynamic effects of different mangrove species (red and black) in Lac Bay?

3.5 Methodology

To investigate the effectiveness of subgrid-based modelling in simulating flow dynamics within Lac Bay's mangrove forest, the systematic approach depicted in Figure 3.7 is used. The study area, Lac Bay, serves as a representative microtidal mangrove ecosystem, providing a good setting for this research.

Following a literature review, an in-depth analysis of the study area will be conducted. This phase addresses the first research question by identifying the geographic and hydrodynamic characteristics of Lac Bay. Data gathering will include collecting vegetation maps, flow characteristics, and boundary conditions. The analysis will focus on understanding the hydrodynamic forcings, spatial variability, and flow patterns both within the tidal creeks and mangrove forest of Lac Bay and in the surrounding area. The key hydrodynamic characteristics will be used to define criteria to calibrate and validate the model later on.

For the hydrodynamic simulations, a suitable base-case model is needed, before implementing the different vegetation methods. With the base-case model, parameters such as model domain, bathymetry, boundary conditions and initial conditions are chosen and will be kept constant during the research. Additionally, a suitable computational grid size will be chosen, based on a sensitivity analysis. The optimal resolution is intended to represent the bathymetry while maintaining computational efficiency. Next, a vegetation representation raster is created, which serves as a key input for implementing different vegetation modelling methods (increased bottom roughness, Baptist method, and porous layer). By using this detailed subgrid raster, we can ensure that each method is applied precisely to the correct locations within the model domain.

The implementation of vegetation drag effects will focus on three methods: increased bed roughness, the Baptist approach, and the porous layer method. The increased bed roughness will be implemented via a spatially varying roughness raster. The Baptist approach will be applied to directly account for vegetation characteristics. The porous layer method will model the porous nature of the mangrove forest. Calibration and validation will be done with predefined criteria. They will provide insight in the performance of the numerical models compared with the observations. The best performing parameter settings from the calibration will be used for the validation. The output of the validation will be used to compare the results of the three vegetation methods. With these criteria, the hydrodynamic characteristics will be compared, in order to see which methods allow for a better simulation of the complex physical processes.

The last step is constructing a hybrid model, which combines different approaches of modelling vegetation. As there are different mangrove types, different methods are likely needed to represent various types better. By modelling the mangrove types with different methods, the effect of the different types on the system can be investigated. Also for this step, the previous criteria are used to calibrate and validate the model and analyse the model performance.

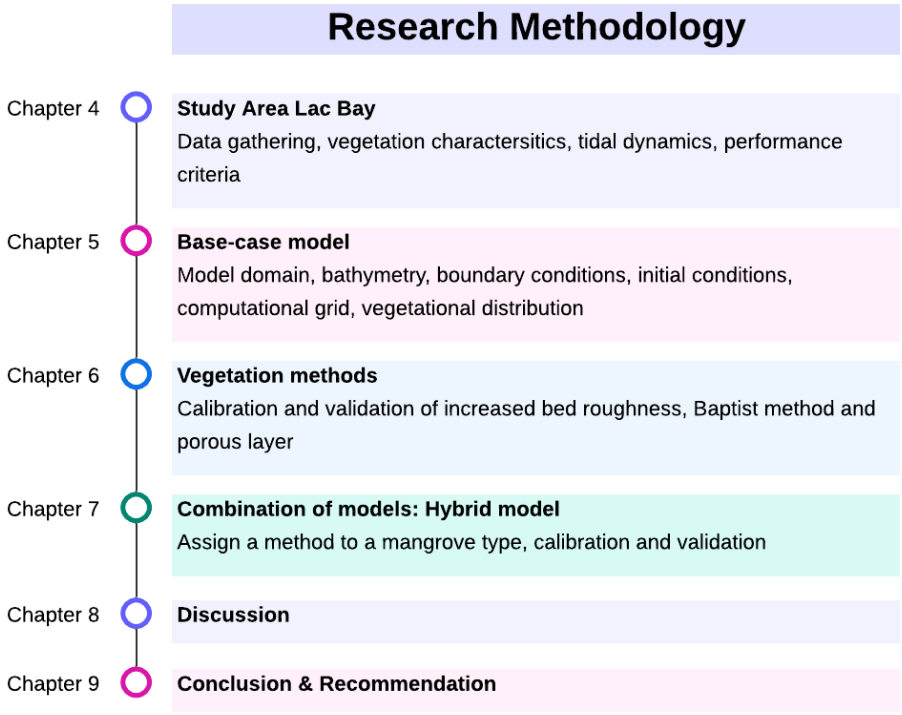

Figure 3.7: Flowchart research methodology.

3.6 Report Organization

In Section 4 the study area will be introduced and the analysis of the hydrodynamics and spatial area will be shown. With these results the performance criteria are formed. Section 5 will show the computational grid sensitivity analysis to explain the set-up of the base-case model. In Section 6 the individual methods will be implemented, calibrated and finally evaluated with the validation. The set-up of the combined methods is elaborated in Section 7, This is followed by Section 8, where the results, uncertainties and other aspects will be discussed. In Section 9.1 the conclusion of this research is presented, which is followed by the recommendations in Section 9.2.

4 Study area analysis

4.1 Lac Bay

Lac Bay is a mangrove and seagrass lagoon, on the south-east coast of the island of Bonaire (Figure 4.1). Within the bay, extensive seagrass meadows are situated which provide an important feeding grounds for juvenile green turtles, but also support a diversity of fish and invertebrates (Smulders et al., 2017; van Zee, 2022). The bay is surrounded by a mangrove forest. Throughout the past century, the mangrove forest has grown towards the bay while losing ground at the back. The die-off in the back of the forest occurs due to reduced tidal exchange. This is caused by overgrowth of the creeks within the forest due to reduced boating in the creeks as it was declared a Ramsar site, which is a protected wetland (List, 2024). This resulted in progressive siltation, blocking water flow to the back (van der Meulen, 2023; van Zee, 2022). Consequently, the backwater area is permanently inundated, and both the soil and water at the back of the forest become hypersaline, creating adverse conditions for mangrove survival (Van Moorsel & Meijer, 1993). Additional evaporation during prolonged low water periods further increases the salinity in both the soil and water, exacerbating hypersalinity (Lott, 2001). Next to mangroves, seagrass also grow within the bay, as mentioned earlier. However, the effect of seagrass on tidal flow is not considered in this research. Therefore, in the context of this study, the term "vegetation" refers exclusively to the mangrove trees.

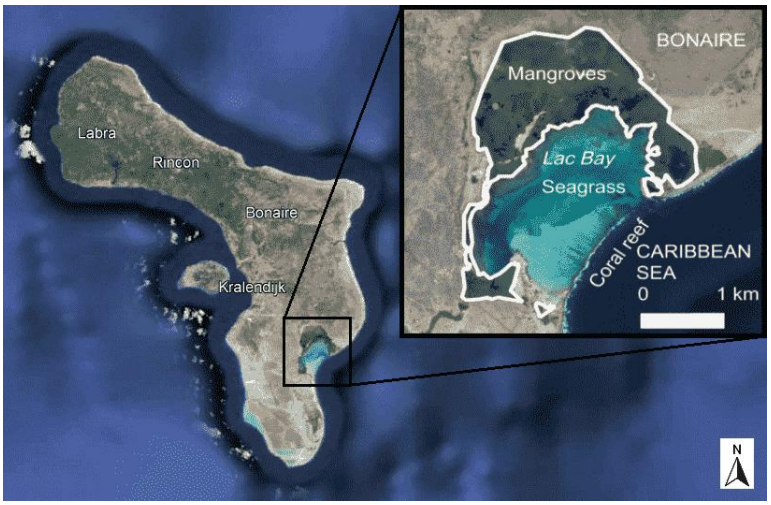

Figure 4.1: A map of Bonaire (Google Earth, 2023) and a close up with land-use of Lac Bay (Smulders et al., 2017)

4.2 Topographic description

Lac Bay covers approximately 700 *ha* (Smulders et al., 2017), of which the mangrove trees are covering around 222 *ha* (Casal et al., 2024) excluding the died-off area. The lagoon is protected by a coral reef on the east coast. This protects the lagoon from waves, resulting in calm water conditions in the bay, while also being a nursery for fish (Debrot et al., 2010). A small opening towards the sea, called Boca di Lac, is located at the north side of the coral reef (Figure 4.2). Within the mangrove forest, a series of small islands (orange) are located from west towards the east: Isla di Yuwana, Isla di Pedro, Isla Rancho, Isla Fogon and Isla di Chico. The latter four islands obstruct the tides from moving in and out of the backwater (Van Moorsel & Meijer, 1993). Next to the islands, two creeks allow the tide to enter the back of the forest, called Awa di Lodo. The eastern creek is Creek di Coco (red), which remains open and is maintained by fishermen (Lott, 2001). At the west boundary Creek di Pedro (blue) is located. Both creeks are indicated by the red lines in Figure 4.2.

4.2.1 Bathymetry

Lac Bay is protected by two headlands on the southwest and the northeast side, which are elevated to 1.0m LVD (Local Vertical Datum). The coral reef is connected to the southwest headland and goes almost to the northeast side. Baco di Lac is the only deeper connection between the open sea and the bay, located at the

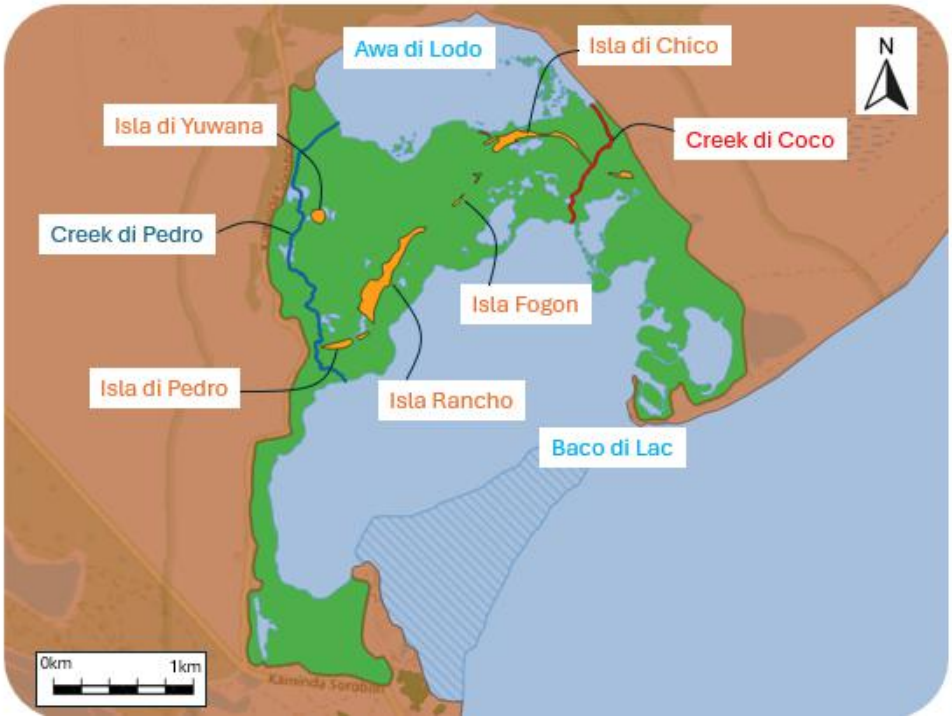

Figure 4.2: A map of Lac Bay with the names of important locations with the mangrove forest (green). The hashed area marks the coral reef

northeast headland, called Cai. Inside the bay the elevation lowers from the coral reef and gradually rises towards the fringe of the forest. The fringe of the forest is surrounding the bay and starts at an elevation of around $-0.05m$ LVD (van Zee, 2022). Inside the forest, no elevation measurements are available, except for the islands, which have a surface elevation of around $0.4 - 0.6m$ LVD. It is important to notice that during high HWL's (high water levels), water flows at some locations over the islands. Awa di Lodo lies lower than the mangrove forest floor. This elevation difference forms a lake with standing water during low tides. The bed level at Awa di Lodo is approximately $-0.5m$ LVD. The exact elevation within the mangrove forest is not known.

Within the mangrove forest the creek system plays an important role. It connects Awa di Lodo with the bay. The Lac Bay area features two creeks, one on the west side and one on the east side. Those creeks bring saline tidal water towards Awa di Lodo. Towards the back of the forest, the creeks gradually disappear as the elevation rises, forming a depression. This elevated area at the far end of the creeks creates conditions that allow mangroves to establish themselves within the creek bed. The presence of these trees in the depression forms a transition zone, blurring the distinction between the creek and the surrounding forest. The west creek has a deeper and wider bathymetry overall, compared with the east creek. The west creek ($2000m$) is twice as long as the east creek ($950m$). Both creeks have several lagoons along the path from the bay towards Awa di Lodo.

4.2.2 Mangrove population

Within the mangrove forest, there are two dominant mangrove types, the *Rhizophora mangle* (red mangroves) and the *Avicennia germinans* (black mangroves), shown in Figure 4.3. The red mangroves are populated more towards the front of the mangrove forest at the bay side. This is because the red mangrove prefers frequently or permanently flooded areas, while the black mangroves grow at higher elevation areas, with lower water levels (Casal et al., 2024). An important characteristic of these mangroves, particularly the red mangroves, is their growth pattern along the creek banks. It has been observed that their roots often extend and hang over the banks into the creeks, creating a natural but significant obstruction to water flow within these creeks. This unique growth pattern not only shapes the physical structure of the creeks but also influences their

Figure 4.3: Photographs from red mangroves (left) and black mangroves (right) within Lac Bay (Picture taken by Kadaster Bonaire)

hydrodynamics. Casal et al. (2024) have mapped the mangrove distribution (Figure 4.4) based on Sentinel-2 data, allowing a clear categorization of the vegetation type within the mangrove forest. A small percentage was unclassified, which will not be used during this research. The total area covered by the red mangroves is 136.0 ha and the black mangroves cover around 77.1 ha. It is important to notice that the data depends on the leaves of the trees, which might cover creeks.

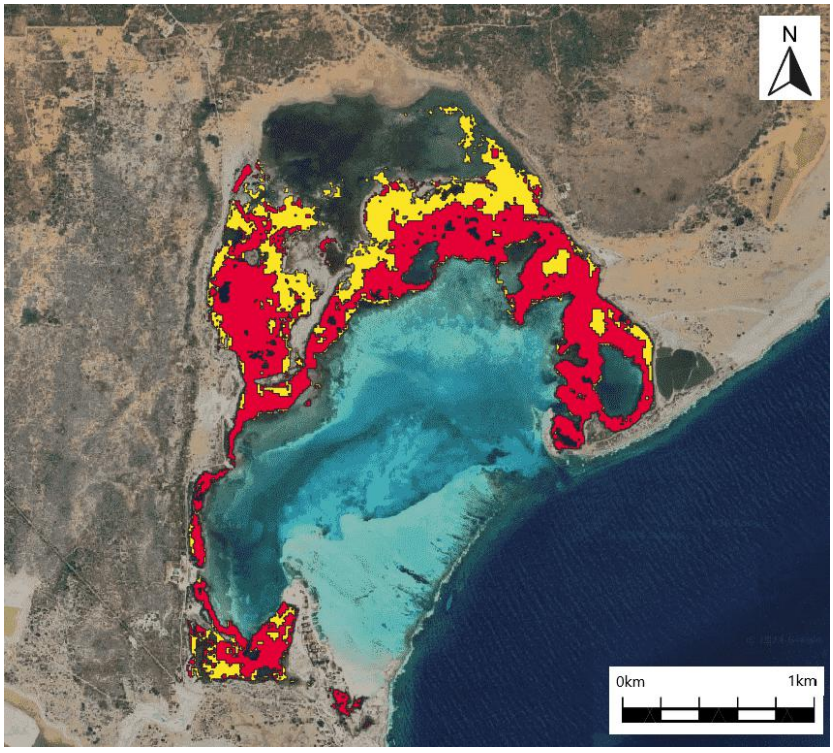

Figure 4.4: The map shows the black mangroves (yellow) and the red mangroves (red) distribution in Lac Bay Bonaire (Casal et al., 2024)

Next to the distribution of the vegetation, the vegetation characteristics play an important role. Gijsman et al. (2024) performed measurements in Lac Bay at several locations. A total of 14 locations were chosen, where $1m^2$ plots were set out to measure the mangrove type (black or red mangroves), root density, root height and root diameter. Only the living portions of the roots were measured, while dead sections were excluded. Table 4.1 shows the average measured values for the red and black mangroves. Also their solid volume fraction and frontal area density is shown. The complete table with all measurements can be found in Appendix A.

Table 4.1: The averaged vegetation characteristics for the red and black mangroves, based on Gijsman et al. (2024).

Characteristic	Black mangrove	Red mangrove
Number of roots, N $[/m^2]$	500	70
Average diameter, D $[m]$	0.010	0.025
Average height, h $[m]$	0.150	0.700
Solid volume fraction, φ $[-]$	0.040	0.035
Frontal area density, a $[/m]$	5.000	1.750

4.3 Tidal dynamics

The following section focuses on the hydrodynamics within Lac Bay. The data used for this analysis was obtained by Gijsman et al. (2024) during a field study conducted from January to March 2022. Measurements were taken at various locations in and around the mangrove forest (Figure 4.5). Water level measurement locations, indicated by red dots in Figure 4.5, were recorded at several key points. These include the west fringe (referred to as fringe), Awa di Lodo, and Cai. Velocity measurement locations, represented by green dots, were taken at two creek locations: the west creek (WC) and the east creek (EC). Within the forest, no measurement locations were available.

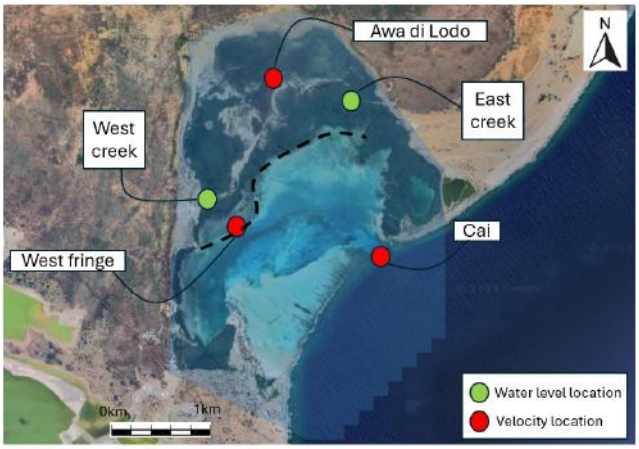

Figure 4.5: Measurement locations for water level (red) and velocities (green). The dotted black line is marking the fringe (Gijsman et al., 2024)

Within the mangrove forest, the tide is the primary driver of water flow. The dominant tidal constituents in Lac Bay are the diurnal constituents K1 and O1, and the semi-diurnal constituent M2. The tidal pattern exhibits variation between neap and spring tides (Figure 4.6). During neap tide, the semi-diurnal constituents are more prominent in the data, while during spring tide, the diurnal component becomes dominant.

4.3.1 Water levels

As mentioned before, during spring tide, the diurnal components become dominant, resulting in approximately one high and one low water occurrence per day. Figure 4.7 shows the data collected between 22.01.2022 and 05.03.2022, displaying three spring-neap cycles. During spring tide, the tidal range at the forest fringe varies: it reaches around $0.45m$ for the first and third periods, while it's approximately $0.32m$ for the second period. At neap tide, the tidal range reduces to around 0.10-0.15m. Notably, all three spring-neap cycles exhibit different behaviours, indicating a region with highly variable tidal dynamics. This variability suggests the presence of additional factors operating on a different timescale than the spring-neap cycles, such as meteorological influences or longer-term oceanographic phenomena.

The backwater area, known as Awa di Lodo, behaves differently from the forest fringe. In Awa di Lodo, the tidal range is significantly smaller, varying between $0.03m$-$0.07m$. van Zee (2022) describes this phenomenon as the "bathtub effect", where during spring tides, the backwater gradually fills. This occurs because before

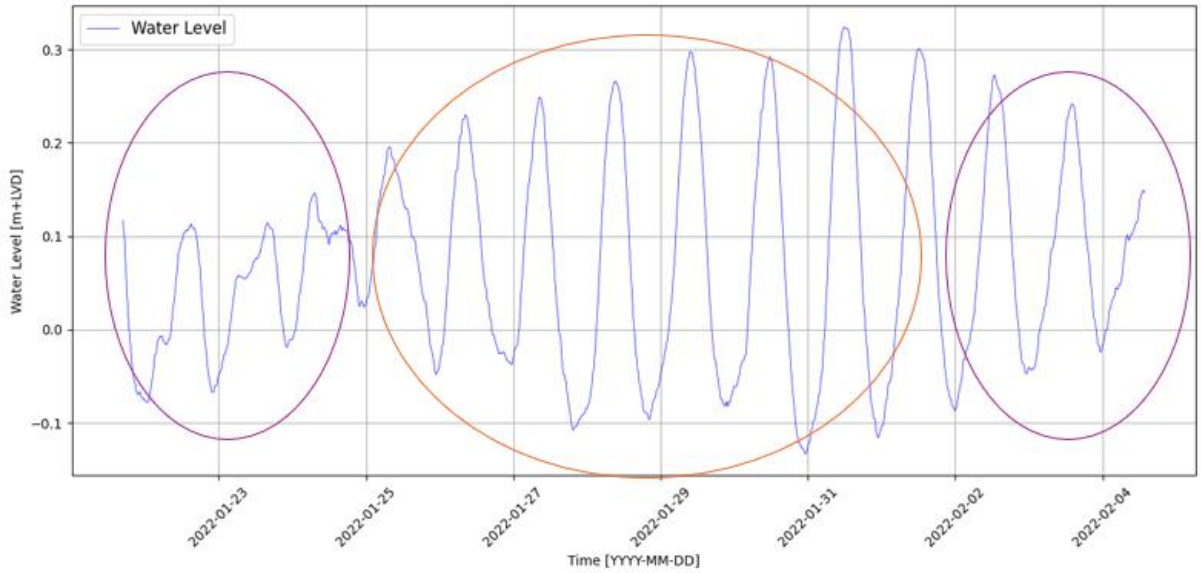

Figure 4.6: Water level measured at Cai, showing semi-diurnal component (purple) and diurnal component (orange) during one spring-neap cycle

water can fully drain back into the bay, the next flood tide enters the mangrove forest, leading to a cumulative increase in water levels. In the second spring-neap cycle, the high water levels (HWLs) are lower than those in the first spring-neap cycle, resulting in less water level variation in the backwater. This is likely due to the reduced water level gradient caused by lower HWLs in front of the forest. Importantly, the water level in Awa di Lodo never falls below $0.02m$ LVD, ensuring that it always contains water, regardless of the tidal state.

The timing of the HWL peaks between the fringe and Awa di Lodo is noteworthy. Before spring tide, water levels at the fringe rise more rapidly compared to Awa di Lodo. During spring tide, the peak at the fringe occurs earlier than at Awa di Lodo, where water levels continue to rise even as they begin to fall at the fringe. This pattern is visible in Figure 4.7 for all three spring-neap cycles, although it's most pronounced in the first and third cycles. This observation demonstrates a significant delay in peak water levels between the fringe and Awa di Lodo, highlighting the complex hydrodynamics of the mangrove system. These findings underscore the intricate interplay between tidal forcing, local topography, and the mangrove forest's hydrological response, contributing to the unique water level dynamics observed in Lac Bay.

4.3.2 Tidal duration asymmetry

Tides consist of a rising and falling phase. In tidal ecosystems, asymmetry often occurs due to factors such as bathymetry, friction, and vegetation. To quantify tidal asymmetry, a ratio is calculated with the time between low water level (LWL) and the subsequent HWL, representing the rising tide, and the time between the HWL and the next LWL, representing the falling tide:

$$A_{duration} = \frac{T_{falling}}{T_{rising}} \tag{4.1}$$

This ratio indicates whether the system is flood-dominant or ebb-dominant. In a flood-dominant system, where the rising tide is shorter ($A_{duration} > 1$), the flood period is shorter, and the ebb period is longer. Figure 4.8 shows the tidal duration asymmetry ratio for Awa di Lodo (red), fringe (green), and Cai (blue). The locations at the fringe of the mangrove forest exhibit ebb-dominant behavior, where the flood phase lasts longer than the ebb phase, especially at higher HWLs. Conversely, in Awa di Lodo, the ratio exceeds one, indicating flood dominance. This means that the flood period is shorter, and the ebb period is longer. During the flood, water is rapidly forced towards Awa di Lodo due to the pressure gradient. However, during the ebb period, water is held back, suggesting that vegetation and bathymetry create significant resistance, slowing the draining flow and extending the ebb period.

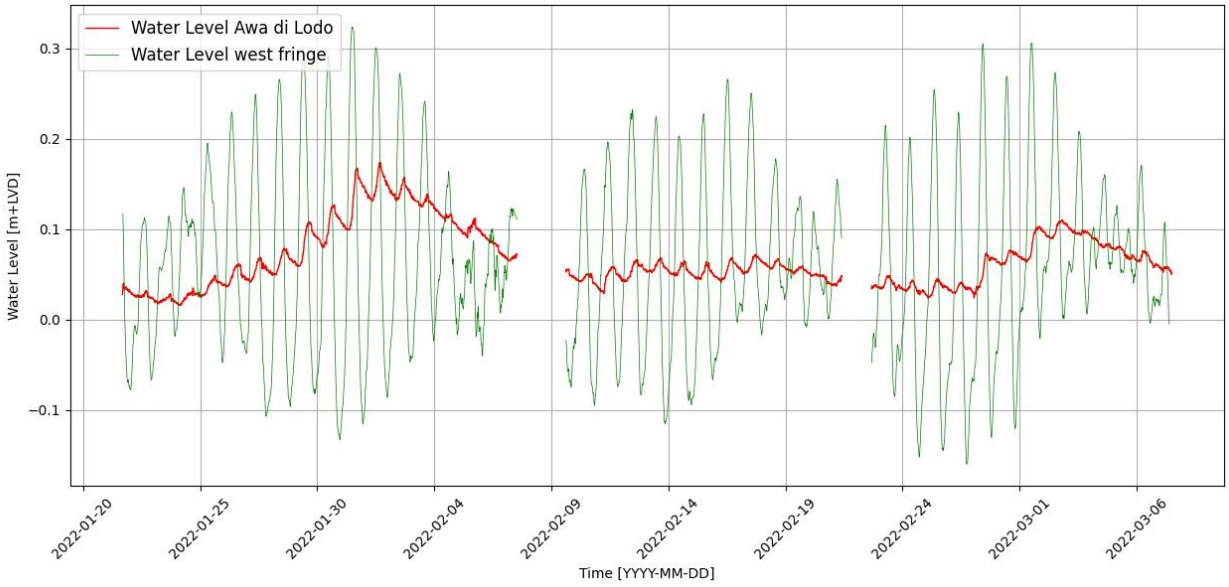

Figure 4.7: The water level measured during the three spring-neap cycle. Locations are the west fringe (green) and at Awa di Lodo (red).

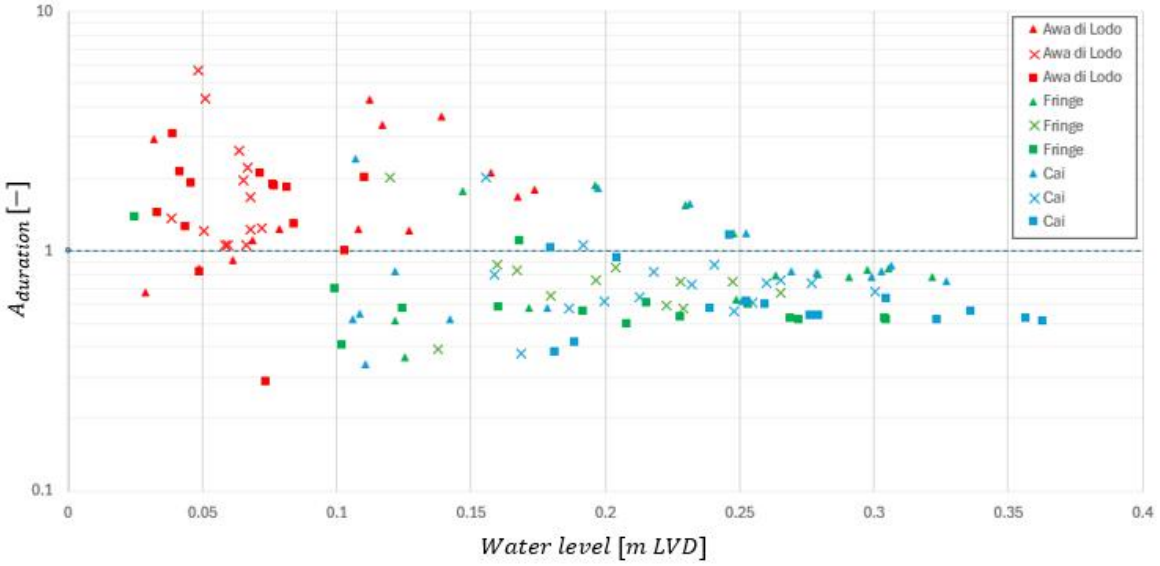

Figure 4.8: Tidal duration asymmetry at different locations around Lac Bay on a logarithmic scale for the first sping-neap cycle (triangle), second sping-neap cycle (cross), and thirs spring-neap cycle (square).A value ***above*** *1 (dotted line) is flood dominant.*

Due to the influence of bathymetry, bottom friction, and vegetation, the HWL is delayed in the back of the mangrove forest. van Zee (2022) calculated a total delay of nearly 4-5 hours between the HWL at Cai and the HWL measured at Awa di Lodo. This delay is linked to the significant water level differences between Awa di Lodo and the fringe, as discussed in Section 4.3.1. Essentially, the tide changes direction 4-5 hours later at Awa di Lodo than at the fringe. These findings demonstrate the substantial influence of the mangrove forest on tidal flow patterns.

4.3.3 Flow velocities

The observed flow velocities in the west and east creek show different behaviour. In the west creek a large difference between the flood and ebb velocities can be seen in Figure 4.9. During flood, the speed increases up to $0.40m/s$ during spring tide, while the maximum ebb flow velocity remains around $0.05m/s$ throughout the entire spring-neap cycle. The total area below the graph indicates a larger volume of water entering during flood compared to the water leaving during ebb. At certain points during the spring-neap cycle, almost no water leaves via the west creek (ebb flow velocity below $0.01m/s$). This raises questions regarding the validity of the measurements, as observations of researchers see water flowing out of the creek. The location of the measurement equipment was located at the side of the creek to ensure passage by boats through the creek. This can be a cause for irregular measurements between flood and ebb.

At the east creek the flow velocities during flood and ebb show a more balanced behaviour, where the maximum flood and ebb velocities are between $0.10m/s$ and $0.15m/s$. A notable observation is the short duration of the maximum flood velocity, which occurs as a single sharp peak. In contrast, the ebb maximum velocity persists for a much longer period. As a result, the total area below the curve representing the ebb period is larger than that during the flood period. This indicates that the outflow during ebb is larger than the total inflow during flood in the east creek. This imbalance between inflow and outflow might be attributed to water entering Awa di Lodo over the islands during high water levels. This additional water input then leaves the area through the east creek during the ebb tide, contributing to the increased outflow observed.

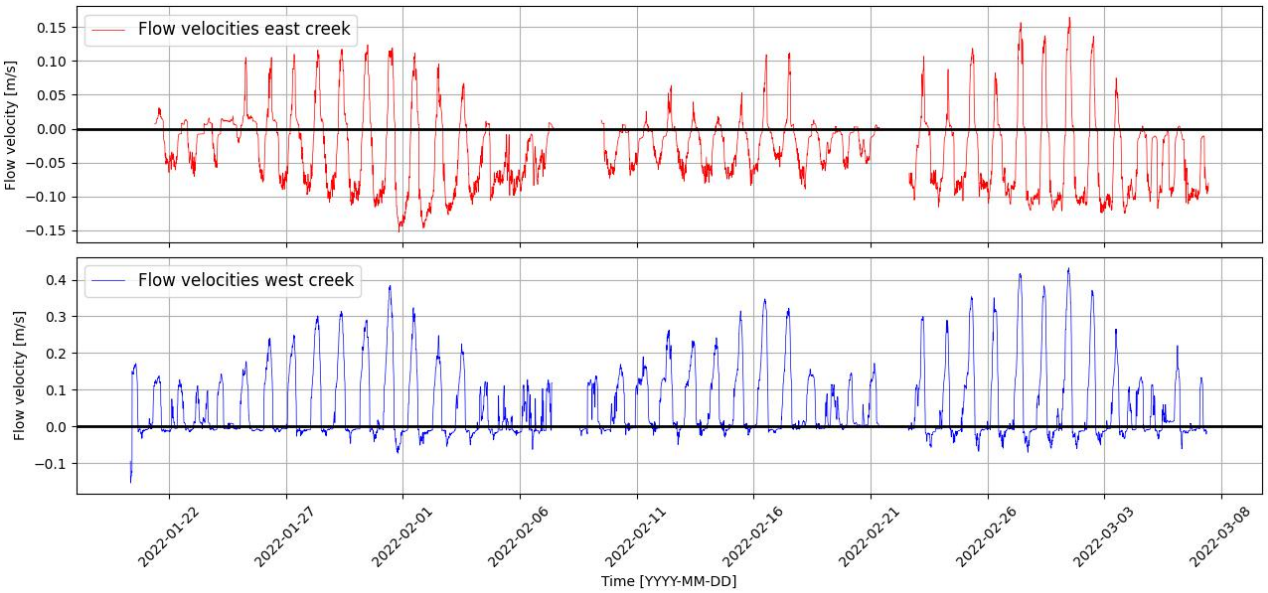

Figure 4.9: Flow velocities at east creek (top) and west creek (bottom). Positive velocities are directed inland and negative velocities are directed towards the bay.

By calculating the tidal velocity asymmetry, a creek can be categorised into either flood or ebb dominant. For this the maximum velocity during ebb is divided by the maximum velocity during flood. A ratio below one is flood dominant.

$$A_{velocity} = \frac{\mid u_{max,ebb} \mid}{\mid u_{max,flood} \mid} \tag{4.2}$$

Figure 4.10 shows the asymmetry in the east and the west creek. It shows that the west creek is flood dominant.

The east creek shows both flood and ebb dominant behaviour. During higher water levels at the fringe the creek shows flood dominant behaviour which is due to the water level gradient between fringe and Awa di Lodo. At the fringe flood dominant behaviour was seen for the tidal duration asymmetry, which supports flood dominant behaviour in the west creek as it is close to the fringe. In flood-dominant systems, the incoming tide has a shorter duration to transport water inland compared to the outgoing tide. This compressed time-frame for the flood tide necessitates higher flow velocities to move the same volume of water. This supports the observed higher flow velocities in the west creek.

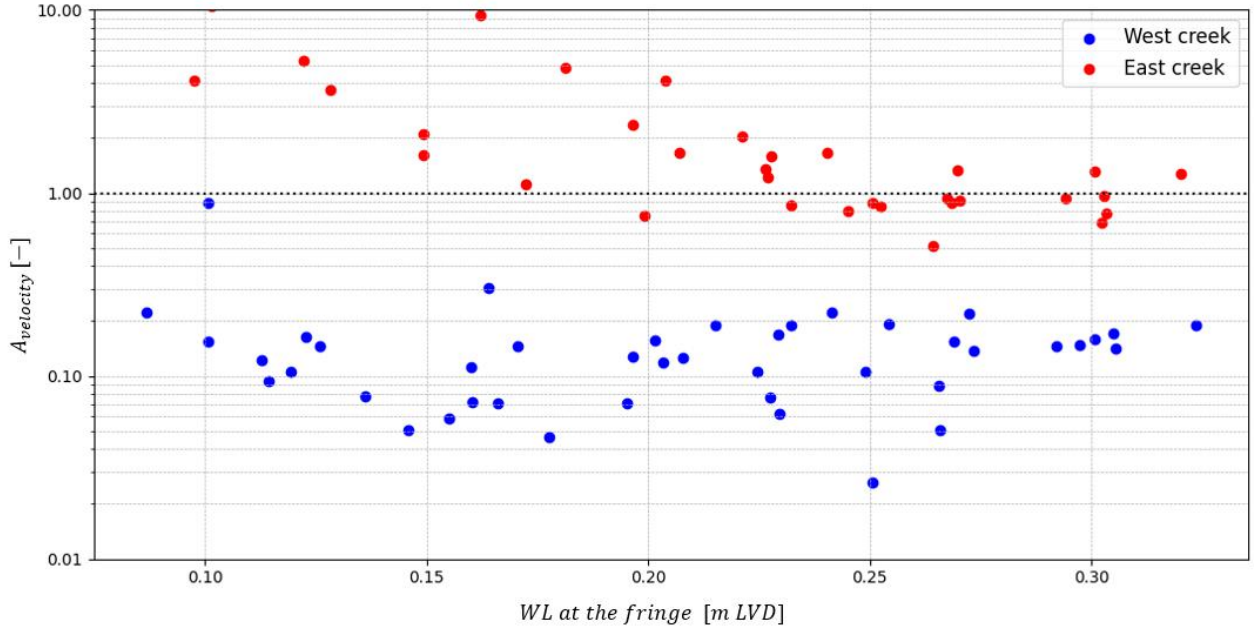

Figure 4.10: Velocity asymmetry in the west creek (blue) and east creek (red) for all three spring-neap cycles. A value ***below*** 1 *(dotted line) is flood dominant.*

The flow velocity measurements in Lac Bay reveal distinct patterns between the east and west creek, reflecting the complex hydrodynamics of the system. Several factors contribute to the differences observed between the two creeks. The proximity of the west creek measurement location to the bay, compared to the east creek, potentially increases its sensitivity to the influence of the incoming tidal wave at the fringe. The presence of lagoons and branches along the east creek may affect its flow velocities. The west creek's greater width presents an interesting dynamic: while it might result in lower flow velocities, it could also allow the flood dominance of the west fringe to have a more significant impact on the measured flow velocities, particularly in areas closer to the bay. Additionally, the dominant easterly wind direction in the area may force more water towards the west fringe, potentially further influencing velocities within the west creek. These factors, combined with the observed tidal asymmetry patterns, underscore the complexity of the hydrodynamics in Lac Bay.

Given the irregular behavior and contradictions observed in the west creek measurements, it has been decided not to consider these observations as a performance criterion. This decision acknowledges the unique challenges presented by the west creek's data while emphasizing the need for further research and more comprehensive measurements to fully understand the intricate relationships governing flow velocities throughout the Lac Bay system. Having only limited data allows a limited comparison between observations and simulation results. Having one measurement in the east creek, which is located in front of the islands misses the effects of those islands in this ecosystem. As mentioned before, there are no measurement locations in the forest, leaving the entire forest a black box in terms of water levels and flow velocities.

4.4 Performance Criteria

From the previous section, several key hydrodynamic characteristics have been identified that are crucial for the calibration and validation of the hydrodynamic model. These characteristics, observed through measurements at locations such as Awa di Lodo and the east creeks, include tidal ranges, water levels, flow velocities, and

tidal duration asymmetry. These variables represent the essential dynamics of the mangrove system and are used to establish quantitative criteria for evaluating the model's performance.

The criteria are prioritised based on their importance in capturing these hydrodynamic features and are applied to assess whether the model accurately reflects the system's behavior. The criteria, listed below in order of priority, serve as the basis for the model calibration and validation process:

- **Tidal Range (Highest Priority)**: The difference between high and low water levels during a tidal cycle, observed at Awa di Lodo. This criterion has the highest priority because it reflects the volume of water exchanged between Awa di Lodo and Lac Bay, a key factor influencing flow velocities and circulation patterns. Accurate simulation of the tidal range is critical for capturing the overall system dynamics.

- **Tidal Duration Asymmetry**: The time difference between the flood and ebb phases of a tidal cycle, measured at Awa di Lodo. This criterion reflects the influence of vegetation on water flow and helps determine whether the model correctly captures the timing of water movement through the system.

- **Absolute Water Level**: Maximum and minimum water levels during a tidal cycle at Awa di Lodo. This criterion ensures that the model accurately simulates the magnitude of water exchange, which is essential for understanding how high and low tides affect the system. By comparing observed and simulated water levels, the model's ability to replicate these critical water dynamics can be assessed.

- **Maximum Velocities (Lowest Priority)**: The maximum flood and ebb velocities observed in the West and East creeks. These velocities provide insight into the inflow and outflow dynamics of the system, helping to assess the accuracy of the model's flow resistance and the simulation of water movement through the creeks. While important, this criterion is given slightly lower priority due to potential uncertainties in the velocity measurements.

These criteria, derived from the hydrodynamic characteristics observed in Lac Bay, are used to evaluate the performance of the hydrodynamic model. Table 4.2 summarises the criteria and the locations where they are applied. The absolute water level is split into HWL and LWL. The maximum velocities is split between flood and ebb. This means a total of 8 criteria values are used.

Table 4.2: The criteria that are used for measuring the performance and comparing the different methods with each other.

Criteria	**Approach**	**Location**	**Abbreviation**
Tidal range	quantitative	Awa di Lodo	TR
Tidal duration asymmetry	quantitative	Awa di Lodo	$A_{duration}$
Absolute HWL	quantitative	Awa di Lodo	HWL
Absolute LWL	quantitative	Awa di Lodo	LWL
Maximumflow velocity Flood	quantitative	East creek	EC_{flood}
Maximum flow velocity Ebb	quantitative	East creek	EC_{ebb}

The performance of the model is evaluated using the Normalised Root Mean Square Error (NRMSE), a standardised metric that compares the model's predictions with observed data.

$$RMSE = \sqrt{\frac{\sum_{i=1}^{n}(y_{\text{simulated,i}} - y_{\text{measured,i}})^2}{n}} \tag{4.3}$$

$$NRMSE = \frac{\text{RMSE}}{\text{mean}(y_{\text{measured}})} \tag{4.4}$$

The NRMSE is calculated by first determining the Root Mean Square Error (RMSE), which measures the average magnitude of differences between the simulated and measured values. The RMSE is then normalised by dividing it by the mean of the measured values, making it dimensionless and comparable across different criteria and scales.

5 Base-case model

Before applying the different types of vegetation representations, it is important to have a realistic base model. This contains the correct bathymetry, boundary and initial condition, computational grid size and vegetation distribution, which defines the locations where the vegetation methods should be used. This base model will be the foundation for this research and should contain the correct information. The aforementioned aspects are discussed separately below.

5.1 Model domain

The model domain is chosen to cover all relevant spatial characteristics of the area. Important aspects of the area that influence the flow behaviour in and around the mangrove forest should be included. These are the whole bay, coral reef, and entrance of the bay. The model domain should be larger than the area of focus (mangrove forest). This is important because a large model domain will allow a more realistic propagation of the tidal wave. Furthermore, this expanded domain ensures that the implemented boundary conditions do not dominate the local hydrodynamics within the study area. This spatial buffer allows the bathymetry and other local features to properly influence water flow patterns, preventing the boundary signals from overshadowing the natural system dynamics. Therefore, the sea area is expanded farther out from the bay in order to achieve that.

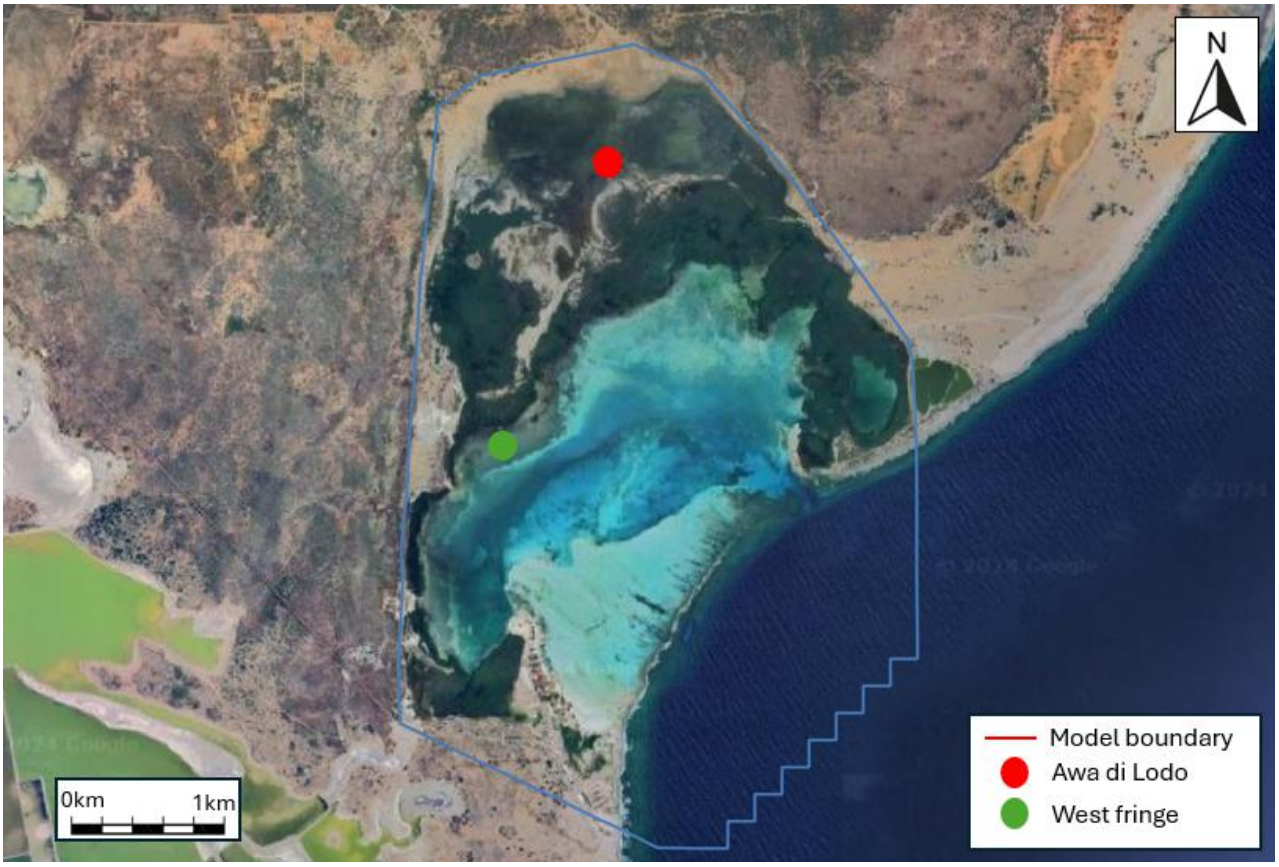

Figure 5.1: The model domain chosen for this research (blue line) with Awa di Lodo (red) and west fringe (green).

The complete model domain is shown in Figure 5.1. The road surrounding Lac Bay serves as the cut-off from the hinterland. The height is 1.0m LVD, which is well above the maximum HWL and will not be submerged by water. Therefore, everything behind it will not be flooded by the tides and is beyond our interest.

5.2 Bathymetry

An elevation map of the area is crucial for this study. The detailed representation of the forest elevation plays a crucial role in accurately simulating water flow patterns within hydrodynamic models. A correct bathymetry is therefore important, especially in the areas around the creeks and islands. The final bathymetry map (Figure 5.2) is combined from two data sources. The elevation point data files from Gijsman et al. (2024) provide detailed measurements for the creeks, islands, and outside land border. The Delft3D data, which is also based on elevation points by Gijsman et al. (2024) and measured transects, offer elevation points across the model domain. This Delft3D dataset is a coarse DEM as it has been processed in Delft3D without subgrid refinement. The Delft3D data served as the foundational layer for the DEM, with elevation points spaced at intervals ranging from 5 to 20 meters, depending on the size of the computational cells. This map is supplemented at the creeks, islands, and border with raw data obtained by Gijsman et al. (2024), as those locations show steep elevation gradients that can be used within 3Di. These measurements had a much higher resolution compared to the $5m$ grid cell edges in Delft3D. The forest platform elevation within this dataset was assumed to be uniform at a height of $-0.05m$ LVD, as there were no specific measurements. The two raw data sets can be seen in Appendix C.

The creek point elevation data consists of a general cross-section obtained from three cross-section measurements, implemented along the thalweg of the creeks. However, this results in cross-sections that overlay each other in corners or lagoons. This resulted in abnormal averaged values, which were removed manually. To obtain a final DEM, the combined elevation points from the creeks and islands, and the Delft3D model were linearly interpolated, which is shown in Figure 5.2. At the ocean boundary, the elevation points stop just outside of the coral reef at an elevation of $-20m$ LVD. To allow the implementation of the boundary conditions, without influencing the hydrodynamics within Lac Bay, the area is expanded uniformly at $-20m$ LVD. This results in a subgrid with a resolution of $0.5m$ by $0.5m$ for the DEM. The use of only one cross section for the entire creek system does not adequately reflect the actual variability within the creek profiles, potentially leading to inaccuracies in hydrodynamic representations.

5.3 Boundary conditions

Boundary conditions are required to force the model. Water level conditions are imposed on the diagonal line at the seaward boundary (Figure 5.1), based on water level measurements from a nearby measurement station, deployed by Gijsman et al. (2024). All other model boundaries at the open sea, including the vertical and bottom sections, are defined as closed boundaries. The measurement station was chosen because a continuous series of measurements was obtained. As only water depths are available, a derivation of the water levels was needed. It was observed by van Zee (2022) that the changes in water level between the ocean and in front of the fringe were similar. Since the west fringe had a continuous and stable measurement, it was used to derive the water level data at sea (Figure 5.3). This was also done because the measurements from the sea were available for a shorter period, which has been extended with the west fringe due to the close similarity. During the calibration, the first spring-neap cycle is used, and for the validation, the second and third spring-neap cycles are used, shown with a red line in Figure 5.3.

5.4 Initial conditions

To reduce the warm-up period for a numerical model, it is useful to implement an initial water level condition. This provides the model with a realistic water level distribution at the start of the simulation. A uniform initial water level is not appropriate for this model due to the significant spatial variations observed in the study area. Measurements indicate that at the simulation start time, Awa di Lodo has a water level of $0.035m$ LVD, while the bay has a water level of $0.119m$ LVD. Given this substantial difference, an initial water level raster was used (see Appendix D). For this initial condition, the area behind the mangrove forest is assigned a water level of $0.035m$ LVD, while the area in front of the forest is set to $0.119m$ LVD. Between these zones, the water levels are linearly interpolated to ensure a smooth transition.

Regarding initial velocities, the numerical model assumes standing water conditions at the start of the simulation, with all flow velocities set to $0m/s$. Despite the initial water level conditions, a warm-up period is still necessary to allow the model to develop realistic flow patterns. For this study, the warm-up period is set to one tidal cycle, which is sufficient to establish correct velocities and water levels throughout the domain. Consequently,

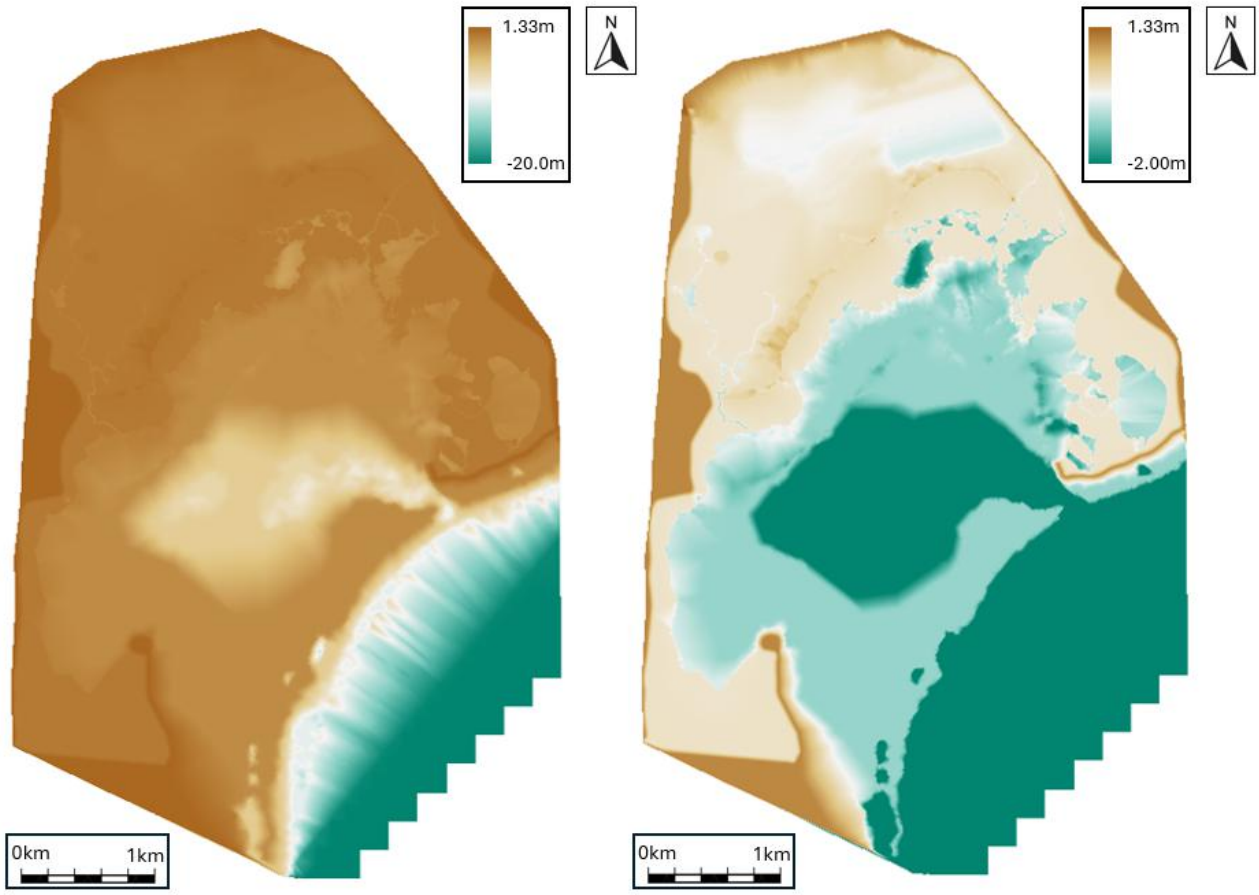

Figure 5.2: DEM of Lac Bay for two colorbars: elevation scale ranging from $-20.0m$ to $1.33m$ LVD (left) and $-2.00m$ to $1.33m$ LVD (right)

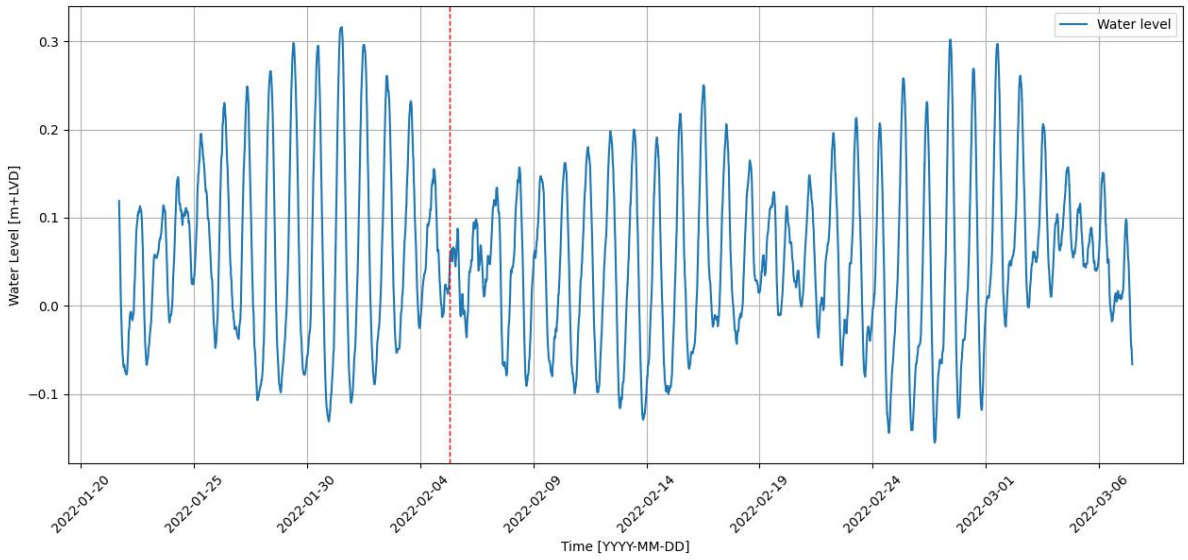

Figure 5.3: The input for the boundary conditions at the model boundary. The red dotted line shows the split between the calibration period (left) and the validation period (right).

data from the first tidal cycle are excluded from the performance criteria evaluations to ensure that only fully developed flow conditions are analysed.

5.5 Computational grid

The computational grid plays a crucial role in numerical modelling, as it balances the computational cost with the precision of representing physical processes occurring within the study area. A finer grid resolution can capture detailed physical interactions more accurately but increases computational time and resource demands. Conversely, a coarser grid reduces computational load, but may oversimplify the representation of processes, potentially affecting the accuracy of the results. To determine the optimal grid resolution, a sensitivity analysis is conducted. The results in simulations with different grid sizes to evaluate their impact on the model's ability to simulate the systems behaviour accurately. For this study, grid resolutions ranging from $\Delta x = 10m$ to $\Delta x = 320m$ are tested, where the grid size edge length is denoted as Δx, to find an appropriate balance between computational efficiency and accuracy of the physical processes being modelled. A grid size of $\Delta x = 5m$ for the entire model was not advised, as it consists of more than 500.000 nodes resulting in very long computational times which is not recommended by 3Di (docs, 2024b).

5.5.1 Computational grid in the study area

To ensure a well-functioning model, it is important for the boundary condition to be located in a grid cell which is mostly covered by the DEM. 3Di cannot use a 2D diagonal boundary condition along the edge. Therefore 1D water level boundary conditions are defined. These boundary conditions provide the 2D grid cells at the boundary with the necessary water level information. These settings are shown in Appendix B. The DEM along the sea-side edge needed to be adjusted to a uniform staircase pattern, with step sizes matching the computational cell dimensions. The 1D boundary conditions are implemented along the staircase edge of the model boundary, where cells with forcings do not contact each other. The purple dots in Figure 5.4 indicate the location of the 1D boundary points. This allows water to flow in and out of the model domain, propagating tidal elevation signals towards the bay and through the mangrove forest. For each tested computational cell size, the DEM is adjusted at the staircase side, to accommodate a diagonal row of cells with 1D boundary conditions (Figure 5.4).

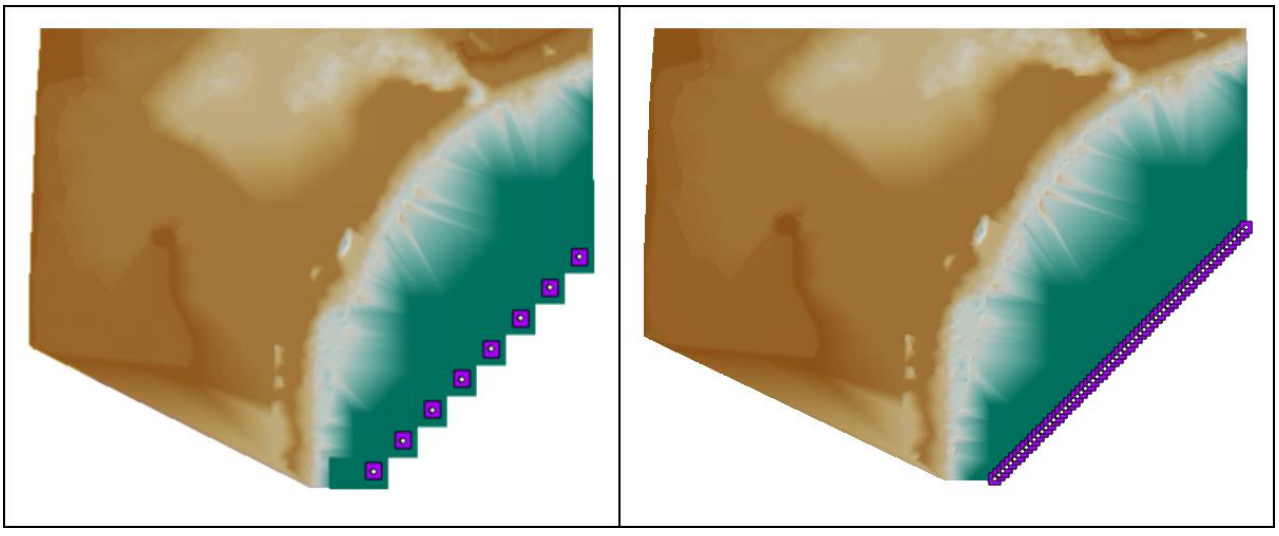

Figure 5.4: A close up of the staircase boundary DEM for a grid size of $\Delta x = 160m$ (left) and for a grid size of $\Delta x = 20m$ (right). The purple dots mark the 1D boundary conditions.

To assess the performance of different computational grid sizes, water levels are evaluated at two locations shown in Figure 5.1. The first location is in front of the fringe at the entrance of the west creek, marked by a green dot. This ensures accurate simulation of the tidal elevation signal reaching the mangrove forest. The second location is in Awa di Lodo, indicated by a red dot, which provides insight into the bathymetry's effect

on water levels within the mangrove forest, which is the main study area. A uniform friction value is used during this sensitivity analysis, with a Chézy coefficient of $60m^{1/2}/s$ representing earthy surface materials.

Figure 5.5 shows the water levels for the first spring-neap cycle at the forest fringe. All grid sizes closely follow the observed data, with minimal variations in timing, likely due to the boundary condition derivation method (Section 5.3). The minimal variations are attributed to the relatively uniform hydrodynamic conditions inside the bay, where even coarser grid cells adequately resolve tidal oscillations.

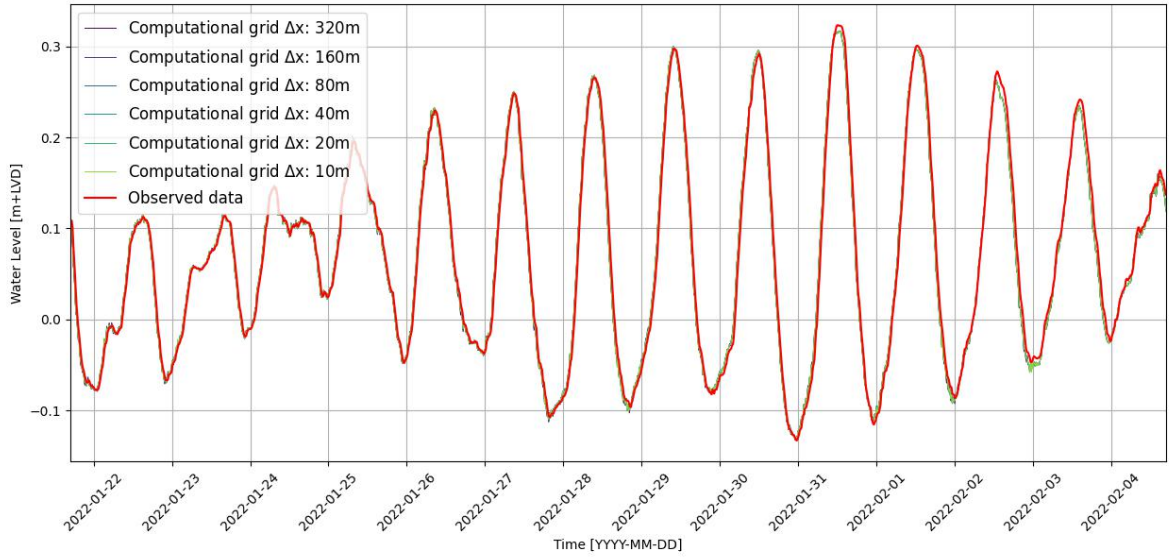

Figure 5.5: The sensitivty analysis results for the water level at the west fringe for grid sizes between $\Delta x = 10m$ and $\Delta x = 320m$. The observed data is indicated with a red line.

At Awa di Lodo, water levels show greater sensitivity to the grid size, which is shown in Figure 5.6. Finer grid sizes align best with observed data, suggesting they better capture complex physical processes and small-scale variations in the bathymetry. As the grid size increases, simulations diverge from observed data, with LWLs becoming exaggerated for grid sizes of $\Delta x = 80m$ and larger. The largest grid size ($\Delta x = 320m$) simulates water levels below $0.0m$ LVD, which is not observed in reality. HWLs show less pronounced exaggeration. This mismatch for coarser grids indicates inadequate representation of small-scale hydrodynamic processes within the mangrove forest.

Computational efficiency is also considered. Table 5.1 presents the computational time required for a spring-neap cycle (14 days) simulation. Grids with $\Delta x = 40m$ or larger complete within 25 minutes. Balancing hydrodynamic accuracy and computational efficiency, a grid size of $\Delta x = 160m$ is chosen for areas outside the mangrove forest. The next section will present a separate sensitivity analysis for the grid within the mangrove forest between the fringe and Awa di Lodo. This is because the results in Figure 5.6 showed the importance of smaller grid sizes for catching the small-scale variations in the bathymetry.

Table 5.1: The computational grid size on the left side and the computational time it takes to simulate one spring neap cycle of 14 days.

computational grid size $[m]$	computational time $[hh:mm:ss]$
$\Delta x = 10$	13:37:00
$\Delta x = 20$	01:58:00
$\Delta x = 40$	00:24:41
$\Delta x = 80$	00:07:14
$\Delta x = 160$	00:02:36
$\Delta x = 320$	00:01:24

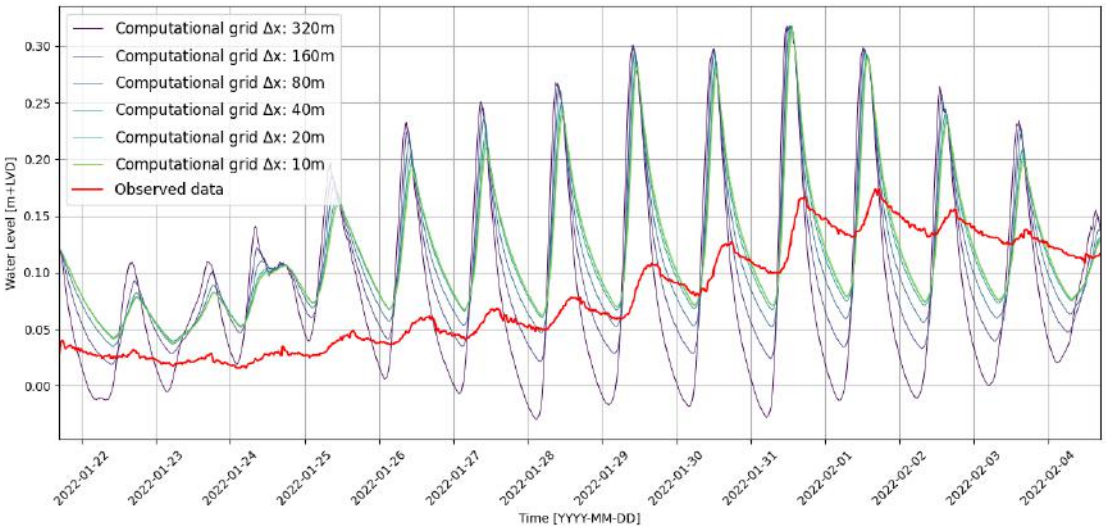

Figure 5.6: The sensitivty analysis results for the water level at Awa di Lodo for grid sizes between $\Delta x = 10m$ and $\Delta x = 320m$. The observed data is indicated with a red line.

5.5.2 Computational grid inside the mangrove forest

As seen in the previous section, a grid size of $\Delta x = 40m$ and smaller start to catch more of the complex physical processes and complex small-scale geometry of the bathymetry within the forest. Therefore, a smaller grid size will be used within the mangrove forest between the fringe and Awa di Lodo. This allows for a more accurate comparison of the flow velocities with the observations and takes the complex bathymetry into account.

An important phenomenon which should be avoided within subgrid modelling are leaking cells. Leaking cells primarily occur due to abrupt bathymetric changes that are not adequately captured by coarse grid resolutions. These cells fail to represent obstacles or elevation changes that occur within them, as each cell is assigned a single average water level. Therefore, water or flow unintentionally escapes into or out of a computational cell. This issue is particularly critical in locations where the bathymetry is not continuously inundated and alternates between wet and dry states.

Important areas are the creeks, the islands and the edge of the forest. To check whether this is the case in Lac Bay, three different areas will be analysed separately: the creeks, the islands and the entire mangrove forest. Creeks and islands were chosen because they represent regions of significant elevation changes over short distances, where bathymetric shifts are common. The mangrove forest is analysed to see whether grid refinement across the entire forest is needed. It functions as a reference and shows whether focusing only on the creeks and islands is sufficient. The sensitivity analysis is done separately from these areas, in order to compare them. Appendix E contains the individual results of the sensitivity analysis.

The most important results are shown in Figure 5.7. The sensitivity analysis showed that grid refinement around the creeks did not lead to changes at Awa di Lodo, indicating that the creek bathymetry is taken into account with computational cells with a size of $\Delta x = 40m$. The grid refinement around the island influenced the water level at Awa di Lodo, indicating that larger computational cells caused leaking cells. The sensitivity analysis results of the grid refinement around the islands were similar to those of the grid refinement in the entire mangrove forest. This is clearly demonstrated in Figure 5.7, where the $\Delta x = 5m$ computational cells for the entire forest perform similarly to the $\Delta x = 10m$ computational cells around the islands. Implementing refinement only around the islands significantly reduces computational time due to the smaller area requiring refined cells.

Figure 5.8 shows the final computational grid used for this research. The grid design incorporates a gradual transition of cell sizes to ensure computational stability and accuracy. Starting from the bay and moving towards the forest, a grid size of $\Delta x = 80m$ is implemented. This intermediate size serves as a transition zone between the larger $\Delta x = 160m$ cells in the open water and the finer resolution required within the mangrove forest, preventing abrupt changes in cell size that could potentially introduce numerical instabilities.

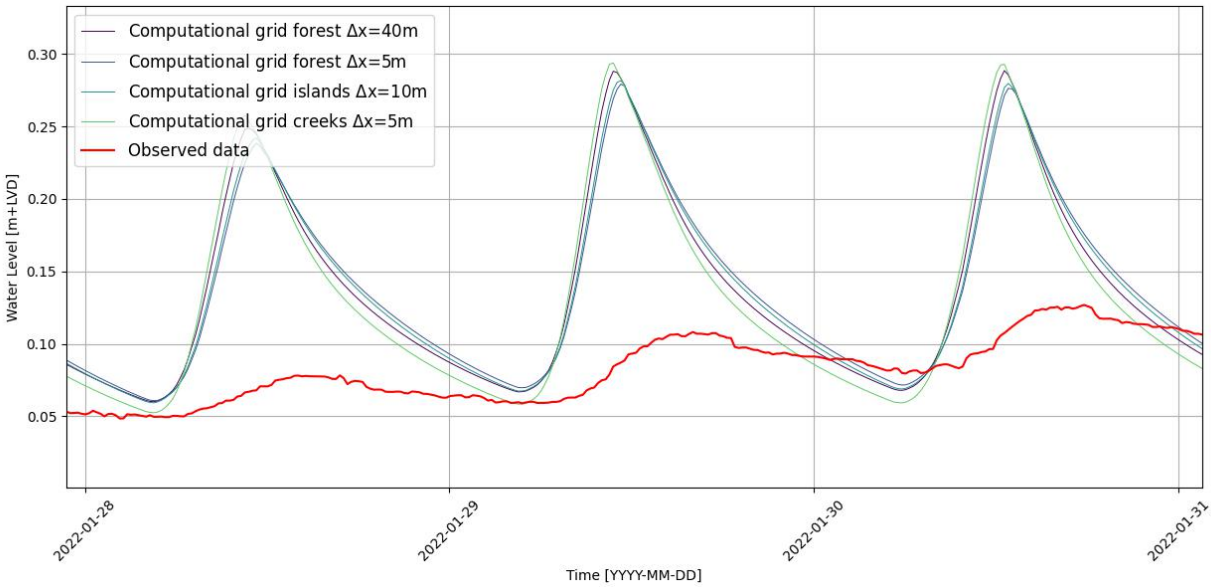

Figure 5.7: The most important results for the grid sensitivity analysis within the mangrove forest between 28.01.2022 and 31.01.2022. The red line indicates the observed data.

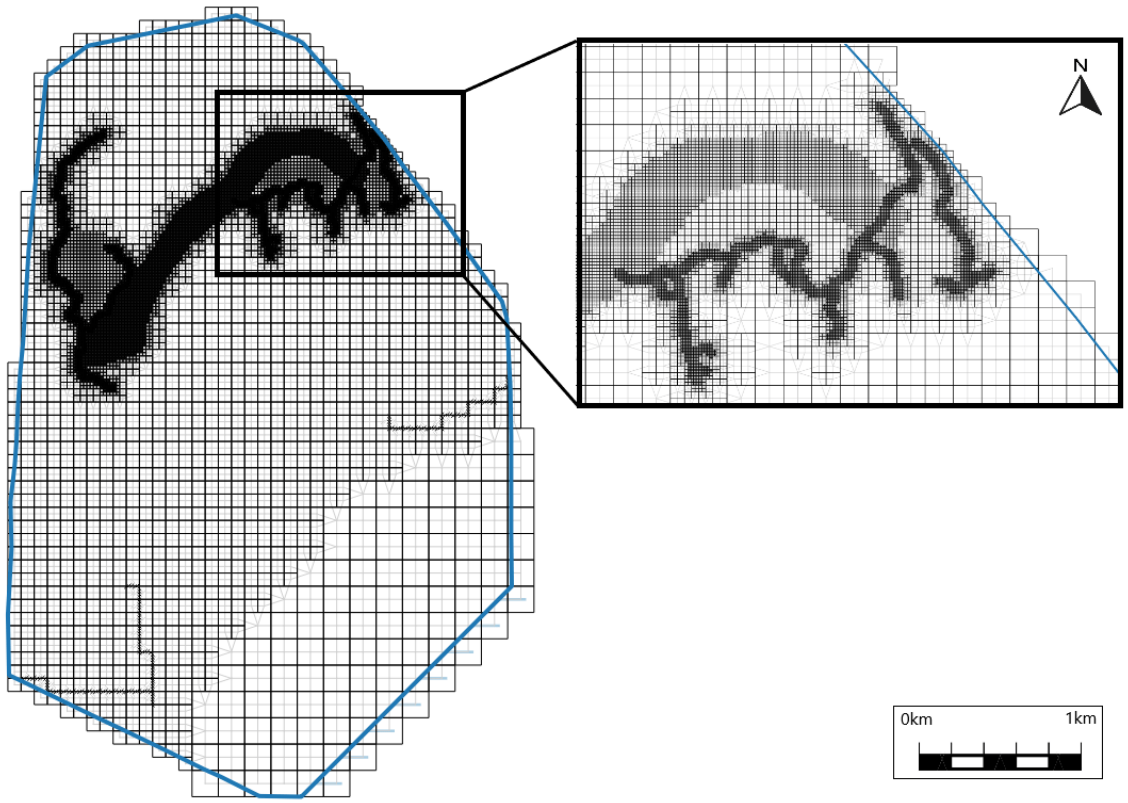

Figure 5.8: The computational grid for this research with the largest computational cells being $\Delta x = 160m$ and the smallest computational cells being $\Delta x = 5m$.

Within the mangrove forest, the grid resolution is refined based on the sensitivity analysis results and the specific requirements of different areas. Around the islands, a grid size of $\Delta x = 10m$ is utilized. This fine resolution is crucial for accurately representing the complex bathymetry in these areas and minimising the occurrence of leaking cells.

For the creeks, an even finer grid size of $\Delta x = 5m$ is employed. The sensitivity analysis suggested that larger cells are good enough for overall water level predictions in front and behind the mangrove forest; however, this finer resolution is necessary for accurately simulating and comparing flow velocities within the narrow creeks. Given that the creeks are approximately $10m$ wide, using $\Delta x = 5m$ cells ensures that we can capture the flow dynamics within the creek channel.

To maintain a smooth transition between these areas of differing resolution, the regions surrounding and between the islands and creeks are assigned a grid size of $\Delta x = 40m$. This intermediate resolution acts as a buffer, allowing for a more gradual change in cell sizes and promoting smoother transitions in the numerical calculations between areas of different resolutions. This carefully designed grid structure balances the need for high resolution in critical areas with computational efficiency. The resulting model achieves a total computational time of 75 minutes for a typical simulation run, providing a good compromise between accuracy and practical run times for the study's objectives.

5.6 Vegetation distribution

Inside the mangrove forest, the vegetation plays an important role in the complex hydrodynamics. Important aspects for implementing vegetational effects in a model are coverage and characteristics. All three approaches require information about the location where vegetation affects the system's hydrodynamics. To incorporate this data effectively into the model, the vegetation information is converted into subgrid data, allowing for a more detailed representation within each computational grid cell.

There is no clear data of how far the trees grow into the creeks, and therefore it is difficult to tell what part of the creek is an 'effective' creek. Figure 5.9 visualises the effective creek width, which is the width of the creek, where water can flow through without the influence of the overhanging vegetation. To implement an effective creek which is wider towards the fringe and reduces towards the back, a dependency on the elevation is defined, called creek delineation height (z_{creek}) . This elevation-based approach doesn't alter the DEM within the model but is used to determine whether water is influenced by vegetation. Figure 5.10 shows the impact on a changing creek delineation height. Through analysis and expert judgment, the creek delineation height is set at $-0.20m$ LVD, resulting in wider creeks at the front that gradually narrow towards the back. This dependency also accounts for vegetation in creek depressions near Awa di Lodo.

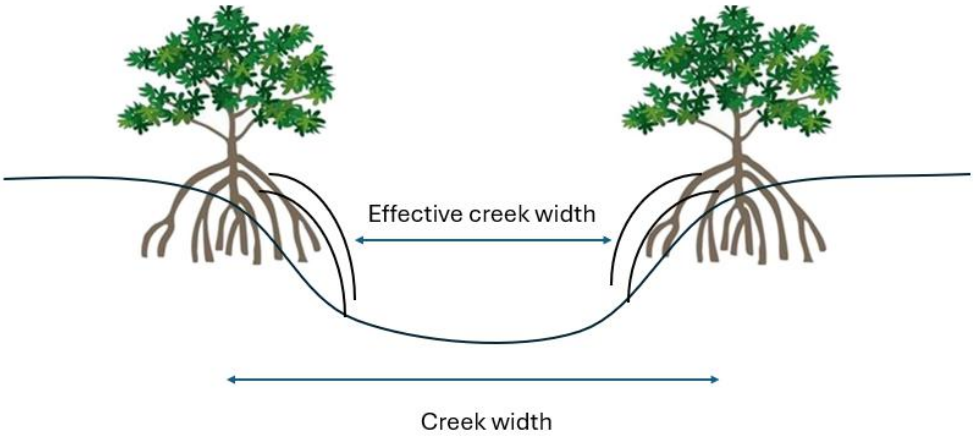

Figure 5.9: A schematisation of the effective creek width within a mangrove forest.

As input for the vegetation, a remote sensing study by Casal et al. (2024) is used. It captures the distribution of the mangrove types within Lac Bay in a raster format. This research focuses on red and black mangroves and because the other types are outside of the main study area, they are not taken into account. The data obtained

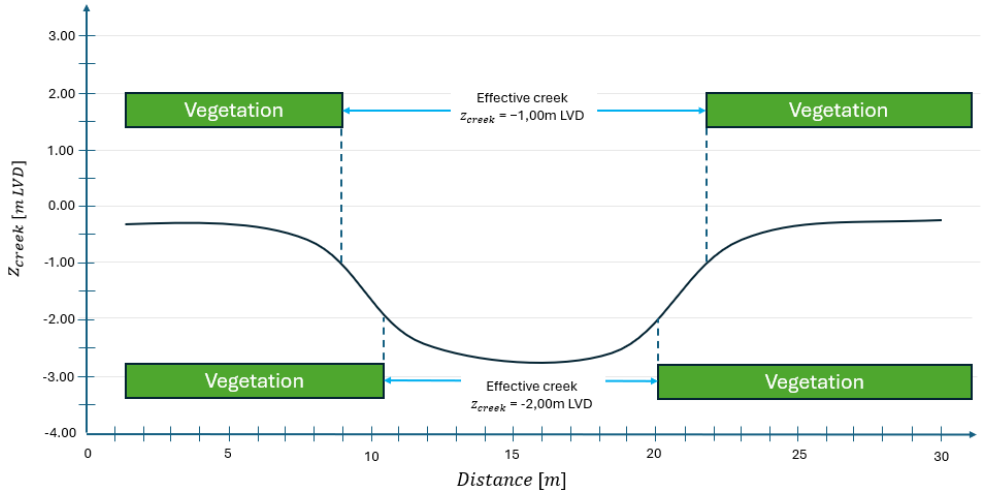

Figure 5.10: A schematisation of the creek delineation height.

is based on sentinel-2 data which uses the leaves of the mangroves. This means that dead vegetation is not taken into account, while around Awa di Lodo large areas are affected by die-off. Since the vegetation overgrows the creeks, they are hardly distinguishable. Therefore, the remote sensing study assigns vegetation inside the creeks. This is where the previous obtained raster about effective creek width is used. The effective creek width is removed from the mangrove distribution. The values in the final vegetation raster that is obtained differentiate between red mangroves (1), black mangroves (2) and the unvegetated part (3), which includes the bay, backwater, land and creeks, as shown in Figure 5.11.

This refined vegetation data is then converted into subgrid input for the model. By using subgrid data, we can represent the vegetation distribution at a higher resolution than the computational grid, allowing for a more accurate simulation of vegetation effects on hydrodynamics within each grid cell. This approach enables us to capture small-scale variations in vegetation cover and their impacts on water flow, even when using larger computational grid cells for efficiency.

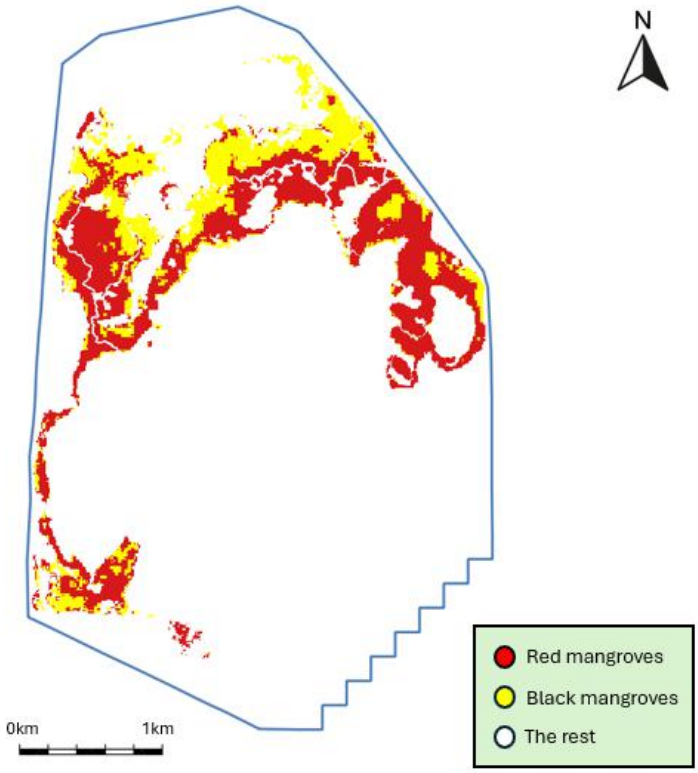

Figure 5.11: The final vegetation raster used in the model. It differentiates between red mangroves (1), black mangroves (2) and unvegetated areas (3).

6 Vegetation methods

In the sections below, the implementation of three vegetation methods is explained. For each method, the implementation is described, followed by the calibration process. Finally a validation of the three representations which performed best is done to compare them. This evaluation will serve as the foundation for the final research question, which addresses a combination of different methods within a single model.

6.1 Increased bed roughness

6.1.1 Introduction

The first method, applied to vegetation implementation, is increasing bed roughness. The previous base case model did not account for vegetation. A roughness raster, based on vegetation distribution, is implemented into the model. This means that vegetation drag and turbulence exerted on the flow within the forest are incorporated into the Chézy value of the bottom roughness. The vegetation raster from Section 5.6 is used to implement the increased bed roughness at the appropriate locations.

Although Lac Bay contains two different mangrove types with varying characteristics (e.g., height and number of roots), calibrating with two distinct types and adjusting their values individually would be currently impossible due to the lack of comparative observations. Moreover, both types have similar solid volume fractions. Therefore, a single Chézy value is assumed for both red and black mangroves. Literature suggests that mangrove forests typically have a Chézy value around $5.00m^{1/2}/s$ (Horstman et al., 2021; Mazda et al., 1995; Stark et al., 2015), which serves as the starting point for calibration. Given the dense vegetation in the forest, the calibration process will test Chézy values ranging from $5.00m^{1/2}/s$ to $0.10m^{1/2}/s$. Although Chézy values below $1.00m^{1/2}/s$ are generally considered unrealistic, they are included to demonstrate the limitations of this method for the modelled system. Figure 6.1 shows the starting raster for the calibration of the bed roughness.

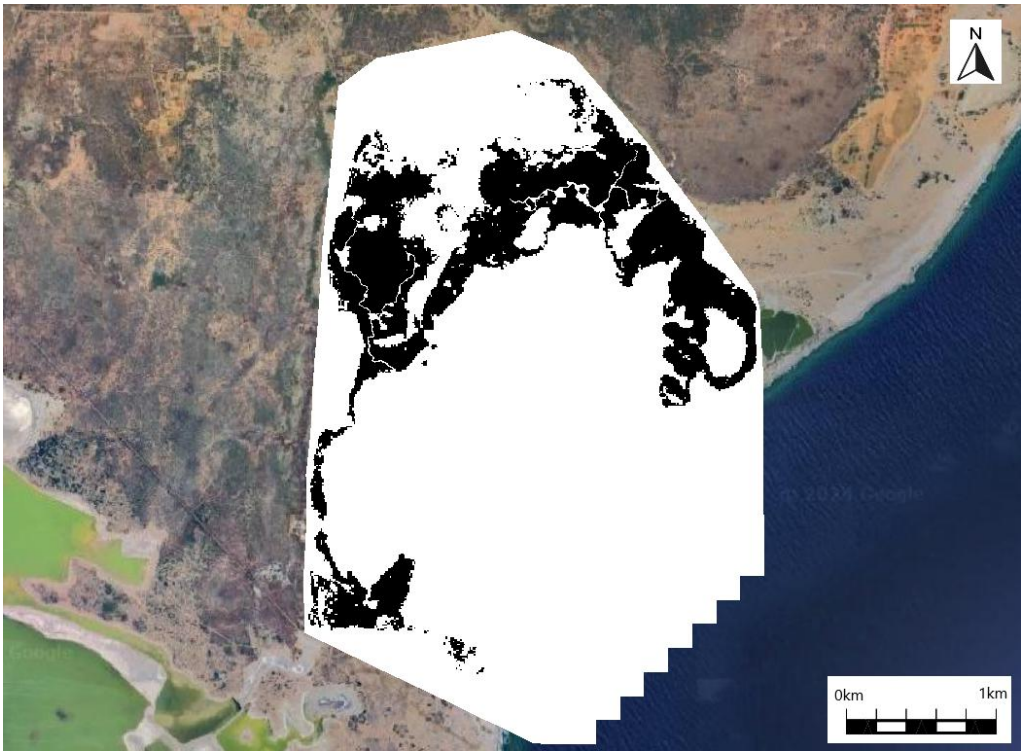

Figure 6.1: The friction raster used for the calibration of the increased bed roughness. A Chézy value of $60.00m^{1/2}/s$ (white), and a Chézy between $5.00m^{1/2}/s$ and $0.10m^{1/2}/s$ (black).

To illustrate why low Chézy values are unrealistic, the Nikuradse roughness height (k_N) is used. This parameter quantifies the effect of surface roughness on flow resistance (Chow, 1959). The Nikuradse roughness height was originally derived from experiments with sand-grain roughness and represents the diameter of roughness

elements that affect flow resistance. The concept was generalised in later years to be applicable under different conditions, such as various ground types including gravel and rocks, as well as vegetation-covered areas. The Nikuradse roughness height for a given Chézy value can be calculated using the following equation, which applies to rough channels (Augustijn et al., 2008):

$$k_N = \frac{12H}{10^{C/18}} \tag{6.1}$$

In mangrove forests, k_N represents the effective root height of the complex vegetation structure. Within the forest, the forest platform is assumed to be at approximately $-0.05m$ LVD. The maximum water level at the fringe lies just below $0.35m$ LVD. This means that the maximum water depth is limited to $0.40m$. Table 6.1 demonstrates this relationship, showing that a Chézy value of $5.00m^{1/2}/s$ corresponds to a roughness height of nearly $2m$. A roughness height greater than the water depth would suggest complete flow obstruction, making continuous water flow physically impossible. This indicates that the Chézy approach, when using very low values, fails to realistically represent the complex flow resistance mechanisms in mangrove forests.

Table 6.1: The conversion from Chézy to Nikuradse roughness height with a water depth of $0.40m$.

Chézy coefficient, C $[m^{1/2}/s]$	**Water depth,** H $[m]$	**Nikuradse roughness height,** k_N $[m]$
60.0	0.40	0.002
20.0	0.40	0.372
5.00	0.40	2.532
1.00	0.40	4.224

6.1.2 Calibration

During the calibration process, only the Chézy value inside the forest was modified. Table 6.2 presents the Chézy values used inside the forest for each of the eight simulation runs conducted. Performance criteria were applied to evaluate these simulations. Figure 6.2 illustrates the simulated water levels at Awa di Lodo for all simulation runs alongside the observations. It is evident that reducing the Chézy value has a particularly significant impact on the HWLs, which show considerable variation across simulations.

Table 6.2: Calibration results comparing Chézy values, showing NRMSE for different criteria. ***Bold values*** *indicate best performance per criterion; green indicates overall optimal Chézy value.*

Chézy coefficient, C $[m^{1/2}/s]$	**TR**	$A_{Duration}$	**HWL**	**LWL**	EC_{flood}	EC_{ebb}
5.00	0.85	0.55	0.54	0.39	0.42	0.67
2.50	0.72	0.51	0.47	0.36	0.37	0.48
1.25	0.45	0.48	0.36	0.35	0.32	**0.16**
1.00	0.32	0.46	0.31	0.34	0.31	0.18
0.75	**0.19**	**0.43**	0.25	0.33	0.30	0.33
0.50	0.72	0.45	**0.18**	**0.29**	**0.29**	0.61
0.25	2.88	0.46	0.32	0.30	0.49	1.13
0.10	6.87	1.28	0.77	0.52	1.87	2.84

The results of the performance criteria are displayed in Table 6.2, with the best-performing simulation run indicated by bold values. Models with a Chézy value of $1.00m^{1/2}/s$ or lower generally outperform those with higher values. Specifically, Chézy values of $0.75m^{1/2}/s$ (highlighted in green) and $0.50m^{1/2}/s$ yield the best results. A Chézy value of $0.75m^{1/2}/s$ performs particularly well in simulating the tidal range, suggesting that it most accurately represents the inflow and outflow of water at Awa di Lodo. Conversely, a Chézy value of $0.50m^{1/2}/s$ performs well in terms of absolute water level values at Awa di Lodo. This is primarily due to the reduction of the offset observed between 25.01.2022 and 28.01.2022, as the high bottom roughness restricts water flow to Awa di Lodo, bringing the simulated values closer to the observations (Figure 6.2). However, this same value ($0.50m^{1/2}/s$) performs poorly in reproducing the tidal range. The impact of very low Chézy values is clearly visible in Figure 6.2. As the Chézy value decreases, the simulated water level curve flattens, and the

tidal wave becomes increasingly dampened. For simulations with Chézy values of $0.25 m^{1/2}/s$ and lower, the modeled friction becomes excessive. This results in a significant reduction of flow towards Awa di Lodo, to the extent that the simulated water levels fail to approach the observed HWLs during spring tide.

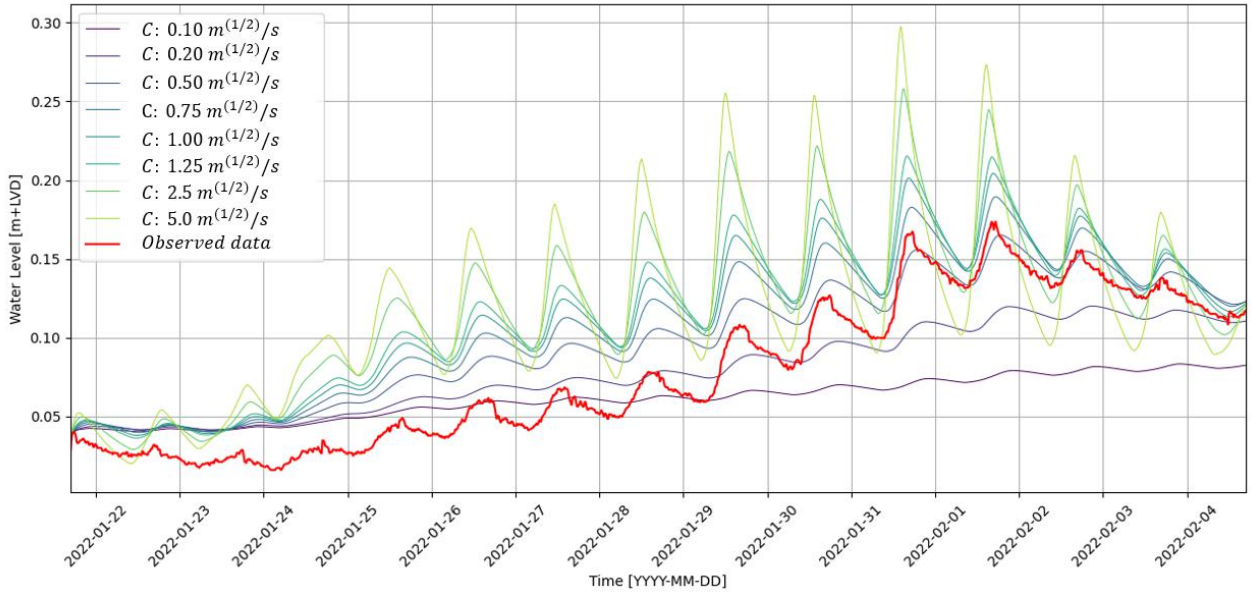

*Figure 6.2: Simulated water levels at Awa di Lodo for varying Chézy coefficients (*0.10-5.00 $m^{1/2}/s$*), with observations indicated in red.*

As the tidal range is the most important criterion, the simulation run with a Chézy value of $0.75 m^{1/2}/s$ is chosen as the best-performing simulation (marked green). However, a Chézy value below $1.00 m^{1/2}/s$ is highly unrealistic, indicating that vegetation cannot be modelled solely through increased bed roughness. This unrealistic value is further emphasized by the resulting Nikuradse roughness height, which significantly exceeds the actual water depth in Lac Bay. Such a discrepancy creates a paradoxical situation where the model represents the entire height of mangroves as a bed roughness element, despite the shallow water conditions. This suggests that other methods should be implemented.

6.2 Baptist approach

6.2.1 Introduction

The Baptist method utilises the distribution of red and black mangroves in Lac Bay. This approach implements vegetation drag separately from bottom roughness, as explained in Section 3.1.3, using four key characteristics. Table 4.1 presents the averaged characteristics derived from measurements by Gijsman et al. (2024). These values are implemented at the subgrid level using the vegetation distribution described in Section 5.6, ensuring a detailed representation of spatial variability.

Baptist et al. (2007) uses a drag coefficient within his method. This coefficient, along with root density, root diameter, and root height, linearly influence the representative Chézy value, as shown in equation 3.2. While the drag coefficient itself does not directly account for measurement uncertainty, it can serve as a proxy for assessing spatial variability in areas where direct measurements were not obtained. The significant variations observed throughout the forest justify testing a range of drag coefficients. If higher drag coefficients yield improved performance, it may indicate substantial spatial variation in vegetation characteristics across unmeasured areas of the dense forest.

For the calibration of the Baptist method, the drag coefficient is selected as the adjustable parameter. In mangrove forests, drag coefficients typically range between 1 and 10 (Gijon Mancheno et al., 2021; Wang et al., 2022). The calibration process begins with a drag coefficient of 1 and increases up to 300 to evaluate extreme scenarios. Although such high values are physically unrealistic, they serve to highlight the potential variability and uncertainties in vegetation characteristics across the forest.

The Baptist method's incorporation of vertical vegetation structure allows for a reduction in bottom roughness, enabling the use of a higher Chézy value within the forest, compared with the previous method. A uniform Chézy value of $20m^{1/2}/s$ is assigned to the forest floor for both mangrove types, accounting for the presence of rough sediment, dead vegetation, and leaf litter. For areas outside the forest, a Chézy value of $60m^{1/2}/s$ is maintained, consistent with the previous method.

6.2.2 Calibration

Table 6.3 shows the drag coefficient used for each simulation run in the left most column. A total of 7 simulations were performed, on which the performance criteria were applied.

Table 6.3: Calibration results comparing Drag coefficient values, showing NRMSE for different criteria. ***Bold values*** *indicate best performance per criterion; green indicates overall optimal Drag coefficient value.*

Drag coefficient, C_D [−]	**TR**	$A_{Duration}$	**HWL**	**LWL**	EC_{flood}	EC_{ebb}
1.00	0.87	0.58	0.56	0.52	0.40	0.68
10.0	0.65	0.51	0.43	0.35	0.36	0.31
20.0	0.52	0.50	0.37	0.34	0.34	**0.16**
50.0	0.27	**0.45**	0.29	0.32	0.31	0.27
100	**0.25**	**0.45**	0.22	0.30	**0.30**	0.47
200	0.87	0.48	**0.19**	0.27	0.32	0.67
300	1.48	0.52	0.22	**0.26**	0.37	0.80

Figure 6.3 shows the water level at Awa di Lodo for all simulation runs using the Baptist method. A very high drag coefficient is needed to bring the simulation results closer to the observations. The criteria results are shown in Table 6.3, where the bold values indicate the best performing simulation run. Increasing the drag coefficient from the starting value results in a better performing model. This only holds until a drag coefficient of 100, after which the improvements stall or get worse.

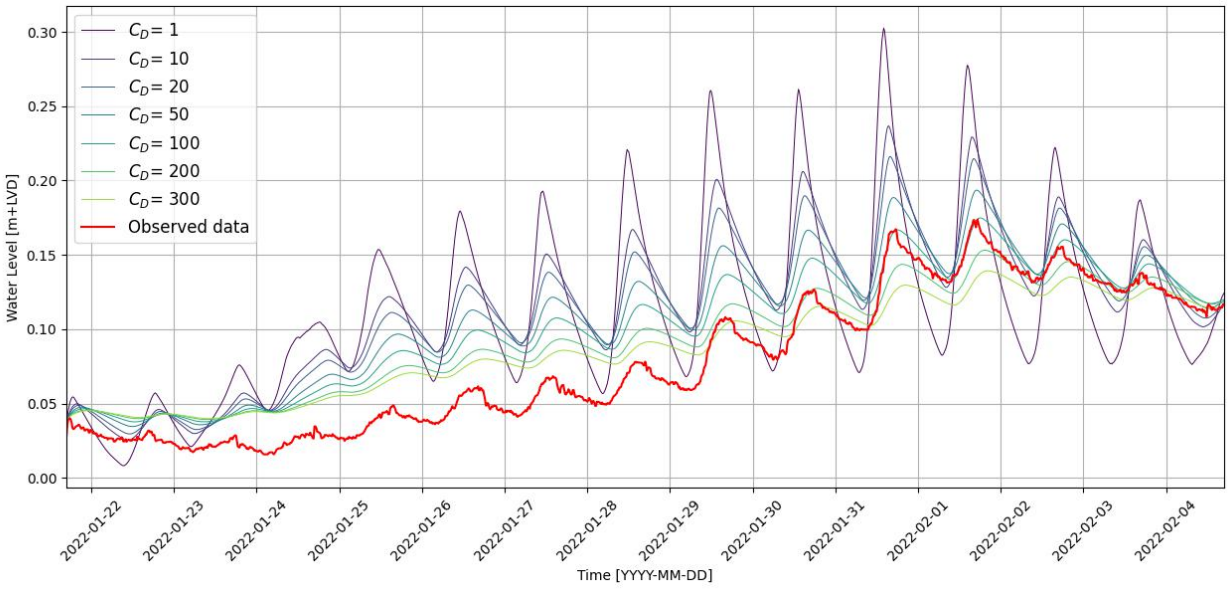

Figure 6.3: Simulated water levels at Awa di Lodo for varying Drag coefficients (1.00-300), with observations indicated in red.

It's important to note the changing tidal asymmetry at different drag coefficient values. As the drag coefficient increases, the tidal asymmetry becomes more pronounced. This is due to the higher drag resulting in increased friction, which in turn leads to lower velocities through the vegetation. The effect is particularly visible in Figure 6.3, where it can be observed that the timing of the peaks is influenced by the changing drag coefficient.

Higher drag coefficients cause a delay in the peak water levels, further emphasising the asymmetry between flood and ebb tides.

Especially the tidal range decreases in performance for the extreme values of 300 for the drag coefficient. For the high and low water levels, a drag coefficient of 100 and higher performs well. As the priority is on the tidal range, and water level and velocity performance are similar for the high drag coefficients, the best performing simulation run is with a drag coefficient of 100, shown in green. Therefore, this value will be used for the validation process.

The unusually high drag coefficient (100) required for optimal performance can be attributed to the high variability between measurements. This suggests that areas which have not been directly measured may have higher characteristic values, such as number of roots or root diameter, indicating much more resistance than the measurements initially indicated. The high drag coefficient required for optimal performance might also suggests that the model may be compensating for other factors not explicitly accounted for, such as complex root structures of the red mangroves or variations in vegetation density that are not captured by the available field measurements.

6.3 Porous layer

6.3.1 Introduction

To implement the porous layer representing the mangrove forest, several parameters need to be defined based on measured characteristics. Within the 3Di software, the porous layer is simulated using the interflow layer functionality, specifically employing Type 3 (docs, 2024a). Type 3 in 3Di is characterised by its dependence on computational cell geometry, where the bottom of the interflow layer is determined by the lowest DEM pixel in the computational cell. The porosity and hydraulic conductivity are applied on a subgrid level. This approach allows for a more nuanced representation of the porous medium. For this implementation, three key parameters must be defined: porosity, hydraulic conductivity, and porous layer height.

A critical aspect of the model is the porous layer height. 3Di requires a uniform height for the porous layer across the entire domain. However, black and red mangroves exhibit different characteristic heights, as shown in Table 4.1. To account for this variation, an initial height of $0.40m$ was chosen, which is slightly lower than the average height between the red and black mangroves. It's important to note that while 3Di models the porous layer below the DEM, the actual vegetation exists above the DEM. To address this discrepancy, the original DEM was elevated by $0.40m$ at mangrove locations.

The porosity of the porous layer was determined using the solid volume fraction from measured characteristics as a starting point. To account for leaves and dead roots, which contribute to the overall volume occupied by mangroves, an additional fraction was added to the solid volume fraction. This resulted in a porosity value of 0.9 within the mangrove forest, indicating that 90% of the volume is water and 10% is occupied by mangroves. In areas without mangrove forest, the porosity was set to 0.0, effectively eliminating the porous layer in these locations.

Hydraulic conductivity represents the ease with which water flows through the porous layer. Due to no flow speed measurements within the forest, this study relied on research by Baltus (2022), who used a hydraulic conductivity of $208m/s$. Considering that the Lac Bay forest is known to be denser compared to the one studied by Baltus (2022), a slightly lower hydraulic conductivity of $200m/s$ was chosen for this model. It's worth noting that in areas outside the forest, where porosity is set to zero, the hydraulic conductivity value does not affect the flow as there is no volume in the porous layer beneath the normal DEM.

Above the porous layer, a Chézy roughness coefficient is defined to represent canopy-scale turbulence. While there is limited literature directly converting canopy-scale turbulence into a Chézy roughness value, this study adopted the approach used by Baltus (2022), applying a Chézy value of $20m^{1/2}/s$. This value serves as an initial estimate for the complex interaction between water flow and the mangrove canopy structure.

6.3.2 Calibration

The first step in the calibration process involved testing the impact of porosity and hydraulic conductivity on the system. Table 6.4 shows the input parameters for the simulation runs, with porosity values ranging from 0.1 to 0.9 and hydraulic conductivity values between $200m/day$ and $10.0m/day$.

*Table 6.4: Calibration results comparing porosity and hydraulic conductivity values, showing NRMSE for different criteria. **Bold values** indicate best performance per criterion; green indicates overall optimal porosity and hydraulic conductivity value.*

Porosity, ϕ $[-]$	**Hydraulic Conductivity,** K $[m/day]$	**TR**	$A_{Duration}$	**HWL**	**LWL**	EC_{flood}	EC_{ebb}
0.9	200	1.54	0.67	0.41	0.36	**2.46**	**4.43**
0.5	200	1.29	0.65	0.37	0.34	4.02	5.46
0.1	200	**1.07**	**0.63**	**0.33**	**0.32**	4.96	6.66
0.9	100	1.53	0.67	0.41	0.36	2.57	4.52
0.9	10.0	1.51	0.67	0.40	0.35	2.75	4.74

Table 6.4 presents the criteria results from these simulations. It is evident that none of the parameter combinations yield satisfactory simulation results, with most values close to 1.00 or higher. While lower porosity values generally increase accuracy, it's important to note that a porosity of 0.1 is highly unrealistic for a mangrove forest and therefore not representative of the actual conditions in Lac Bay.

Figure 6.4 illustrates the effect of these parameter changes on the water level at Awa di Lodo. The results reveal that reducing the porosity of the porous layer leads to an increase in water level at Awa di Lodo. This phenomenon occurs because lower porosity corresponds to reduced volume storage within the porous layer. Consequently, less water is retained within the layer, resulting in more water being pushed into Awa di Lodo.

Variations in hydraulic conductivity showed minimal impact on water levels. This lack of sensitivity might be attributed to the relatively low range of hydraulic conductivity values tested. Even at $200m/day$, water in the simulation may not have sufficient time to reach Awa di Lodo. Further reducing this value only decreases the likelihood of water movement, effectively nullifying its impact on the results.

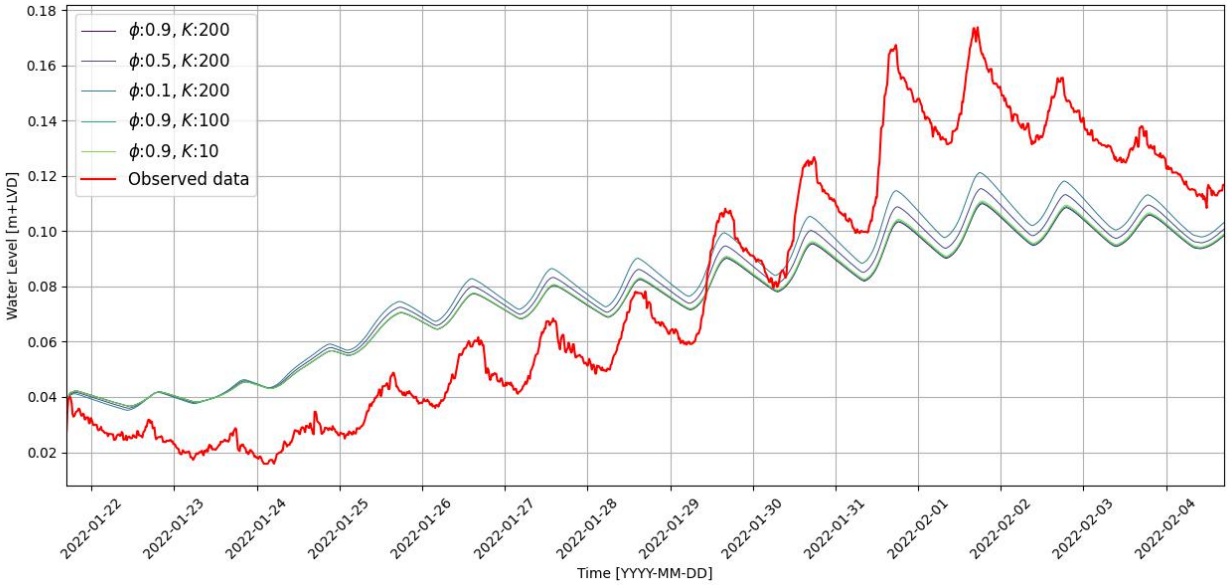

*Figure 6.4: Simulated water levels at Awa di Lodo for varying porosity (*0.9-0.1*) and hydraulic conductivity (*200-10 m/day*), with observations indicated in red.*

The poor performance of the model, particularly in the eastern creek, can be attributed to the porous layer effectively "blocking" the flow towards Awa di Lodo. This suggests that the layer height may be too high at that location, or the hydraulic conductivity is significantly underestimated. The uniform porous layer height of $0.40m$ used across all runs seems problematic, as it results in a root height of $0.035m$ LVD. Given that peak water levels during spring tide only slightly exceed $0.30m$ LVD, this setup may have unintentionally obstructed the tidal exchange between the bay and Awa di Lodo by raising the DEM too much.

Given these observations, it becomes clear that adjusting the porous layer height is a critical next step in the calibration process. The subsequent calibration efforts will focus on optimising this parameter, using the settings from the first simulation, marked green in Figure 6.4, as the baseline. These initial settings were chosen based on their representation of the study area and expert judgment.

As the height might influence the system too much, a second calibration run is performed by adjusting the height of the porous layer. For this run, constant values are chosen for porosity and hydraulic conductivity. The porosity is set to 0.9 and the hydraulic conductivity is maintained at $200m/day$. Table 6.5 lists the various porous layer heights tested in the left column.

Table 6.5: Calibration results comparing porous layer height values, showing NRMSE for different criteria. ***Bold values*** *indicate best performance per criterion; green indicates overall optimal porous layer height value.*

Porous Layer height, h_p $[m]$	**TR**	$A_{Duration}$	**HWL**	**LWL**	EC_{flood}	EC_{ebb}
0.20	0.59	0.51	0.43	0.41	**0.20**	**0.69**
0.25	**0.35**	**0.39**	**0.19**	**0.30**	**0.20**	2.94
0.40	1.54	0.67	0.41	0.36	2.46	4.43
0.60	1.62	0.74	0.46	0.40	5.01	4.73

Figure 6.5 shows the water level results at Awa di Lodo for different porous layer heights. The figure clearly demonstrates that the porous layer height significantly influences water levels. Lowering the height increases both the tidal range and absolute water levels. This occurs because a lower height presents less obstruction by the mangroves to water flow, allowing tidal exchange between the bay and Awa di Lodo at lower water levels.

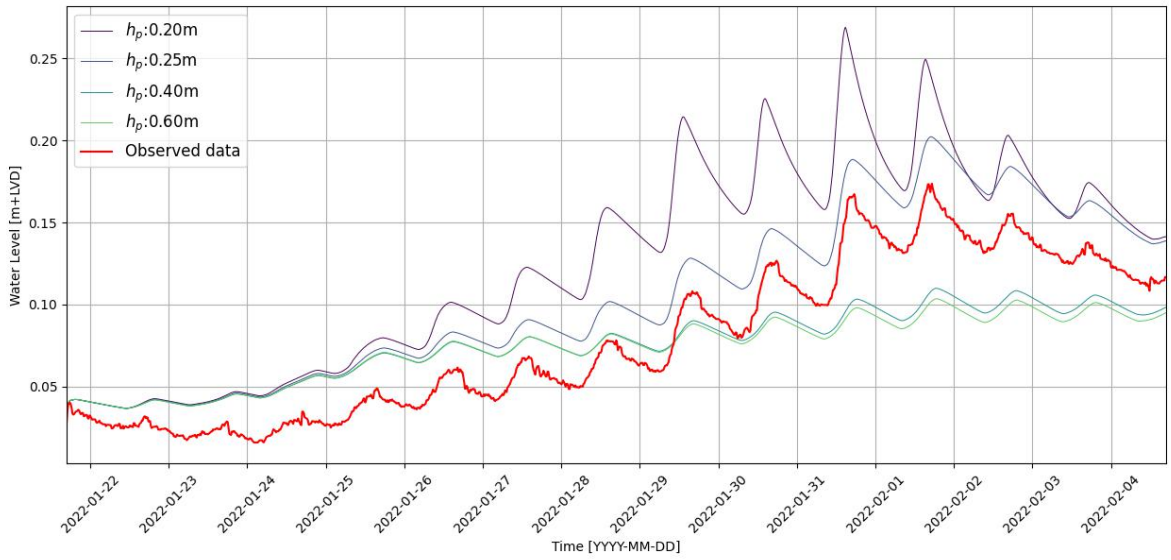

Figure 6.5: Simulated water levels at Awa di Lodo for varying porous layer height (0.20-0.60 m), with observations indicated in red.

Table 6.5 presents the criteria analysis results for this calibration phase.The simulation with a height of $0.25m$ shows behavior similar to the observations, albeit with a consistent upward shift above the measured water levels. This improved performance is particularly evident in the east creeks, where the lower porous layer height allows for better water flow, as reflected in the results.

The simulation with a porous layer height of $0.25m$ (marked in green) yields good results across most criteria, performing exceptionally well in terms of tidal range and tidal duration asymmetry. Based on these results, a porous layer height of $0.25m$ is selected for the validation phase.

6.4 Validation

To evaluate the performance of the three methods representing vegetation (roughness coefficient, Baptist method, and porous layer), their validation was tested on the performance criteria. The optimal parameter settings for each vegetation method, as determined during calibration, are presented in Table 6.6.

Table 6.6: Parameter values used for the three vegetation methods, which were obtained by the calibration.

Vegetation representation method	Parameters
Increased bed roughness	$C = 0.75m^{1/2}/s$
Baptist method	$C_D = 100$
Porous layer method	$\phi = 0.9$, $K = 200m/s$, $t = 0.25m$

Figure 6.6 illustrates the water level at the fringe for the validation period. A small shift in water levels between observations and simulations is evident during the first spring-neap cycle, with simulated levels consistently lower. This is reduced between the first and second spring-neap cycles, where simulations and observations align more closely. The observed shift may be due to the methodology used to obtain the boundary conditions (Section 5.3).

It is important to note that there is a gap in the observations between the first and second spring cycles, corresponding to a period when measurement equipment was changed. This gap has been excluded from the performance criteria calculations to ensure comparison only where observational data is available.

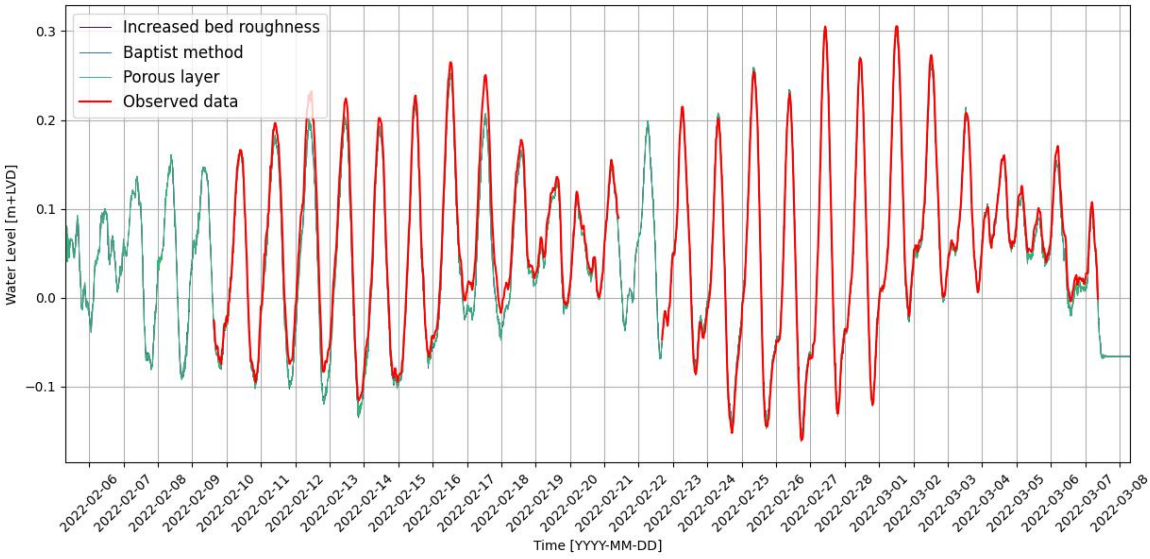

Figure 6.6: Water level at the west fringe (validation period) comparing three methods: increased bed roughness (purple), Baptist method (green), and porous layer (blue), with observations indicated in red.

Table 6.7 presents the results for the performance criteria across the three methods. The results are mixed, with no single method excelling in all criteria. Overall performance is lower than during the calibration phase.

*Table 6.7: Validation results comparing three vegetation methods, with **bold value** indicating best performance per criterion.*

Simulation method	TR	$A_{Duration}$	HWL	LWL	EC_{flood}	EC_{ebb}
Increased bed roughness	0.40	0.46	0.31	0.38	**0.40**	**0.74**
Baptist method	**0.37**	0.53	**0.27**	**0.34**	0.42	0.82
Porous layer	0.59	**0.43**	**0.27**	0.37	0.54	2.96

The Baptist method performs well in simulating water levels at Awa di Lodo and tidal range, suggesting that

it most accurately represents the volume of water reaching the back of the mangrove forest. The simulated vegetation resistance in this method allows an appropriate amount of water to reach Awa di Lodo while preserving the tidal signal entering the forest at the bay.

While the bottom roughness method yields the most accurate velocities through the east creek, it's important to note that the unrealistic Nikuradse height used in this method does not accurately model a realistic mangrove forest. The porous layer performs very bad in the east creek, especially during ebb, which might be due to the low water levels that are obstructed to flow back.

Interestingly, the porous layer method performs best in simulating tidal duration asymmetry, most closely matching the observed time between high and low water levels. A trade-off between accurate tidal range and duration asymmetry is evident across all methods, suggesting that improvements in one metric often come at the expense of the other.

Figure 6.7 compares the water levels at Awa di Lodo for all three methods. The roughness method consistently simulates higher water levels compared to the other methods, indicating insufficient resistance to water flow by vegetation. The porous layer and Baptist methods yield similar results in terms of water reaching Awa di Lodo. However, the porous layer's obstruction effect is evident during ebb periods, where water drains less easily back to the bay, resulting in a reduced tidal range. The Baptist method maintains a more visible tidal range throughout the simulation.

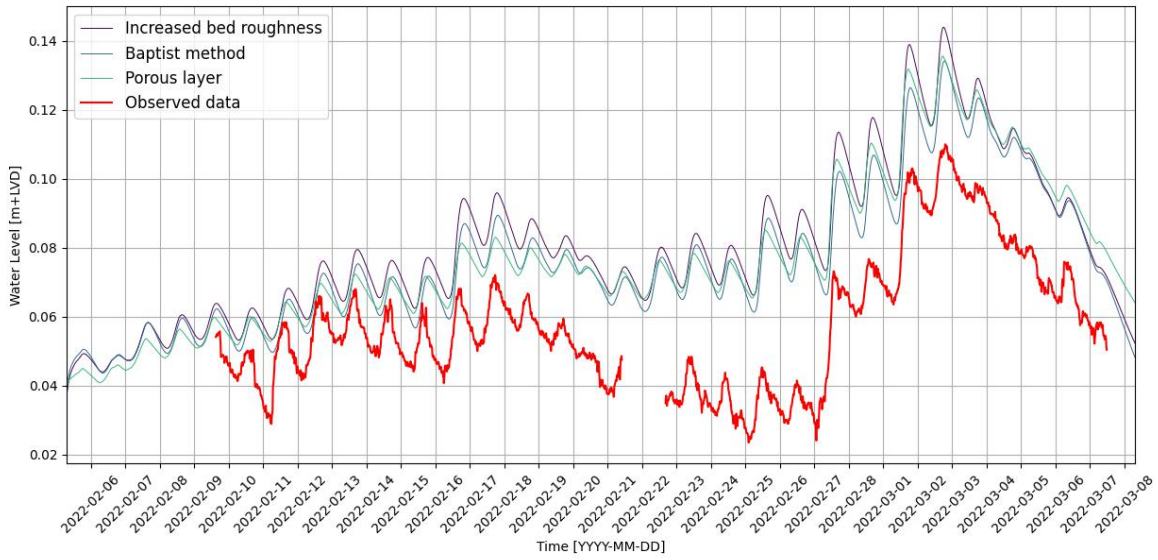

Figure 6.7: Water level at Awa di Lodo (vaidation period) comparing increased bed roughness (purple), Baptist method (blue), and porous layer (green), with observations in red.

All three methods exhibit a constant shift between simulated water levels and observations, particularly noticeable during low water levels in the second spring-neap cycle. This consistent discrepancy suggests that certain system dynamics are not fully captured by any of these methods individually.

Figure 6.8 illustrates velocities in the east creek. During flood periods in the second spring-neap cycle, all methods produce results similar to observations. However, discrepancies are evident during the first spring-neap cycle's flood period and throughout ebb periods. The porous layer method shows minimal water flow through the east creek, likely due to its obstruction effect. The roughness and Baptist methods simulate similar peak velocities during ebb, but these peaks are shorter in duration compared to observations. Observed ebb flows maintain high velocities for extended periods, an observation not replicated in the simulations. This suggests that all models underestimate water flow through the east creek compared to observations.

In conclusion, the validation results underscore the challenge of representing two distinct mangrove types (black and red mangroves) with a single vegetation method. The structural differences between these mangrove types, as evidenced by field observations and imagery (see Figure 4.3), are not adequately captured by any single method. The porous layer and Baptist methods each represent certain aspects of the different mangrove types

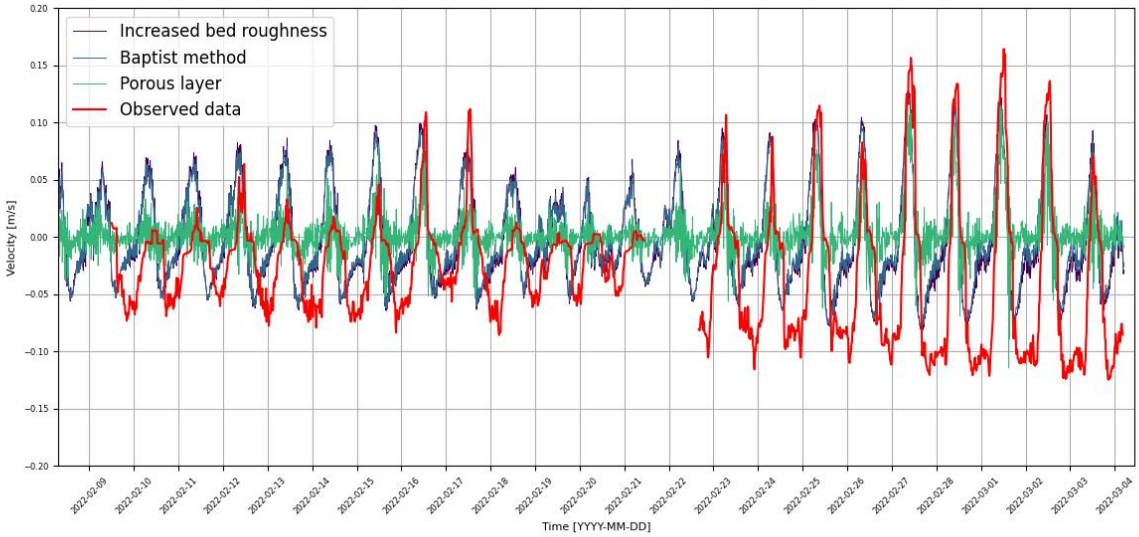

Figure 6.8: The flow velocities in the east creek during the validation period for all three individual methods. The observations are indicated with a red line.

more accurately, but neither fully captures the complexity of both types simultaneously. This limitation is rooted in the fundamental differences in mangrove characteristics and their interactions with hydrodynamics, as supported by both theoretical understanding and empirical observations.

7 Combination of methods: Hybrid model

7.1 Introduction

Previous chapter has demonstrated that applying a single method to model both mangrove types simultaneously fails to produce accurate simulations. This discrepancy arises from the distinct characteristics of the two mangrove species present in Lac Bay, as explained in Section 4. These differences suggest that each species may be more accurately represented by a different modelling approach. Drawing on insights from earlier research questions, a hybrid model is proposed that employs specific methods for each mangrove type. These methods will be calibrated independently by adjusting individual parameters or characteristics. This approach not only aims to improve model outcomes but also demonstrate the influence of each mangrove type and its corresponding modelling method on the simulated ecosystem.

Red mangroves in Lac Bay form a dense forest characterized by complex root structures (Figure 4.3). Their aerial roots, reaching heights up to $0.70m$, create an intricate, entangled network. Unlike straight, vertical roots, these follow curved, unpredictable pathways, often branching into multiple sub-roots. This complexity introduces significant uncertainties in predicting root distribution and growth patterns. Consequently, water flow through this dense, labyrinthine root system is likely to exhibit diffusive behavior. To account for these characteristics and inherent uncertainties, a porous layer approach presents the most realistic representation for modeling red mangroves.

In contrast, black mangroves are distinguished by their numerous pencil-like pneumatophores, which protrude vertically from the soil at the forest's edge (Figure 4.3). These roots exhibit a more uniform, structured arrangement compared to the intertwining roots of red mangroves. The Baptist method, which represents vegetation as straight, uniform structures, aligns well with the characteristics of black mangrove roots. Therefore, employing the Baptist method for black mangroves offers the most accurate representation within the model.

To initialise the hybrid model, the previously established individual settings for both the Baptist method and the porous layer approach will be used. The porous layer will be activated exclusively in areas dominated by red mangroves, while the Baptist method will be applied only to regions where black mangroves predominate. Initial values for key parameters - such as porous layer height, porosity, and drag coefficient - are derived from previous simulations. While these starting values may not be optimal, they provide a foundation for subsequent calibration and sensitivity analysis, allowing for refinement of the hybrid model's performance.

7.2 Calibration

To identify the key effects of different mangrove types on hydrodynamics, a separate calibration for the porous layer (representing red mangroves) and the Baptist method (representing black mangroves) is performed. It begins by analysing the Baptist method, focusing on adjustments to the drag coefficient and stem height. Table 7.1 presents the parameter values used and the resulting performance criteria.

Table 7.1: Calibration results for Baptist method varying drag coefficient and vegetation height. ***Bold values*** *indicate best performance per criterion; green shows optimal Baptist method settings.*

Vegetation height, h $[m]$	**Drag coefficient,** C_D $[-]$	**TR**	$A_{Duration}$	**HWL**	**LWL**	EC_{flood}	EC_{ebb}
0.15	50	0.56	0.52	0.35	**0.31**	0.47	0.49
0.15	100	0.50	**0.51**	0.33	**0.31**	0.42	0.42
0.15	200	0.43	**0.51**	**0.31**	**0.31**	**0.38**	0.35
0.15	300	**0.39**	**0.51**	**0.31**	**0.31**	0.60	**0.29**
0.20	100	0.49	**0.51**	0.33	0.31	0.42	0.42
0.25	100	0.48	**0.51**	0.33	0.31	0.42	0.42

The calibration results reveal that adjusting the stem height has minimal influence on the simulated mangrove ecosystem in Lac Bay. This limited sensitivity can be attributed to the local hydrodynamic conditions: in most areas where black mangroves grow, water levels exceeding $0.15m$ occur only during spring flood events. Consequently, modifications to the pneumatophore height have negligible effects on flow velocities through the vegetation under typical conditions.

The drag coefficient, while still having a relatively small impact, shows more noticeable effects on the model outcomes. Figure 7.1 illustrates the influence of varying drag coefficients on water levels at Awa di Lodo. The observed behavior is similar to that seen in the previous chapter's calibration of the Baptist method, albeit with reduced sensitivity due to the smaller area covered by black mangroves.

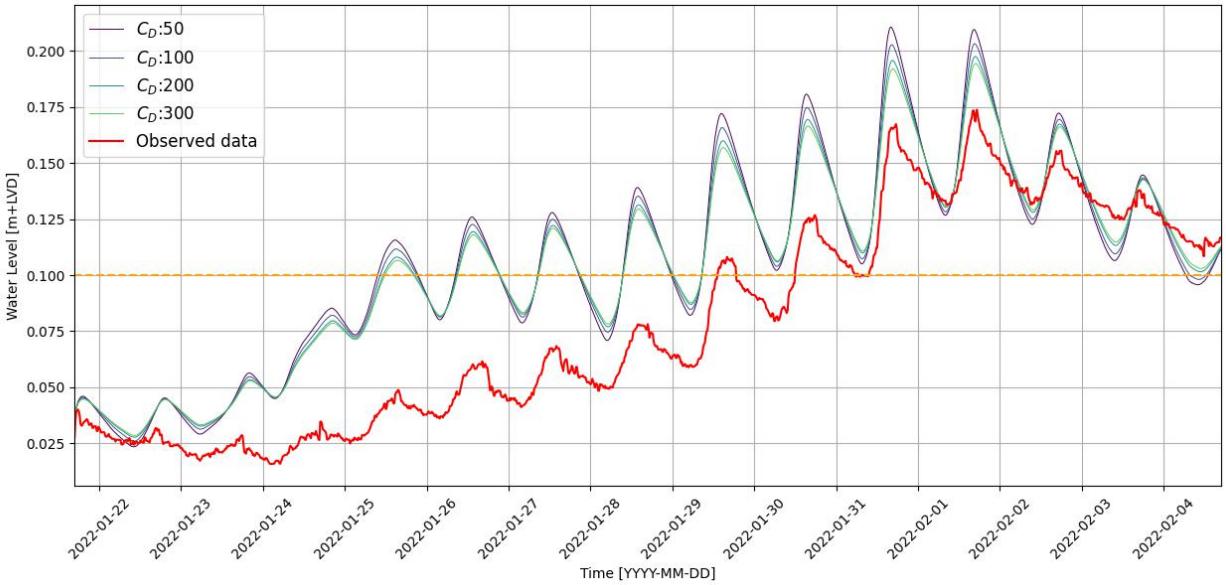

Figure 7.1: Water level at Awa di Lodo during calibration for drag coefficients (50-300), with observations in red and reference line in yellow

As the drag coefficient increases, a consistent trend is observed: both the HWL and the tidal range decrease. This relationship can be explained by the increased resistance to flow that higher drag coefficients represent. Specifically, a higher drag coefficient simulates greater interaction between the water and the vegetation, leading to increased energy dissipation and, consequently, reduced water levels and tidal ranges. It's important to note that while these changes affect the magnitude of water levels, they do not significantly alter the tidal wave's asymmetry. In the east creek, velocity performance criteria show more pronounced changes, with drag coefficients of 100 and 200 yielding the most accurate results. Detailed results for all simulations are provided in Appendix I.

The relatively high optimal drag coefficient (100) suggests that our initial measurements may have underestimated the hydraulic resistance of the black mangrove areas. This could be due to several factors. Some pneumatophores may have been missed during field measurements, or the spatial extent of black mangroves might be greater than initially mapped. Additionally, the high drag coefficient may be compensating for small-scale bathymetric features not captured in the model's resolution. Other sources of hydraulic resistance, such as leaf litter or sediment characteristics, may also be implicitly represented by the increased drag coefficient.

Given these considerations and the minimal impact of stem height adjustments, it has been decided to proceed with the initial stem height value of $0.15m$ and a drag coefficient of 100 for black mangroves. This choice balances the need to represent observed hydrodynamics accurately while acknowledging the uncertainties in our vegetation and bathymetry data.

The calibration of the porous layer representing red mangroves involved adjusting two key parameters: the height of the porous layer and the creek delineation height where red mangroves cover both sides of the creek. Notably, these adjustments did not alter the DEM but instead expanded the area where mangroves grow and where the porous layer is applied.

The modification of the creek delineation height stems from the assumption that vegetation growth into the creeks reduces their effective width. By applying this adjustment specifically to red mangroves, the complete blocking of the connection between the fringe and Awa di Lodo was avoided. In previous simulations, the creek delineation height was set at $-0.20m$ LVD. For the calibration, the creek delineation height was lowered to

$-0.30m$ LVD, reducing the effective creek width. Table 7.2 presents the parameters used in the calibration and the resulting performance criteria.

Table 7.2: Calibration results for porous layer method varying height and effective creek width. ***Bold values*** *indicate best performance per criterion; green shows optimal porous layer settings.*

Creek delineation height, z_{creek} $[m\ LVD]$	**Porous layer height,** t $[m]$	**TR**	$\boldsymbol{A_{Duration}}$	**HWL**	**LWL**	$\boldsymbol{EC_{flood}}$	$\boldsymbol{EC_{ebb}}$
-0.20	0.25	0.50	0.51	0.33	0.31	0.42	0.42
-0.20	0.30	0.39	0.55	0.29	0.32	0.44	0.37
-0.20	0.40	0.36	0.58	0.29	0.35	0.48	0.34
-0.30	0.25	0.20	**0.46**	0.27	0.32	**0.30**	**0.17**
-0.30	0.30	**0.18**	0.47	**0.23**	**0.31**	**0.30**	0.28
-0.30	0.35	0.33	0.49	0.24	0.32	**0.30**	0.33

The reduction of the effective creek width significantly impacts the tidal range. By increasing the overall resistance of the mangroves to the tidal wave, the tidal range decreases. This effect occurs because a narrower creek allows less water to pass through, altering the tidal signal. Interestingly, the tidal asymmetry remains largely unaffected by these changes.

Figure 7.2 shows the impact of varying porous layer heights with a creek delineation height of $-0.2m$ LVD. The primary effects are observed during high water levels of the spring-neap cycle. As the porous layer height increases, the mangrove forest acts as a higher obstacle, blocking even higher water levels.

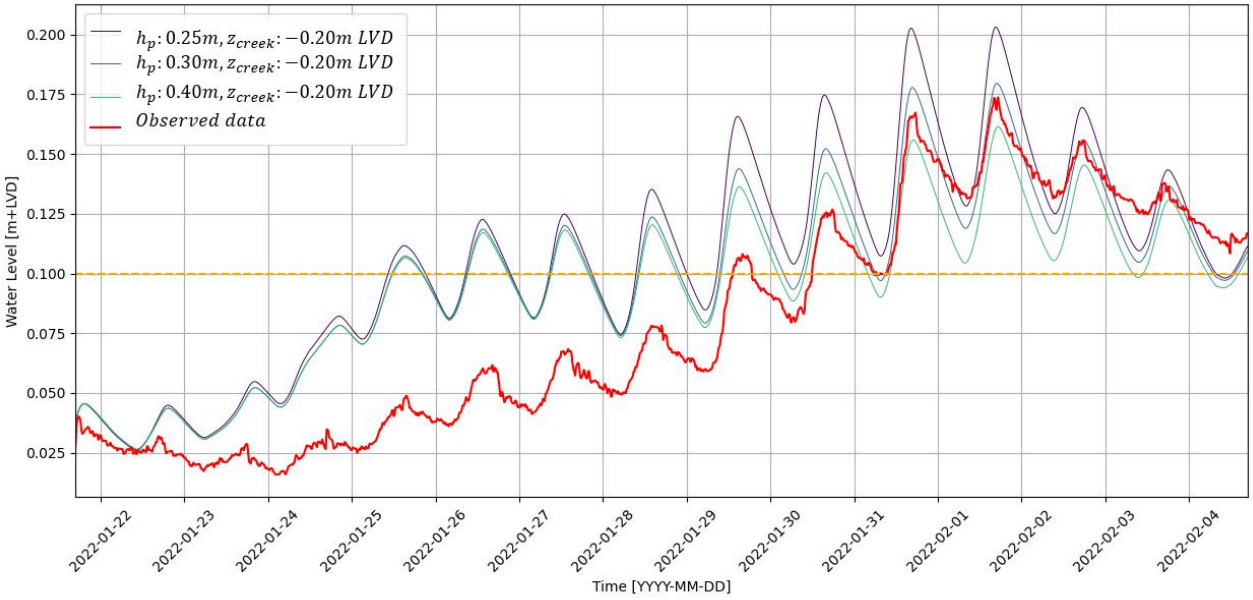

Figure 7.2: Water level at Awa di Lodo with red mangrove distribution at $z_{creek} = -0.20m$ *LVD, showing porous layer heights of* $0.25m$ *(purple),* $0.30m$ *(blue), and* $0.40m$ *(green). Observations in red; reference line in yellow.*

Figure 7.3 shows similar effects but with a creek delineation height of $-0.30m$ LVD. In this scenario, changes are most pronounced at the beginning of the spring-neap cycle. The yellow reference line in both figures helps visualise these differences. In Figure 7.2 the water levels between 25.01.2022 until 29.01.2022 are above the yellow line and show only a little increase. In Figure 7.3 the water level starts below the yellow line and an actual change in water level at Awa di Lodo can be seen, which the observations also show. Notably, all simulations with a creek delineation height of $-0.30m$ LVD exhibit an improved tidal range.

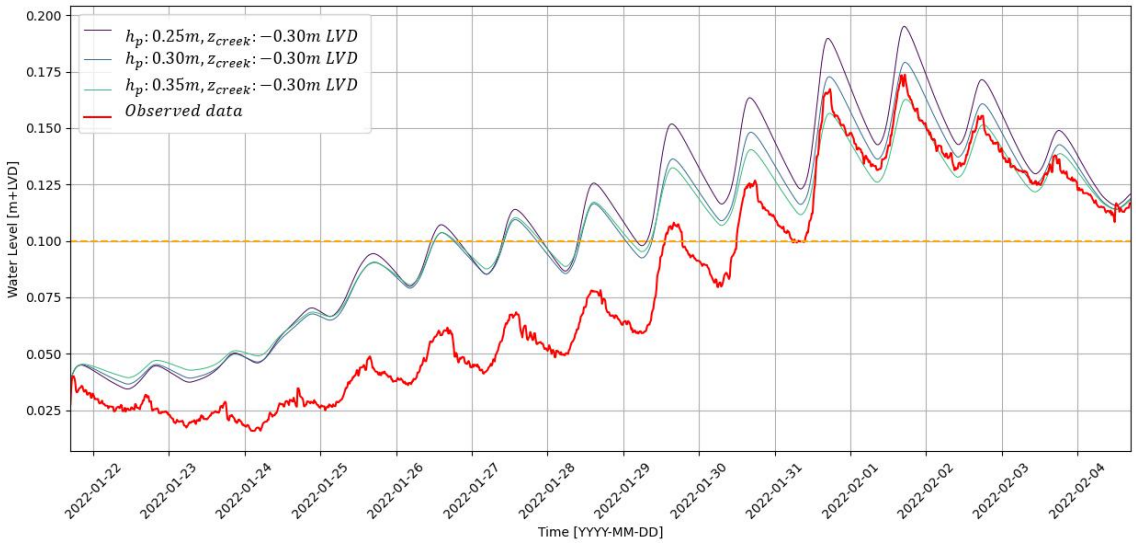

Figure 7.3: Water level at Awa di Lodo with red mangrove distribution at $z_{creek} = -0.30m$ LVD, showing porous layer heights of $0.25m$ (purple), $0.30m$ (blue), and $0.35m$ (green). Observations in red; reference line in yellow.

The calibration results for flow velocities within the east creek are presented in Figure 7.4. Adjusting the creek delineation height to $-0.30m$ LVD significantly influences creek flow. A wider effective creek results in higher velocities, while a narrower effective creek reduces flow velocities. The impact is more pronounced in the east creek due to its location deeper in the forest and its shallower depth. The ideal effective creek width likely lies between the $-0.20m$ LVD and $-0.30m$ LVD dependencies. However, all simulations struggle to accurately represent observed velocities during low water levels at neap tide.

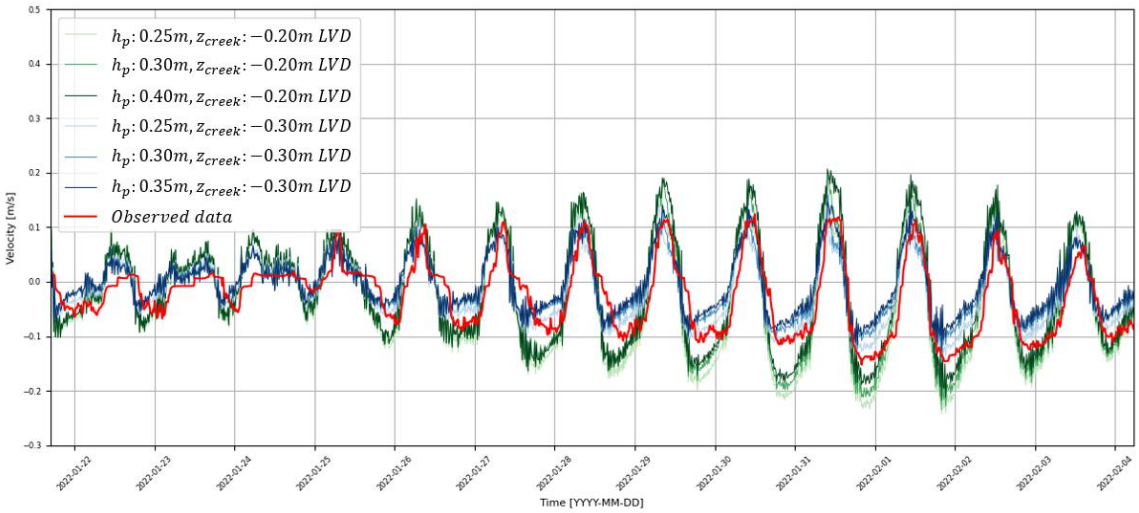

Figure 7.4: East creek velocities during porous layer calibration: $z_{creek} = -0.20m$ LVD (green) and $z_{creek} = -0.30m$ LVD (blue), with observations in red.

Based on these calibration results, the optimal parameters for the hybrid model are selected. For the red mangroves, a porous layer height of $0.30m$ and a creek delineation height of $-0.30m$ LVD. For the black mangroves, the previously calibrated values are used: a drag coefficient of 100 and a vegetation height of $0.15m$ for the Baptist method.

This calibration process highlights the complex interactions between mangrove forests and hydrodynamics in Lac Bay. The adjustments to the porous layer and creek delineation height allow for a more nuanced representation of the red mangrove areas, capturing their impact on water levels and flow velocities throughout the spring-neap cycle.

7.3 Validation

The finalised parameters from the calibration process were applied to the validation dataset to compare the performance of the hybrid model against individual methods. Table 7.3 presents the outcomes, including results from individual vegetation representation methods for comparison. The hybrid model demonstrates significant improvement, particularly in simulating the tidal range, which indicates a more accurate representation of water volume flowing through the forest to the back of the system.

*Table 7.3: Comparison of individual methods (black, **bold** indicating best performance) and hybrid model results (green).*

Simulation method	TR	$A_{Duration}$	HWL	LWL	EC_{flood}	EC_{ebb}
Increasing bed roughness	0.40	0.46	0.31	0.38	**0.40**	**0.74**
Baptist	**0.37**	0.53	**0.27**	**0.34**	0.42	0.82
porous layer	0.59	**0.43**	**0.27**	0.37	0.54	2.96
Hybrid	0.30	0.41	0.29	0.35	0.43	0.51

While the hybrid model does not consistently outperform individual methods in all criteria such as water levels and velocities, it exhibits superior overall performance. Notably, the hybrid model shows marked improvement in crucial aspects that indicate the accuracy of water exchange between the bay and Awa di Lodo, specifically the water flow through creeks and the forest.

Figure 7.5 shows the water level at Awa di Lodo during the validation period, comparing the hybrid model with individual methods. The hybrid model demonstrates good performance in simulating peak water levels while maintaining an accurate tidal range that closely matches observations. In contrast, individual methods would likely require simulating higher resistance to approach the peak HWLs during spring tide, which would consequently reduce the tidal range and deviate from observations.

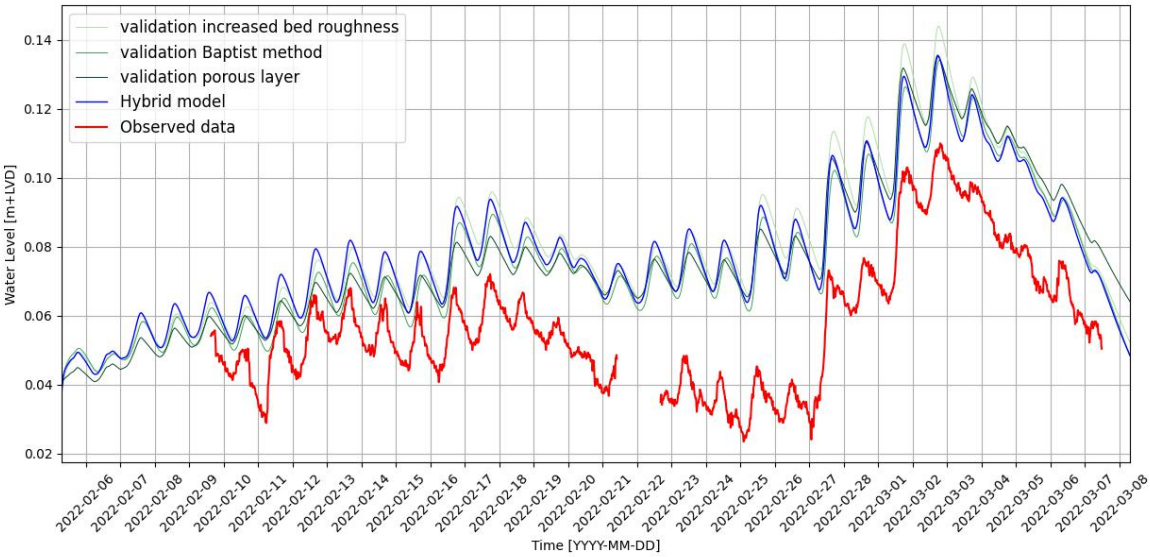

Figure 7.5: Water level at Awa di Lodo (validation) comparing individual methods (green) and the hybrid model (blue), with observations in red.

The hybrid model shows particularly good agreement with observations towards the end of the second spring-neap cycle of the validation data, accurately capturing the rapid lowering of water levels. However, both the

hybrid model and individual models exhibit a consistent shift from observations during very low water levels at neap tide, suggesting a systematic discrepancy in this regime. This was also something noted by van Zee (2022). This persistent shift suggests that a key factor influencing the system is not being accounted for. Given that the tidal range in the hybrid model aligns reasonably well with observations, the cause of this discrepancy likely stems from another process affecting water levels. Results for water levels at the fringe, presented in Appendix J, show good agreement with observations.

Figure 7.6 presents the velocities in the east creek during the validation period. The hybrid model shows good agreement with observations for peak velocities during flood conditions. However, some deviations occur during ebb, particularly in the second spring-neap cycle. The model slightly under-predicts maximum flow velocities and simulates shorter periods of peak flow compared to observations. Notably, the observed velocity during ebb remains almost constant throughout the entire ebb phase, a characteristic not replicated in the simulations.

These discrepancies in velocity predictions may be attributed to the calibration process prioritising accurate representation of the behavior at Awa di Lodo. The focus on calibrating water levels can potentially lead to greater inaccuracies in flow velocities. This trade-off highlights the complex nature of hydrodynamic modelling in mangrove ecosystems and the challenges in simultaneously optimising all aspects of the model.

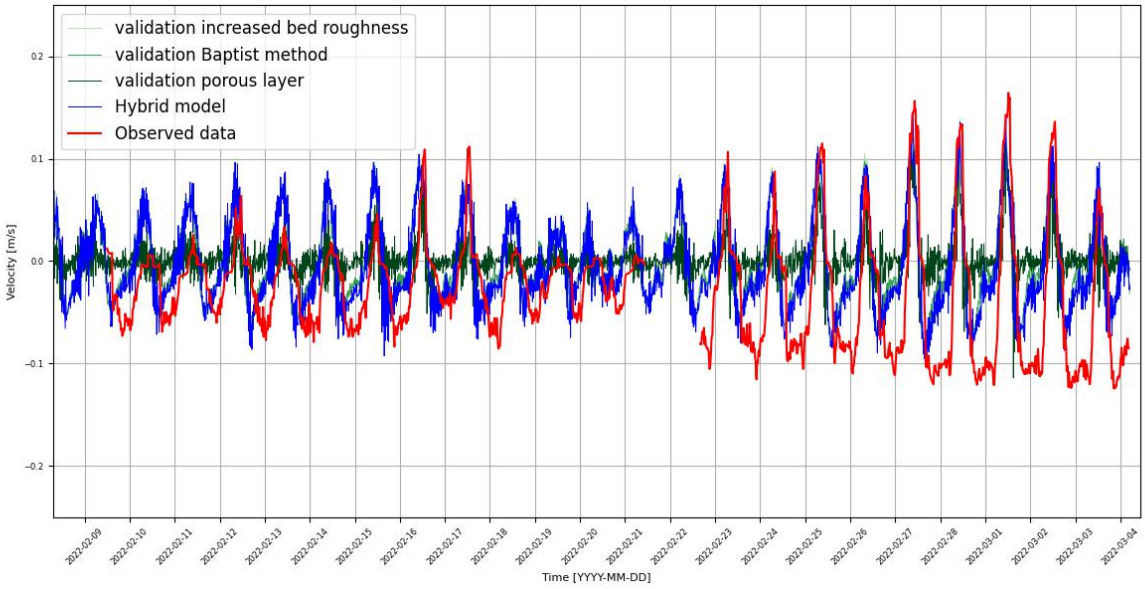

Figure 7.6: East creek velocities during the validation period comparing the individual methods (green) with the hybrid model (blue), with observations in red.

The validation results demonstrate that the hybrid model provides a more comprehensive and accurate representation of the hydrodynamics in Lac Bay's mangrove ecosystem compared to individual methods. While some discrepancies persist, particularly in the tidal range and ebb flow velocities, the hybrid model successfully captures key hydrodynamic features and improves upon the performance of single-method approaches. These findings underscore the potential of hybrid modelling techniques in complex coastal environments and provide a foundation for further refinement of mangrove ecosystem simulations.

8 Discussion

8.1 Measurement and Flow Pattern Uncertainties

Challenges in Data Collection
Data collection in the complex mangrove forest environment presented significant limitations for accurate hydrodynamic modelling, essentially creating a black box situation. The sparse measurement network, with only one measurement point at the entrance of the east creek before the islands and three cross-sectional profiles, restricted the ability to capture the system's tidal dynamics. The dense mangrove vegetation severely limited accessibility for direct elevation measurements. This resulted in a simplified DEM based on interpolation and generalised creek cross-sections, particularly affecting the accuracy in shallow water regions where minor elevation changes can substantially alter flow patterns. Additionally, the vegetation data used do not account for died-off areas, which still create resistance to water flow. This missing resistance, combined with the measurement limitations, introduces considerable uncertainty in the model's representation of water movement through the system.

Inconsistencies in Observational Data
The limited availability of velocity measurements for different mangrove types further compounds these inconsistencies. The calibration process employed identical parameters for both black and red mangroves, effectively averaging their hydrodynamic characteristics. This homogenisation undermines the ability to differentiate the distinct effects of each mangrove type on tidal dynamics, complicating model calibration and validation. The absence of specific velocity measurements within the forest for either mangrove type inhibited the exploration of alternative methodologies to capture these differences.

In conclusion, the various challenges encountered during data collection, coupled with inconsistencies in observational data and uncertainties in model parameters, underscore the complexities of accurately modelling hydrodynamic behaviour in mangrove ecosystems. Future research efforts should focus on enhancing data collection methods, improving DEM accuracy, and addressing the specific hydrodynamic characteristics of different mangrove types to facilitate more precise model calibration and validation.

8.2 Model Development and Methodological Choices

Subgrid Modelling Approach
The complexities of modelling mangrove forests, particularly in regions such as Lac Bay where distinct species such as red (*Rhizophora mangle*) and black (*Avicennia germinans*) mangroves coexist, need a careful approach to model. The subgrid modelling approach employed in this research enhances the ability to represent detailed vegetation characteristics at the same resolution as the DEM. This method allows for a more nuanced spatial distribution of mangrove structures, particularly along creek systems and at forest edges. However, this approach presents both benefits and challenges. A notable advantage is the capability to incorporate a high level of detail without significantly increasing computational time. This is particularly beneficial in creeks, where larger computational cells can obscure flow velocity representation.

Vegetation Representation Methods
The use of the Baptist method enabled a detailed implementation of vegetation characteristics. When mangrove trees exhibit different traits, these can be easily defined on the subgrid scale. However, a more challenging aspect was the implementation of the porous layer. This layer maintains a consistent height throughout the entire model domain and cannot be adjusted based on local variations within the study area. Consequently, an average height must be applied, which may be suitable for smaller areas or uniform mangrove types. However, as the area increases, the height may vary significantly, thereby increasing the uncertainty associated with this method.

During the individual implementation of the porous layer in 3Di in Section 6.3, both mangrove types were assigned the same porosity, as the solid volume fraction was nearly identical for both. However, the height of the porous layer was determined as the average height of the roots between the two mangrove types. It was later recognised that adjusting the porosity in relation to the layer height might yield a more realistic representation. For instance, black mangroves, having shorter roots and not covering the area above, would have higher porosity, thereby increasing the total percentage of void space. In contrast, red mangroves, which have higher roots than the porous layer, would have a lower porosity. Although this adjustment would have offered a more accurate implementation, results indicated that varying the porosity had minimal impact on the

water level at Awa di Lodo. This suggests that the changes in porosity likely have a negligible effect on the overall outcomes of the model.

DEM and Vegetation Distribution
The hydrodynamic modelling of Lac Bay faced challenges in accurately representing vegetation distribution along creeks. Initial assumptions of vegetation-free creek channels proved incorrect, as mangroves were observed overhanging banks. The DEM became crucial for estimating vegetation-affected areas, with a threshold-based classification system depending on the elevation. However, this elevation-based approach proved problematic, as mangroves often grow directly into creeks, indicating elevation alone cannot reliably predict vegetation presence.

The concept of an "effective" creek area—where no vegetation grows—was introduced for more accurate modelling. Inconsistencies in tree coverage suggested DEM variations at lower elevations, further complicating vegetation mapping. While the current elevation-based method remains the best available approach given data constraints, it introduces considerable uncertainty. Future research should focus on obtaining precise above-water measurements of creek widths and vegetation presence to enhance model accuracy and better represent real-world conditions.

Hybrid Modelling Approach To further enhance model accuracy, a hybrid modelling approach was adopted, combining the strengths of the porous layer and Baptist methods. The reasons for combining different methods stemmed from the need to accurately represent the distinct hydrodynamic characteristics of red and black mangroves. The choice for assigning a certain method to a certain mangrove type was based on the assumed behaviour of the flow. Because red mangroves have dense, interlocking root networks with roots growing in all directions bringing large uncertainties in the layer, the porous layer was best fitting to it. Unlike red mangroves, black mangroves possess pneumatophores-thin, vertical aerial roots that are less effective at obstructing water flow (Mullarney & Henderson, 2018). These roots are in a similar set-up as the Baptist method uses, which is why it is applied to black mangroves.

8.3 Model Sensitivities and Parameter Impacts

Mangrove Properties and Hydrodynamic Effects
The sensitivity of vegetation parameters, such as height and drag coefficient, emphasises the distinctions between these mangrove types. The height of the porous layer is critical, as it determines the water level needed for tidal waves to flow over the dense root structures of red mangroves. When the tidal wave remains below this height, water predominantly flows through the creeks, bypassing the roots. Conversely, black mangroves, which occupy areas farther back in the forest and cover about 30% of the region, exhibit lower spatial coverage and less dense root structures, consisting of pneumatophores that are less effective at obstructing water flow. As a result, changes in vegetation height for black mangroves had minimal impact on hydrodynamic conditions, largely due to the consistently low water levels in these areas.

Creek Width Sensitivity
Creek width sensitivity emerged as a critical factor in modelling hydrodynamics. Reducing the effective creek width, based on the creek delineation height, significantly influenced hydrodynamic behaviour, particularly affecting water levels at Awa di Lodo and the overall tidal range. As the modelled creek width narrowed, the volume of water flowing through the creeks decreased, leading to lower water levels due to reduced exchange efficiency.

The challenges in accurately representing creek overgrowth are important. The mangrove trees often overhang the creek banks, complicating the determination of the effective creek width. While a narrower creek width visibly impacts water levels, it does not significantly alter flow velocities measured in the middle of the creeks, likely because those points are closer to open water compared to more isolated backwater regions. Capturing the dynamics of creek vegetation, particularly in a complex environment like Lac Bay, is essential for improving model accuracy.

Calibration Sensitivities
To compare simulation results with observations of tidal dynamics within mangrove forests, the NRMSE was employed. This metric measures how far the simulations deviate from actual observations, with values closer to zero indicating better model performance. However, it was often difficult to interpret whether the result is too high or too low because the NRMSE provides only a relative measure of error without context. This absence of

directional information complicates the calibration process. When adjusting parameters, it becomes difficult to determine the appropriate course of action, whether to increase or decrease a particular parameter. Specifically, if two parameter values produced the same NRMSE, significant insights could be overlooked. For instance, if one parameter consistently resulted in flow values that were too high, while another produced values that were too low, the NRMSE would suggest equivalent performance, hindering further investigation. To enhance clarity, introducing a second criterion that indicates the direction of change in hydrodynamic behavior might be beneficial, allowing for more informed parameter adjustments.

Furthermore, the limitations of using averaged parameters for different mangrove types became evident during the calibration procedure. Parameters were adjusted uniformly for both red and black mangroves, resulting in a composite value that averaged their unique hydrodynamic characteristics. This averaging was particularly noticed, as the initial parameter values derived from individual models failed to accurately simulate tidal dynamics in the hybrid model. The absence of velocity measurements specifically for either mangrove type hindered the differentiation of their distinct hydrodynamic effects. Consequently, exploring alternative methodologies to account for these differences was impractical within the scope of this research for the individual methods.

The hybrid modelling approach, despite its complexities, provides a clearer understanding of the specific influences each mangrove type exerts on hydrodynamics. By linking changes in parameters to distinct vegetation types, the model enhances insights into the intricate interactions within the mangrove ecosystem. This nuanced understanding is crucial for advancing future modelling efforts in similar coastal environments.

8.4 Addressing Model-Observation Discrepancies

Evaporation Effects
In the high-temperature and windy environment of Lac Bay, evaporation could have a significant impact on water levels. To explore this, an evaporation term was introduced into the model, represented as an outflow. This term removes water from the system at a specific rate, with the value used in simulations based on the average daily evaporation, calculated from annual evaporation data.

Figure 8.1 shows the validation period with the hybrid model with ($6mm/day$) and without the evaporation. As it is a constant value added to the simulation, the whole simulation shifts downward, closer to the observations at Awa di Lodo. It has only minor influences on the velocities, which can be seen in Appendix K.

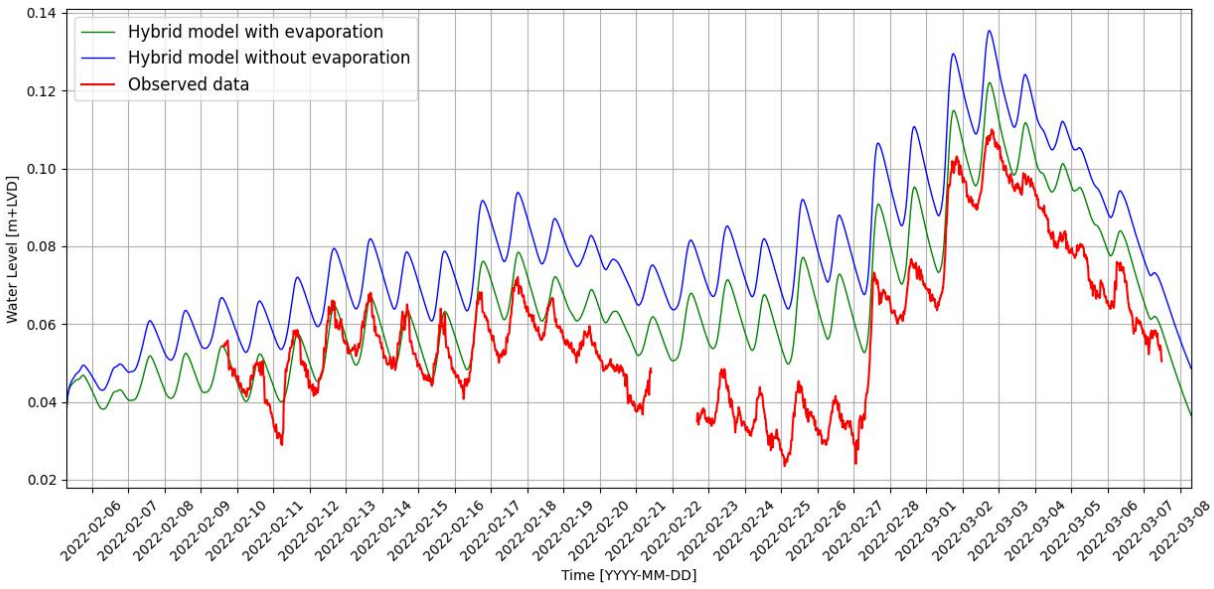

Figure 8.1: Water level at Awa di Lodo during the validation period with evaporation (green) and without evaporation (blue). Observations are indicated with a red line.

The results based on inclusion of the evaporation term showed a notable improvement in the model's performance, suggesting that evaporation may indeed be a key factor behind the observed over-prediction in water levels. This points not only to the importance of incorporating evaporation into the model but also indicates that other physical processes, beyond tidal dynamics, are contributing to the system's behaviour.

Although this provides a baseline, in reality, evaporation is a highly seasonal factor that can fluctuate depending on variables such as sun exposure, wind strength, and salinity levels. These dynamic conditions can influence the overall water balance in the system. Monitoring evaporation rates more closely during future measurements will therefore be essential, not only for improving model accuracy but also for understanding its broader impact on the local ecosystem. By incorporating more precise, seasonal evaporation data, the model's overall predictive capabilities are enhanced.

9 Conclusion and Recommendations

9.1 Conclusion

This study investigated the hydrodynamic forcings, spatial extent and flow characteristics of Lac Bay's tidal creeks and mangrove forest, emphasising the intricate interactions within this ecosystem. Lac Bay exhibits complex tidal dynamics, particularly within the mangrove forest, where tidal wave amplitudes of nearly$0.40m$ during spring tides at the forest fringe are significantly reduced to just a few centimetres at Awa di Lodo, Awa di Lodo, due to dense mangrove vegetation. The system shows notable variability between spring-neap cycles, with the first and third cycles showing tidal ranges of around $0.45m$, while the second cycle only reached about $0.32m$, indicating influences beyond typical tidal forcing, such as meteorological or longer-term oceanographic phenomena. The bathymetry and vegetation characteristics create distinct flow patterns, where the mangroves significantly alter flow timing, creating a 4-5 hour tidal peak lag between Cai and Awa di Lodo. Several uncertainties persist in understanding the complete system dynamics, including questionable west creek measurements, limited data within the forest itself creating a significant knowledge gap about internal forest dynamics, and other aspects such as creek geometry and vegetation density. These insights highlight both the critical role of mangrove forests in modulating water flow and tidal exchange, while also emphasising the need for more comprehensive monitoring to fully understand this complex ecosystem.

To achieve an optimal balance between computational efficiency and accuracy in modelling the hydrodynamics of Lac Bay, a variable-resolution computational grid was implemented on a high resolution DEM. The sensitivity analysis demonstrated that larger grid cells ($\Delta x = 160m$) were sufficient for the bay area, where water levels showed minimal variations between different grid sizes due to uniform hydrodynamic conditions. However, within the mangrove forest, particularly around the islands, finer grid resolution ($\Delta x = 10m$) was essential to prevent leaking cells and accurately capture complex bathymetry. The creeks obtained a finer resolution ($\Delta x = 5m$) to accurately simulate flow velocities within their narrow channels and facilitate easier post-processing of the results. A gradual transition between different grid sizes was implemented using intermediate cell sizes ($\Delta x = 80m$ and $\Delta x = 40m$) to ensure computational stability. This optimised grid design achieved a computational time of 75 minutes for a simulation run, successfully balancing the need for accurate representation of small-scale hydrodynamic processes with computational efficiency.

A key insight from this study is that no single method adequately captures the complex hydrodynamics of mangrove forests. The Chézy roughness method produced unrealistic values, failing to represent key dynamics. The porous layer approach primarily influenced signal asymmetry but did not effectively reproduce tidal amplitude variations, which were largely controlled by the Baptist method. Moreover, applying the same calibration method to both red and black mangroves led to averaged calibrations that could not account for the distinct hydrodynamic properties of each species. This averaging reduced the model's ability to realistically simulate species-specific interactions with water flow, highlighting the limitations of individual methods to model hydrodynamics in diverse mangrove ecosystems.

The hybrid model demonstrates that combining distinct modelling approaches for different mangrove species yields more accurate hydrodynamic simulations in Lac Bay than a single-method approach, confirming that the unique physical characteristics of red and black mangroves require specialised modelling strategies. Calibration revealed that for black mangroves, modelled using the Baptist method, stem height adjustments had minimal impact due to local hydrodynamic conditions, while the drag coefficient showed modest effects with an optimal value of 100, suggesting possible underestimation of initial hydraulic resistance measurements. In contrast, red mangrove parameters, modelled using a porous layer approach, significantly influenced tidal dynamics when adjusting both porous layer height and creek delineation height (from $-0.20m$ to $-0.30m$ LVD). Validation results confirm the hybrid model's superior overall performance compared to individual methods, particularly in simulating tidal range and water exchange between the bay and Awa di Lodo. While the model excels at simulating peak water levels while maintaining accurate tidal ranges, some systematic discrepancies persist during neap tide low water levels, and flow velocity predictions, though accurate during flood conditions, show deviations during ebb phases. These results demonstrate that a species-specific hybrid approach better captures the complex hydrodynamics of mixed mangrove forests, though further refinement may be needed to address specific condition discrepancies.

Additionally, all models revealed discrepancies between predicted and observed results, especially during neap tides. Water levels and velocities were more accurately predicted during HWLs than during LWLs, indicating

that some physical processes, such as evaporation, might not be fully accounted for in the models. Furthermore, the effective width of creeks played a crucial role in controlling water flow, underscoring the importance of accurate vegetation representation around the creeks.

In conclusion, this research demonstrates the necessity of a detailed, multi-method approach to improve our understanding of mangrove hydrodynamics, especially in environments such as Lac Bay. The use of a hybrid model, along with species-specific calibrations, enhances accuracy significantly. Although certain processes during neap tides remain unclear, this study lays a robust foundation for future research.

9.2 Recommendations

One of the most significant gaps in the current understanding is the effect of evaporation across the study area. Given the promising results of initial studies, measuring evaporation during the next field campaign is vital. Continuous and precise evaporation measurements across the entire area will help to refine the hydrological balance and improve the accuracy of future models. The implementation of evaporation in the model needs proper development to accurately represent this physical process, ensuring that the measured data can be effectively utilised in future simulations.

A crucial aspect for future research is investigating the mangrove distribution and creek system characteristics in the back forest area, particularly around the depressions connecting to Awa di Lodo. Special attention should be given to measuring and analysing the effective creek width and its variation throughout the system. Understanding how the creek width changes from the entrance to the back of the forest will provide valuable insights into the system's hydraulic behavior and its interaction with mangrove growth patterns. This knowledge will improve the representation of creek geometry in future modelling efforts.

To ensure a more comprehensive understanding of the tidal dynamics in Lac Bay, future measurement campaigns should prioritise several key observational efforts. A critical aspect is improving flow velocity measurements within the creek system by establishing multiple measurement locations to gain deeper insight into spatial variations of tidal wave propagation. Adding a measurement point behind the islands is essential to better understand their blocking effect on the tidal wave, particularly during low water levels. Additionally, installing measurement instruments within the forest interior, despite its density, will provide valuable data on how the forest impacts flow patterns and tidal movement, improving the application of vegetation methods.

The simulation methods used in this research deserve further investigation, particularly regarding the promising results of hybrid models. Validation through studies in other mangrove ecosystems would be valuable, especially concerning the effectiveness of Baptist's method for black mangroves and the porous layer for red mangroves. Additional research should focus on understanding the effects of porosity and hydraulic conductivity, as their impact was relatively minor in this study. A dedicated study area with red mangroves, including detailed characteristic measurements and porous layer analysis, would provide crucial insights into the application and effectiveness of the porous layer method.

The DEM requires significant improvement, particularly with the new AHN (Actueel Hoogtebestand Nederland) dataset potentially enhancing the accuracy of boundary areas above water level. Key improvements should include detailed creek bathymetry measurements instead of using one general cross-section for the entire creek system. Additionally, higher resolution measurements around islands and along boundaries will allow for more accurate representation of the topography and hydrodynamics within these complex environments.

References

Adame, M. F., Connolly, R. M., Turschwell, M. P., Lovelock, C. E., Fatoyinbo, T., Lagomasino, D., Goldberg, L. A., Holdorf, J., Friess, D. A., Sasmito, S. D., Sanderman, J., Sievers, M., Buelow, C., Kauffman, J. B., Bryan-Brown, D., & Brown, C. J. (2021). Future carbon emissions from global mangrove forest loss. *Global Change Biology*, *27*(12), 2856–2866. https://doi.org/https://doi.org/10.1111/gcb.15571

Alongi, D. M. (2008). Mangrove forests: Resilience, protection from tsunamis, and responses to global climate change. *Estuarine, Coastal and Shelf Science*, *76*(1), 1–13. https://doi.org/https://doi.org/10.1016/j.ecss.2007.08.024

Alongi, D. M. (2015). The impact of climate change on mangrove forests. *Current Climate Change Reports*, *1*. https://doi.org/10.1007/s40641-015-0002-x

Andersson, E. (2007). https://www.flickr.com/photos/tanukikun/1425469489

Asari, N., Suratman, M. N., Ayob, N., & Hamid, N. (2021, October). Mangrove as a natural barrier to environmental risks and coastal protection. https://doi.org/10.1007/978-981-16-2494-0_13

Augustijn, D., Huthoff, F., & van Velzen, E. (2008). Comparison of vegetation roughness descriptions. *Water Engineering & Management*. https://ris.utwente.nl/ws/portalfiles/portal/5373465/Augustijn08comparison.pdf

Baltus, O. (2022). *Representing spatially variable bathymetry and vegetation in a hydrodynamic model: A subgrid-based case study in the whitianga estuary, new zealand* [Master's thesis, University of Twente]. https://www.utwente.nl/en/et/cem/research/wem/education/msc-thesis/2022/baltus.pdf

Baptist, M., Babovic, V., Uthurburu, J. R., Keijzer, M., Uittenbogaard, R., Mynett, A., & Verwey, A. (2007). On inducing equations for vegetation resistance. *Journal of Hydraulic Research*, *45*(4), 435–450. https://doi.org/10.1080/00221686.2007.9521778

Barnes, E. (2022). Mangroves as a solution to climate crisis. https://www.worldwildlife.org/stories/mangroves-as-a-solution-to-the-climate-crisis

Bosboom, J., & Stive, M. J. (2021, January). *Coastal dynamics*. TU Delft Open. https://doi.org/10.5074/T.2021.001

Breda, A., Saco, P. M., Sandi, S. G., Saintilan, N., Riccardi, G., & Rodríguez, J. F. (2021). Accretion, retreat and transgression of coastal wetlands experiencing sea-level rise. *Hydrology and Earth System Sciences*, *25*(2), 769–786. https://doi.org/10.5194/hess-25-769-2021

Casal, G., Trégarot, E., Cornet, C. C., McCarthy, T., & van der Geest, M. (2024). A cost-effective method to map mangrove forest extent, composition, and condition in small islands based on sentinel-2 data: Implications for management. *Ecological Indicators*, *159*, 111696. https://doi.org/https://doi.org/10.1016/j.ecolind.2024.111696

Casulli, V. (2009). A high-resolution wetting and drying algorithm for free-surface hydrodynamics. *International Journal for Numerical Methods in Fluids*, *60*(4), 391–408. https://doi.org/https://doi.org/10.1002/fld.1896

Casulli, V., & Stelling, G. S. (2011). Semi-implicit subgrid modelling of three-dimensional free-surface flows. *International Journal for Numerical Methods in Fluids*, *67*(4), 441–449. https://doi.org/https://doi.org/10.1002/fld.2361

Cheng, H., Wang, Y.-S., Fei, J., Jiang, Z.-Y., & Ye, Z.-H. (2015). Differences in root aeration, iron plaque formation and waterlogging tolerance in six mangroves along a continues tidal gradient. *Ecotoxicology*, *24*. https://doi.org/https://doi.org/10.1007/s10646-015-1474-0

Chow, V. (1959). *Open-channel hydraulics*. McGraw-Hill.

Cooper, C. (2022). Mangrove forest loss is slowing toward a halt, new report shows. *Mongabay*. https://news.mongabay.com/2022/11/mangrove-forest-loss-is-slowing-toward-a-halt-new-report-shows/

de Vos, W.-J. (2004). Wave attenuation in mangrove wetlands. red river delta, vietnam. https://repository.tudelft.nl/islandora/object/uuid:4d8f93b5-8efa-4663-a29a-448a50c45525?collection=education

Debrot, A., Meesters, E., Leon, & Slijkerman, D. M. (2010). Lac bonaire - restoration action spear points, september 2010. https://edepot.wur.nl/155336

docs, 3. (2024a). 2d interflow [3Di documentation site for the implementation of the 2D Interflow layer]. https://docs.3di.live/h_interflow.html

docs, 3. (2024b). Problem solving - limitations to model size [3Di documentation site for limitations to model size]. https://docs.3di.live/f_problem_solving.html

Furukawa, K., & Wolanski, E. (1996). Sedimentation in mangrove forests. *Mangroves and Salt Marshes*, *1*. https://doi.org/https://doi.org/10.1023/A:1025973426404

Gijon Mancheno, A., Jansen, W., Winterwerp, J. C., & Uijttewaal, W. S. J. (2021). Predictive model of bulk drag coefficient for a nature-based structure exposed to currents. *Scientific Reports*, *11*. https://doi.org/10.1038/s41598-021-83035-0

Gijsman, R., Horstman, E., van der Wal, D., Friess, D., Swales, A., & Wijnberg, K. (2021). Nature-based engineering: A review on reducing coastal flood risk with mangroves. *Frontiers in Marine Science*, *8*. https://doi.org/10.3389/fmars.2021.702412

Gijsman, R., Engel, S., van der Wal, D., van Zee, R., Johnson, J., van der Geest, M., Wijnberg, K., & Horstman, E. (2024, October). *Field measurement data of hydrodynamic and morphological processes in the mangrove forest of Lac Bay, Bonaire, Caribbean Netherlands*. Zenodo. https://doi.org/10.5281/zenodo.13904523

Gijsman, R., Horstman, E., Swales, A., MacDonald, I. T., Bouma, T. J., van der Wal, D., & Wijnberg, K. M. (2023). Mangrove forest drag and bed stabilisation effects on intertidal flat morphology. *Earth Surface Processes and Landforms*, *49*(3), 1117–1134. https://doi.org/https://doi.org/10.1002/esp.5758

Google Earth. (2023). https://earth.google.com/web/search/Bonaire/@12.19442666,-68.26400061,61.09841882a,75733.79753846d,35y,0h,0t,0r/data=CigiJgokCS8Ksvx5WjNAES0Ksvx5WjPAGZASxiekJUFAIfqaFkeWhFDAOgMK

Hanipah, A., Guo, Z., & Zahran, E. (2018). Hydrodynamics modelling of a river with mangrove forests, 14 (4 pp.)–14 (4 pp.) https://doi.org/10.1049/cp.2018.1511

Haughey, R. R. (2017). Modelling the hydrodynamics within the mangrove tidal flats in the firth of thames. https://hdl.handle.net/10289/11129

Hoff, R., Hensel, P., Proffitt, E., Delgado, P., Shigenaka, G., Yender, R., & Mearns, A. (2010). Oil spills in mangroves: Planning response considerations. https://doi.org/10.13140/2.1.3588.5765

Horstman, E., Bryan, K. R., & Mullarney, J. C. (2021). Drag variations, tidal asymmetry and tidal range changes in a mangrove creek system. *Earth Surface Processes and Landforms*, *46*(9), 1828–1846. https://doi.org/https://doi.org/10.1002/esp.5124

Horstman, E., Dohmen-Janssen, C. M., & Hulscher, S. J. (2013). Flow routing in mangrove forests: A field study in trang province, thailand. *Continental Shelf Research*, *71*, 52–67. https://doi.org/https://doi.org/10.1016/j.csr.2013.10.002

Horstman, E., Dohmen-Janssen, C., Bouma, T., & Hulscher, S. (2015). Tidal-scale flow routing and sedimentation in mangrove forests: Combining field data and numerical modelling. *Geomorphology*, *228*, 244–262. https://doi.org/https://doi.org/10.1016/j.geomorph.2014.08.011

Hu, K., Chen, Q., Wang, H., Hartig, E. K., & Orton, P. M. (2018). Numerical modeling of salt marsh morphological change induced by hurricane sandy. *Coastal Engineering*, *132*, 63–81. https://doi.org/https://doi.org/10.1016/j.coastaleng.2017.11.001

Järvelä, J. (2002). Flow resistance of flexible and stiff vegetation: A flume study with natural plants. *Journal of Hydrology*, *269*(1), 44–54. https://doi.org/https://doi.org/10.1016/S0022-1694(02)00193-2

Jennerjahn, T. C., Gilman, E., Krauss, K. W., Lacerda, L. D., Nordhaus, I., & Wolanski, E. (2017). Mangrove ecosystems under climate change. In V. H. Rivera-Monroy, S. Y. Lee, E. Kristensen, & R. R. Twilley (Eds.), *Mangrove ecosystems: A global biogeographic perspective: Structure, function, and services* (pp. 211–244). Springer International Publishing. https://doi.org/10.1007/978-3-319-62206-4_7

Kandasamy, K. (2021, October). Mangroves: Types and importance. https://doi.org/10.1007/978-981-16-2494-0_1

Krauss, K., Allen, J., & Cahoon, D. (2003). Differential rates of vertical accretion and elevation change among aerial root types in micronesian mangrove forests. *Estuarine, Coastal and Shelf Science*, *56*(2), 251–259. https://doi.org/https://doi.org/10.1016/S0272-7714(02)00184-1

Larsen, L. G. (2019). Multiscale flow-vegetation-sediment feedbacks in low-gradient landscapes. *Geomorphology*, *334*, 165–193. https://doi.org/https://doi.org/10.1016/j.geomorph.2019.03.009

Lee, S. (2009). Tropical mangrove ecology: Physical and biotic factors influencing ecosystem structure and function. *Australian Journal of Ecology*, *24*, 355–366. https://doi.org/10.1046/j.1442-9993.1999.00984.x

List, R. (2024). The list of wetlands of international importance [List of ramsar site published in september 2024]. https://www.ramsar.org/sites/default/files/2023-08/sitelist.pdf

Lott, C. E. (2001). Lac bay: Then and now... https://www.dcbd.nl/document/lac-bay-then-and-now%E2%80%A6-historical-interpretation-environmental-change-during-1900s-site

Lucas, R., Lule, A. V., Rodríguez, M. T., Kamal, M., Thomas, N., Asbridge, E., & Kuenzer, C. (2017). Spatial ecology of mangrove forests: A remote sensing perspective. In V. H. Rivera-Monroy, S. Y. Lee, E. Kristensen, & R. R. Twilley (Eds.), *Mangrove ecosystems: A global biogeographic perspective: Structure, function, and services* (pp. 87–112). Springer International Publishing. https://doi.org/10.1007/978-3-319-62206-4_4

Marek, P. (2024). http://www.mangrove.at/mangrove_roots.html

Mazda, Y., Kanazawa, N., & Wolanski, E. (1995). Tidal asymmetry in mangrove creeks. *Hydrobiologia*, *295*. https://doi.org/https://doi.org/10.1007/BF00029110

Mazda, Y., Kobashi, D., & Okada, S. (2005). Tidal-scale hydrodynamics within mangrove swamps. *Wetlands Ecology and Management*, *13*. https://doi.org/https://doi.org/10.1007/s11273-005-0613-4

Mazda, Y., Magi, M., Ikeda, Y., Kurokawa, T., & Asano, T. (2006). Wave reduction in a mangrove forest dominated by sonneratia sp. *Wetlands Ecology and Management*, *14*. https://doi.org/10.1007/s11273-005-5388-0

Mazda, Y., Wolanski, E., King, B., Sase, A., Ohtsuka, D., & Magi, M. (1997). Drag force due to vegetation in mangrove swamps. *Mangroves and Salt Marshes*. https://doi.org/https://doi.org/10.1023/A:1009949411068

Menéndez, P., Losada, I. J., Beck, M. W., Torres-Ortega, S., Espejo, A., Narayan, S., Díaz-Simal, P., & Lange, G.-M. (2018). Valuing the protection services of mangroves at national scale: The philippines. *Ecosystem Services*, *34*, 24–36. https://doi.org/https://doi.org/10.1016/j.ecoser.2018.09.005

Merzdorf, J. (2020). Nasa study maps the roots of global mangrove loss. https://climate.nasa.gov/news/3009/nasa-study-maps-the-roots-of-global-mangrove-loss/

Mullarney, J. C., & Henderson, S. M. (2018). Flows within marine vegetation canopies. In *Advances in coastal hydraulics* (pp. 1–46). World Scientific. https://doi.org/10.1142/9789813231283_0001

Nepf, H. M. (2012). Flow and transport in regions with aquatic vegetation. *Annual Review of Fluid Mechanics*, *44*(Volume 44, 2012), 123–142. https://doi.org/https://doi.org/10.1146/annurev-fluid-120710-101048

Norris, B. K., Mullarney, J. C., Bryan, K. R., & Henderson, S. M. (2017). The effect of pneumatophore density on turbulence: A field study in a sonneratia-dominated mangrove forest, vietnam [Sediment- and hydro-dynamics of the Mekong Delta: from tidal river to continental shelf]. *Continental Shelf Research*, *147*, 114–127. https://doi.org/https://doi.org/10.1016/j.csr.2017.06.002

Popescu, I. (2014). Computational hydraulics - numerical methods and modelling. IWA Publishing. https://doi.org/https://doi.org/10.2166/9781780400457

Smulders, F., Vonk, J., Engel, M. S., & Christianen, M. (2017). Expansion and fragment settlement of the non-native seagrass halophila stipulacea in a caribbean bay. *Marine Biology Research*, *13*, 1–8. https://doi.org/10.1080/17451000.2017.1333620

Stark, J., Van Oyen, T., Meire, P., & Temmerman, S. (2015). Observations of tidal and storm surge attenuation in a large tidal marsh. *Limnology and Oceanography*, *60*(4), 1371–1381. https://doi.org/https://doi.org/10.1002/lno.10104

Stevens, M. (2019). https://www.flickr.com/photos/matthewstevens/49067853958

Tusinski, A., & Verhagen, H. (2014). The use of mangroves in coastal protection. *Coastal Engineering Proceedings*, *1*, 45. https://doi.org/10.9753/icce.v34.management.45

van der Meulen, R. (2023). Salinity and sediment issues in the backwaters of mangrove forests measuring of the sediment depths and electrical conductivity in the mangrove forests of lac bay , bonaire. *BSc Thesis*. https://www.dcbd.nl/sites/default/files/documents/Thesis_BIL_Rik_vd_Meulen.pdf

Van Moorsel, G., & Meijer, M. (1993). Base-line ecological study van het lac op bonaire. https://www.researchgate.net/publication/328007211_Base-line_ecological_study_van_het_Lac_op_Bonaire

Van Santen, P., Augustinus, P., Janssen-Stelder, B., Quartel, S., & Tri, N. (2007). Sedimentation in an estuarine mangrove system [Morphodynamics of the Red River Delta, Vietnam]. *Journal of Asian Earth Sciences*, *29*(4), 566–575. https://doi.org/https://doi.org/10.1016/j.jseaes.2006.05.011

van Zee, R. (2022, July). *The role of creeks for tidal exchange in the mangrove forest of lac bay, bonaire* [Master's thesis, University of Twente]. http://essay.utwente.nl/92109/

Versteeg, H., & Malalasekera, W. (2007). An introduction to computational fluid dynamics. Pearson Education Limited. https://www.researchgate.net/profile/Ghassan-Smaisim/post/FEM_mesh_generator/attachment/59d655b479197b80779acc78/AS%3A526908706508800%401502636233004/download/110+Versteeg+2007+an+introduction+to+computational+fluid+dynamics+the+finite+volume+method+2nd+edition.pdf

Volp, N. D., van Prooijen, B. C., & Stelling, G. S. (2013). A finite volume approach for shallow water flow accounting for high-resolution bathymetry and roughness data. *Water Resources Research*, *49*(7), 4126–4135. https://doi.org/https://doi.org/10.1002/wrcr.20324

Wamsley, T. V., Cialone, M. A., Smith, J. M., Atkinson, J. H., & Rosati, J. D. (2010). The potential of wetlands in reducing storm surge [A Forensic Analysis of Hurricane Katrina's Impact: Methods and Findings]. *Ocean Engineering*, *37*(1), 59–68. https://doi.org/https://doi.org/10.1016/j.oceaneng.2009.07.018

Wang, Y., Yin, Z., & Liu, Y. (2022). Experimental investigation of wave attenuation and bulk drag coefficient in mangrove forest with complex root morphology. *Applied Ocean Research*, *118*, 102974. https://doi.org/https://doi.org/10.1016/j.apor.2021.102974

Zhang, K., Liu, H., Li, Y., Xu, H., Shen, J., Rhome, J., & Smith, T. J. (2012). The role of mangroves in attenuating storm surges. *Estuarine, Coastal and Shelf Science*, *102-103*, 11–23. https://doi.org/https://doi.org/10.1016/j.ecss.2012.02.021

Appendix

A Vegetation data measurement

Below in Table A.1 the measured characteristics can be seen. A total of 14 locations were visited and measured. To obtain the average values for the red and black mangroves, the locations which were covered 100% by a certain type were used. Figure A.1 shows the locations for the different measurement locations.

Table A.1: The measured vegetation data by the field research of Gijsman et al. (2024)

Plot nr	Presence of *Rhizophora*?	Presence of *Avicennia*?	Root density $[m^{-2}]$	Root height $[m]$	Root diameter $[m]$	solid volume fraction $[-]$	Frontal area density $[m^{-1}]$
1	Yes	Yes	86	0.159	0.006	0.002	0.516
2	No	Yes	525	0.144	0.008	0.026	4.2
3	Yes	No	19	0.606	0.030	0.013	0.57
4	Yes	Yes	134	0.177	0.004	0.002	0.536
5	No	Yes	168	0.080	0.003	0.001	0.504
6	Yes	No	51	0.637	0.021	0.018	1.071
7	Yes	No	77	0.573	0.032	0.062	2.464
8	Yes	No	63	1.039	0.010	0.005	0.63
9	No	Yes	590	0.129	0.011	0.056	6.49
10	No	Yes	422	0.196	0.006	0.012	2.532
11	Yes	No	90	0.519	0.024	0.041	2.16
12	Yes	No	119	1.320	0.031	0.090	3.689
13	Yes	No	43	0.560	0.022	0.016	0.946
14	Yes	No	55	0.520	0.021	0.019	1.155

Figure A.1: Locations of the vegetation measurement plots (van Zee, 2022)

B 1D boundary settings

In Table B.1 the settings for the 1D boundary conditions are shown. The 1D boundary condition is connected via a channel to a manhole in the computational cell. The channel settings are shown in Table B.2. The channel length is not very important in this case, because the changes in water levels are minor. The width and the height need to be the same size as the computational grid. The settings for the manholes are shown in Table B.3. Via the manholes the information from the 1D boundary conditions is given to the 2D environment.

Table B.1: The setings used in the 1D boundary conditions in 3Di.

Parameter	**Value**
boundary_type	water level
input	timeseries

Table B.2: The channel settings for connecting the 1D boundary conditions with the manholes in 3Di.

Parameter	**Value**
Calculation type	Isolated
Channel length $[m]$	160
Node initial water level $[m]$	0.00
Node storage area $[m^2]$	0.00
Reference level $[m]$	-20.0
Width $[m]$	160
Height $[m]$	160

Table B.3: The manhole settings that give the 1D boundary condition information to the 2D environment in 3Di.

Parameter	**Value**
Calculation type	Embedded
Bottom level $[m]$	-20.0
Surface level $[m]$	-20.0
Drain level $[m]$	-20.0
Width $[m]$	160
Length $[m]$	160

C Raw data-files for the DEM

Figure C.1 shows the two raw data sets for the entire study area. On the left are the elevation data points obtained from Delft3D. The right side shows the elevation data points obtained from Gijsman et al. (2024). To give a better view of the detail of both raw data files, a close-up is made from a creek section, which is shown in Figure C.2. The raw data obtained from Gijsman et al. (2024) has much more detail on the elevation compared to the Delft3D data. This is also the reason why the data obtained from Gijsman et al. (2024) is used for the areas where the bathymetry changes a lot. For the other areas the elevation points from Delft3D are used to fill up the gaps in the raw data from Gijsman et al. (2024).

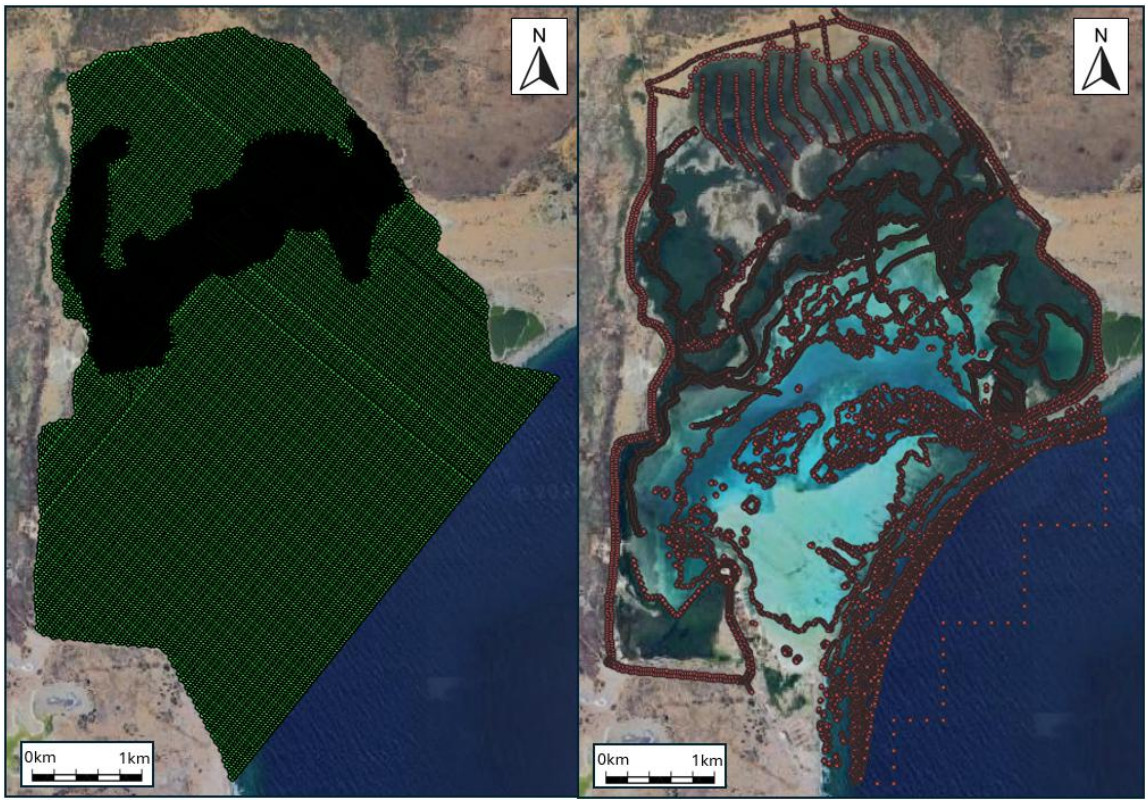

Figure C.1: The raw data obtained from Delft3D (left) and measurements from Gijsman et al. (2024) (right

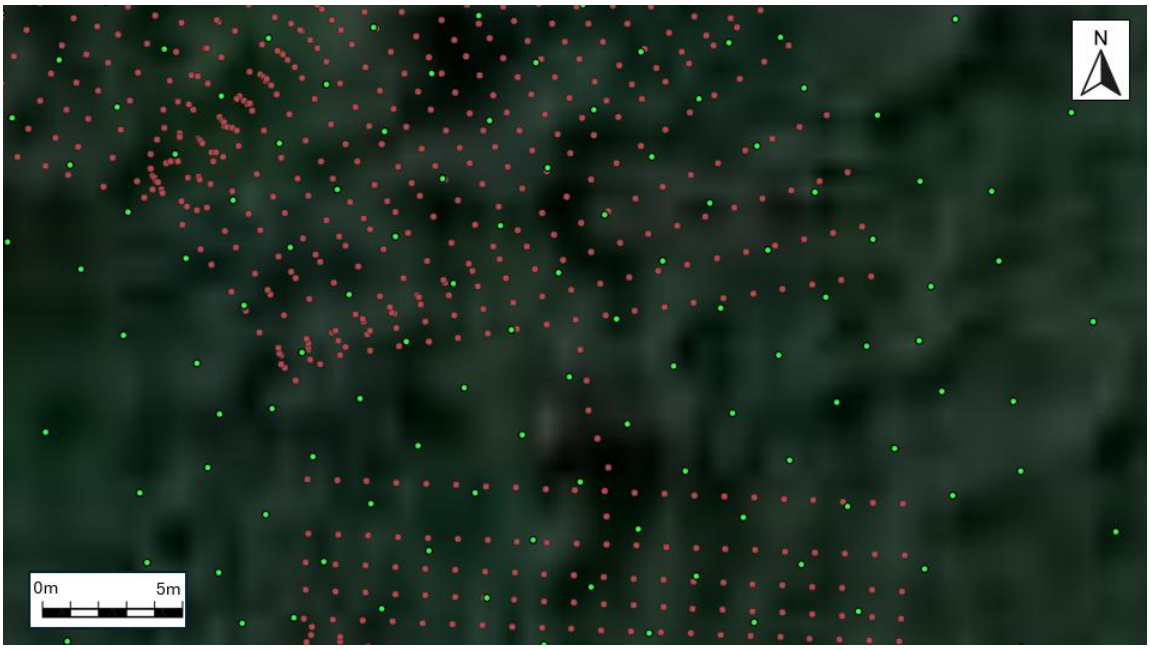

Figure C.2: A close-up of the raw data on a creek location.

D Initial Water Level

Figure D.1 shows the initial water level raster used in all simulations. An interpolation is used within the forest to get a linear relation between Awa di Lodo and the fringe. A value of $0.035m$ LVD is used at Awa di Lodo (white) and a value of $0.119m$ LVD is used at the bay area (dark blue).

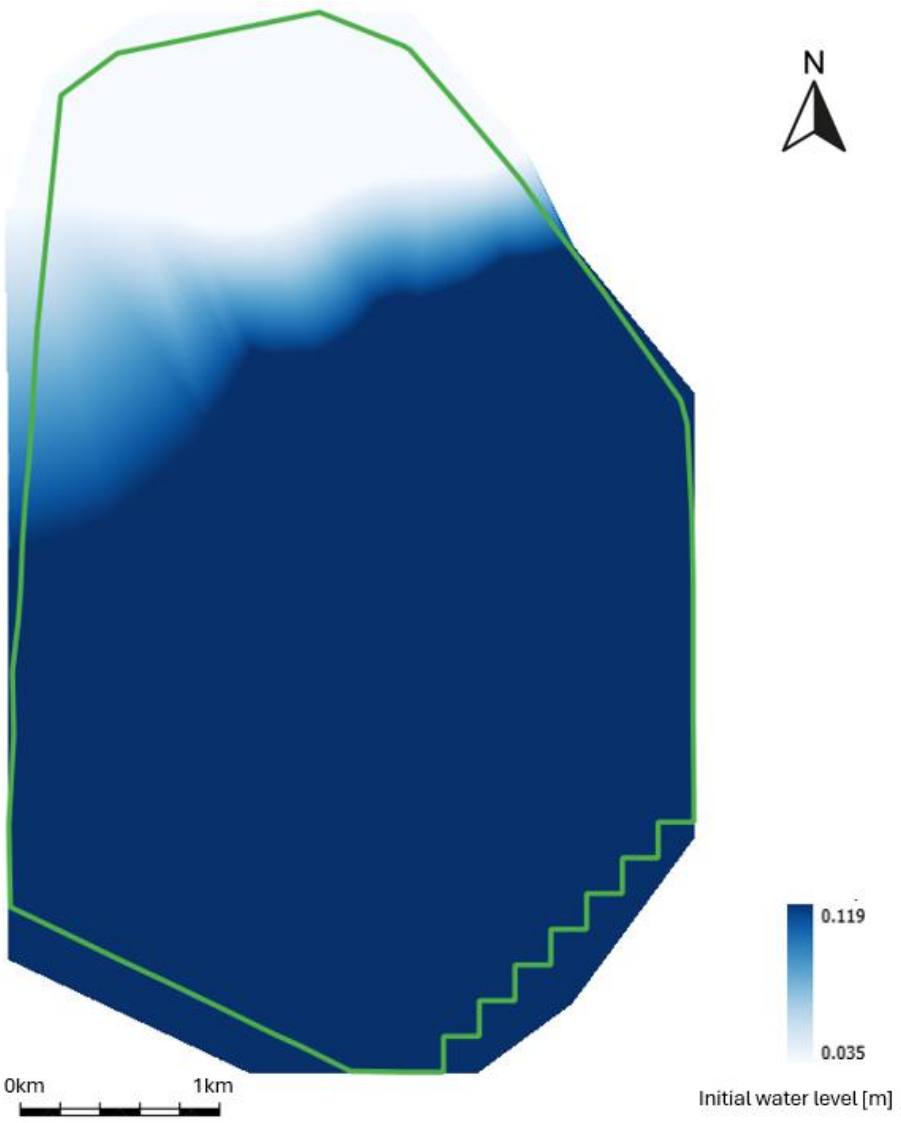

Figure D.1: Initial water level raster used within 3Di.

E Grid refinement sensitivity analysis

Three different areas have been chosen to be analysed for the grid refinement: The whole forest (area between the bay and Awa di Lodo), the creeks and the islands. It is assumed that the most important areas where complex physical processes will happen are within the forest. The creek and islands are important to analyse due to the change in bathymetry and the connection with the forest. To compare the performance, the water level at Awa di Lodo will be compared. Lower water levels simulate more resistance due to the bathymetry, which is an important aspect of the system. The grid refinement will be between the resolution of $\Delta x = 40m$ and $\Delta x = 5m$.

Figure E.1 shows the change in water level at the back of Awa di Lodo between the period of 27th of January until 31st of January, when applying grid refinement within the forest. A shorter period is chosen, because the

differences are small and are better visualised. These simulations are used to be able to compare them with the creek and islands areas.

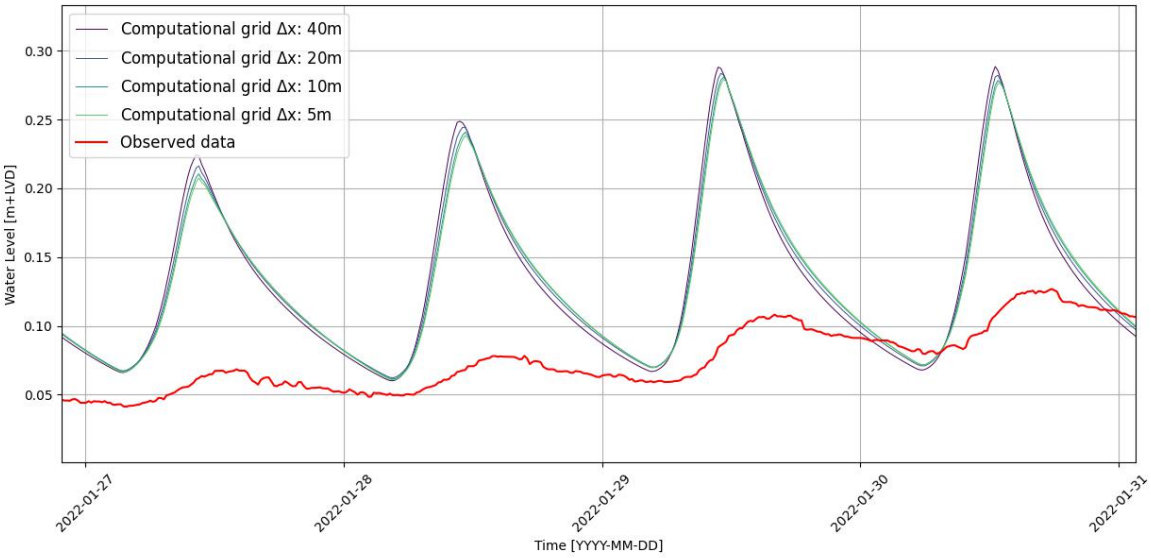

Figure E.1: Water level at Awa di Lodo for the grid refinement sensitivity analysis around the forests. Grid sizes between $\Delta x = 5m$ and $\Delta x = 40m$ are used. The observations are indicated with a red line.

Figure E.2 show the change in water level at Awa di Lodo between the period of 27th of January until 31st of January, when applying grid refinement around the islands. It clearly shows the effect of the bathymetry of the islands. Larger computational grid cells allow leaking cells, which means that water can skip the higher bathymetry within the computational cell.

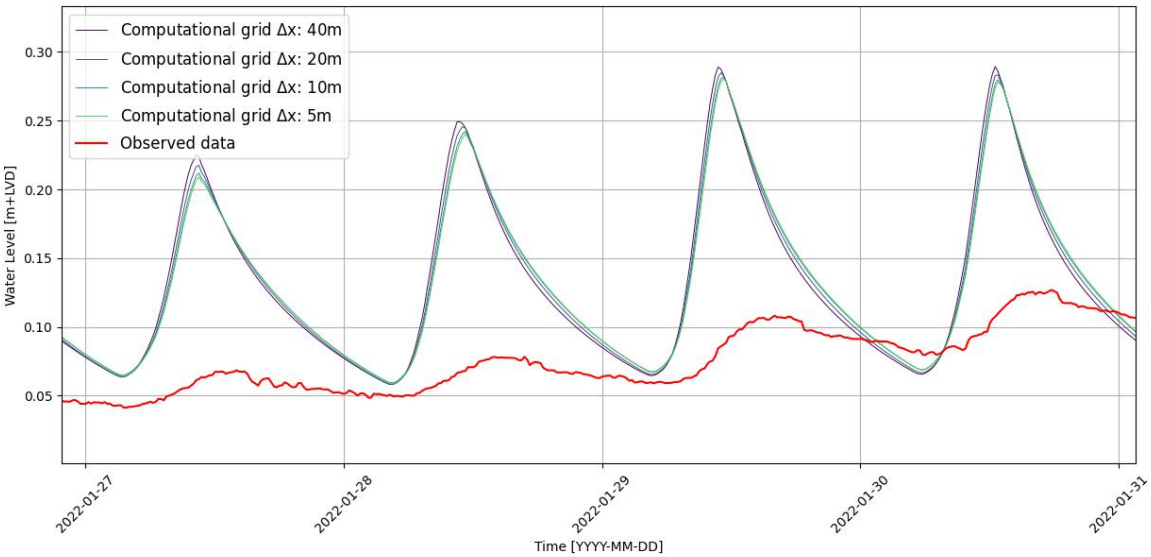

Figure E.2: Water level at Awa di Lodo for the grid refinement sensitivity analysis around the islands. Grid sizes between $\Delta x = 5m$ and $\Delta x = 40m$ are used. The observations are indicated with a red line.

Figure E.3 show the change in water level at Awa di Lodo between the period of 27th of January until 31st of January, when applying grid refinement around the creeks. Increasing the computational cells around the creeks does not influence any large difference, indicating that the different computational grid sizes take the similar physical processes into account.

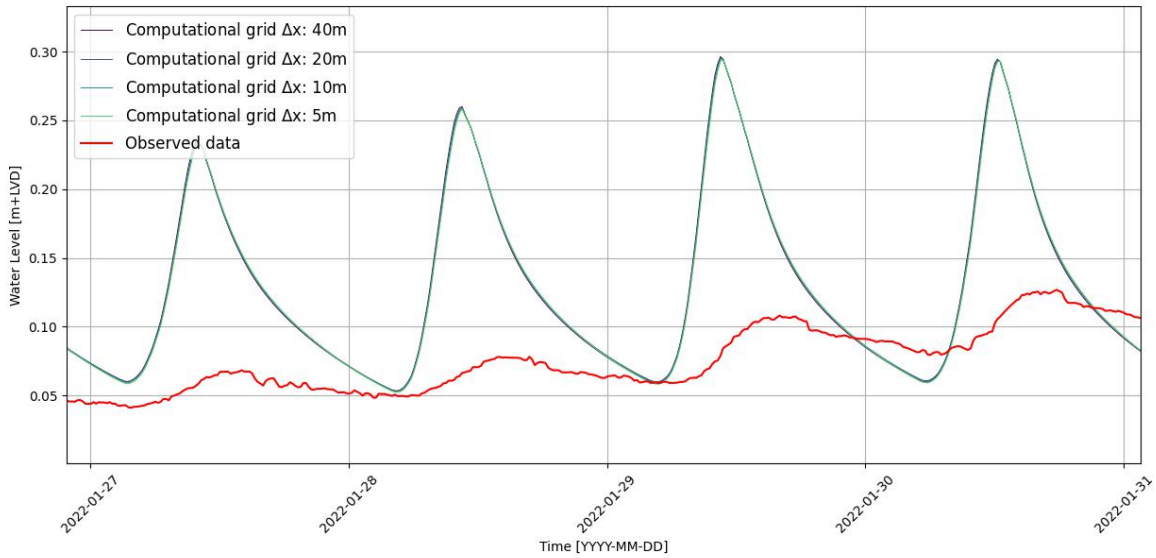

Figure E.3: Water level at Awa di Lodo for the grid refinement sensitivity analysis around the creeks. Grid sizes between $\Delta x = 5m$ and $\Delta x = 40m$ are used. The observations are indicated with a red line.

Analysing the results, show that especially the islands are important to take into account. As there is no change between the resolution of $\Delta x = 5m$ and $\Delta x = 10m$, the $\Delta x = 10m$ grid is chosen around the islands. As the results are the same as the forest with $\Delta x = 10m$, the rest of the forest no grid refinement is needed. In general, grid refinement is not needed within the creeks, however to compare simulations and observations of velocities within the creek, a resolution of $\Delta x = 5m$ is chosen. To allow a smooth transition between islands and creeks, the grid will not go back to a resolution of $\Delta x = 80m$, but is set to a resolution of $\Delta x = 40m$.

F Calibration results for increased bed roughness

Below the results from the calibration process for the water level at the west fringe and the velocities in the east creek can be seen for the roughness method. These simulations were used to calculate the criteria that were used for choosing the best performing parameter settings. Figure F.1 shows the water level in front of the mangrove forest. It can be seen that the simulation results are almost the same as the observations. This means that the tidal signal enters the mangrove forest for all cases correctly. All the criteria outcomes depend on the implementation and the effect of the modelled mangrove forest. If the criteria are not good enough, it means that there is a physical process missing within the forest or backwater.

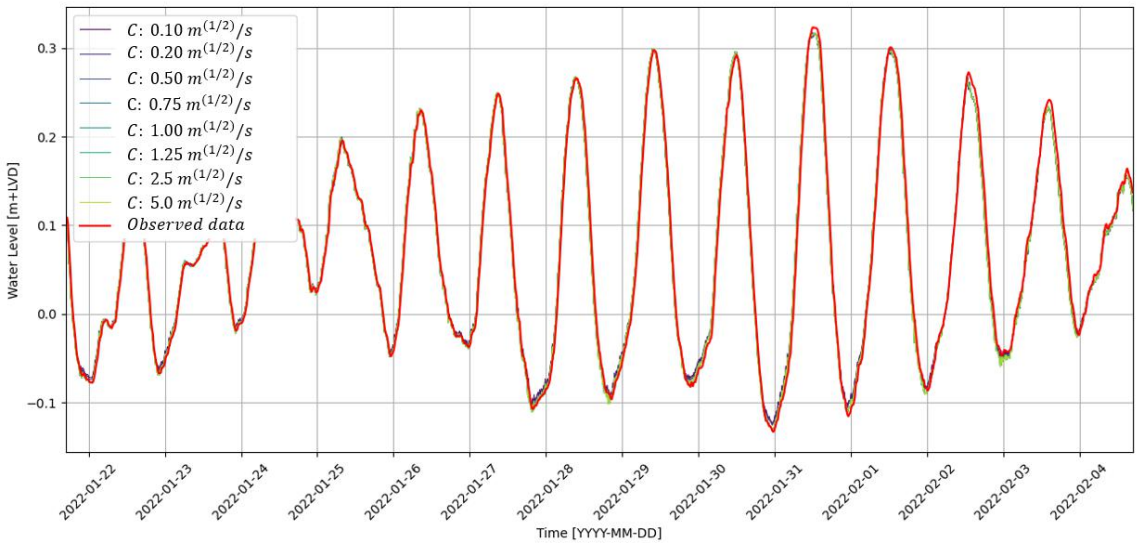

Figure F.1: The water level at the west fringe for the different Chézy friction coefficient values compared with the observations (red line)

Figure F.2 shows the velocities simulated in the east creek. The simulations are much more similar to the observations at this location. It can be seen that when changing the Chézy friction coefficient, during flood there are no large changes. However during ebb, the Chézy friction has a higher influence on the velocities.

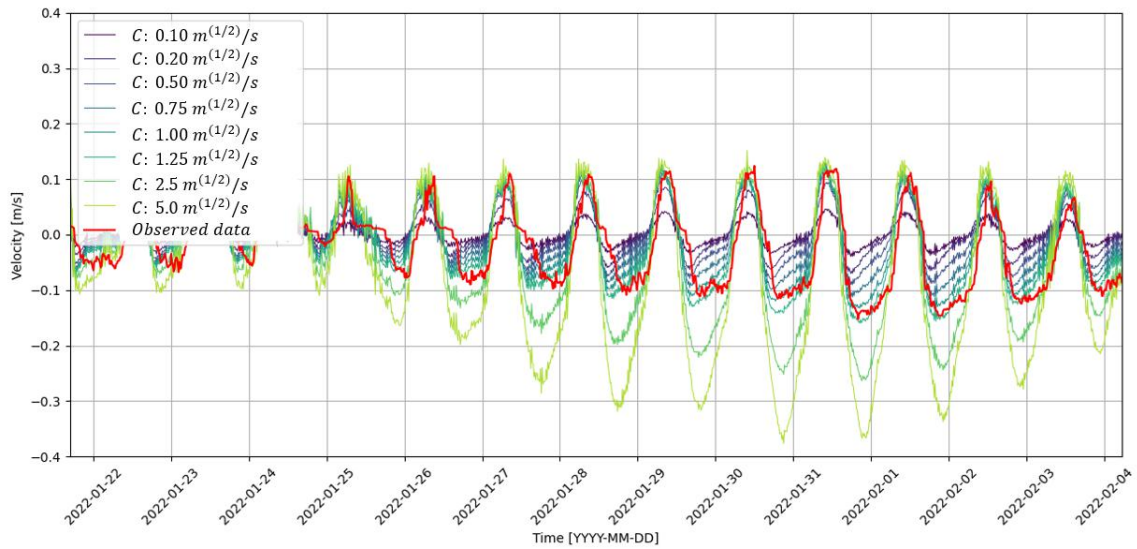

Figure F.2: The velocity in the east creek for the changing Chézy friction coefficient. The observations are indicated with a red line.

G Calibration results for Baptist method

Below the results from the calibration process for the water level at the west fringe and the velocities in the east creek can be seen for the Baptist method. These simulations were used to calculate the criteria that were used for choosing the best performing parameter settings. Figure G.1 shows the water level in front of the mangrove forest. It can be seen that the simulation results are almost the same as the observations. This means that the tidal elevation signal enters the mangrove forest for all cases correctly. All the criteria outcomes depend on the implementation and the effect of the modelled mangrove forest. If the criteria are not good enough, it means that there is a physical process missing within the forest or backwater.

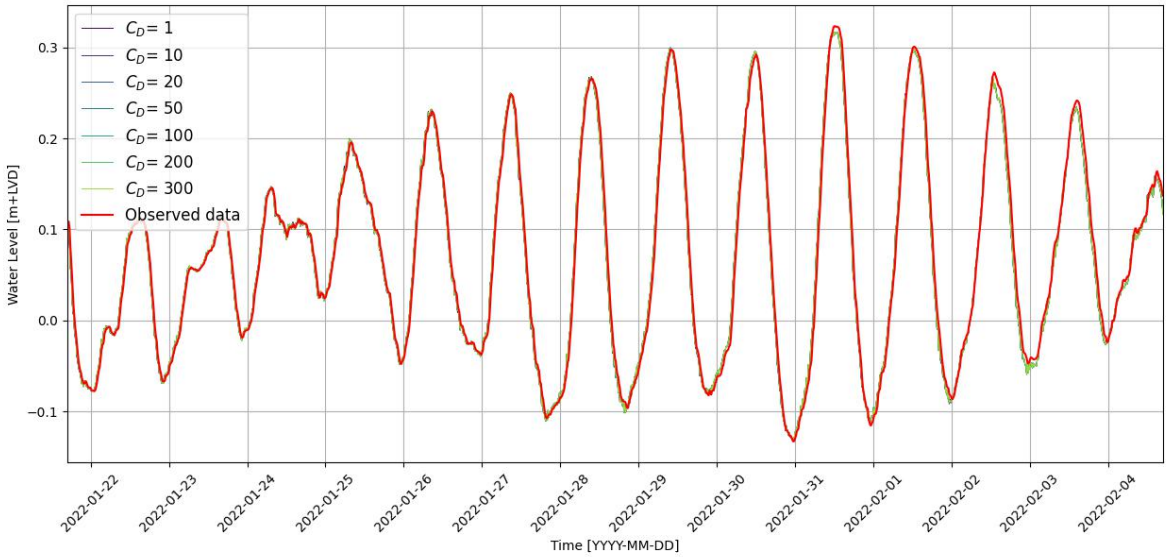

Figure G.1: The water level at the west fringe for the different drag coefficient values compared with the observations (red line)

Figure G.2 shows the velocities simulated in the east creek. The simulations are much more similar to the observations at this location. It can be seen that when changing the drag coefficient, during flood there are no large changes. However, during ebb, the drag coefficient has a higher influence on the velocities.

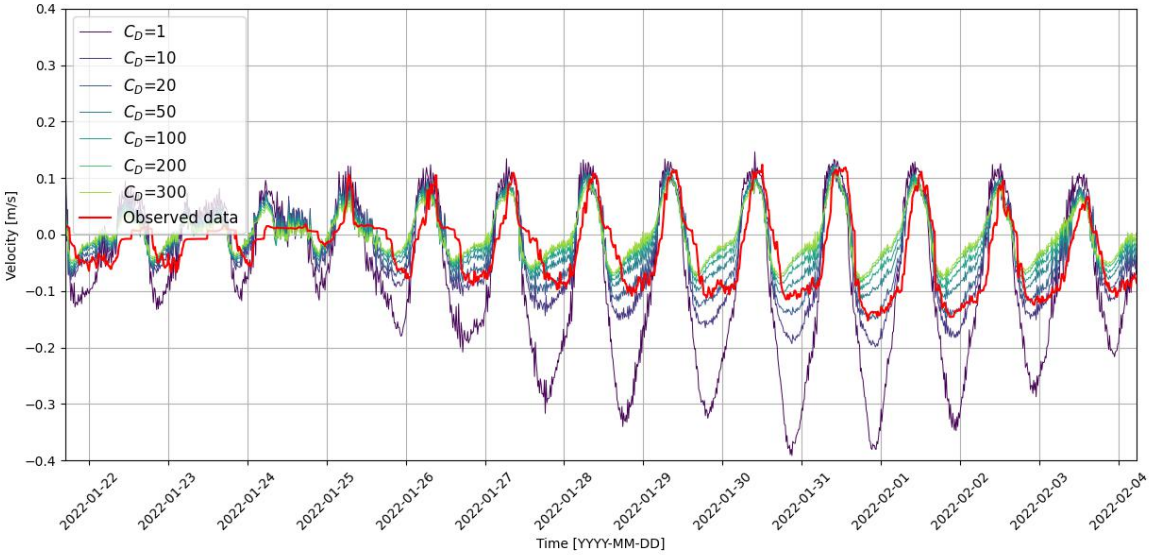

Figure G.2: The velocity in the east creek for the changing drag coefficient. The observations are indicated with a red line.

H Calibration results for the porous layer

Below, the results from the calibration process for the water level at the west fringe and the velocities in the east creek can be seen for the porous layer. These simulations were used to calculate the criteria for choosing the best-performing parameter settings. Figure H.1 shows the water level in front of the mangrove forest for the first calibration run, changing the porosity and hydraulic conductivity. Figure H.2 shows the water level in front of the mangrove forest for the second calibration run, changing the porous layer height. The simulation results are almost identical to the observations, indicating that the tidal signal enters the mangrove forest correctly in all cases. All criteria outcomes depend on the implementation and the effect of the modelled mangrove forest. If the criteria are not satisfactory, it suggests that there is an issue within the forest.

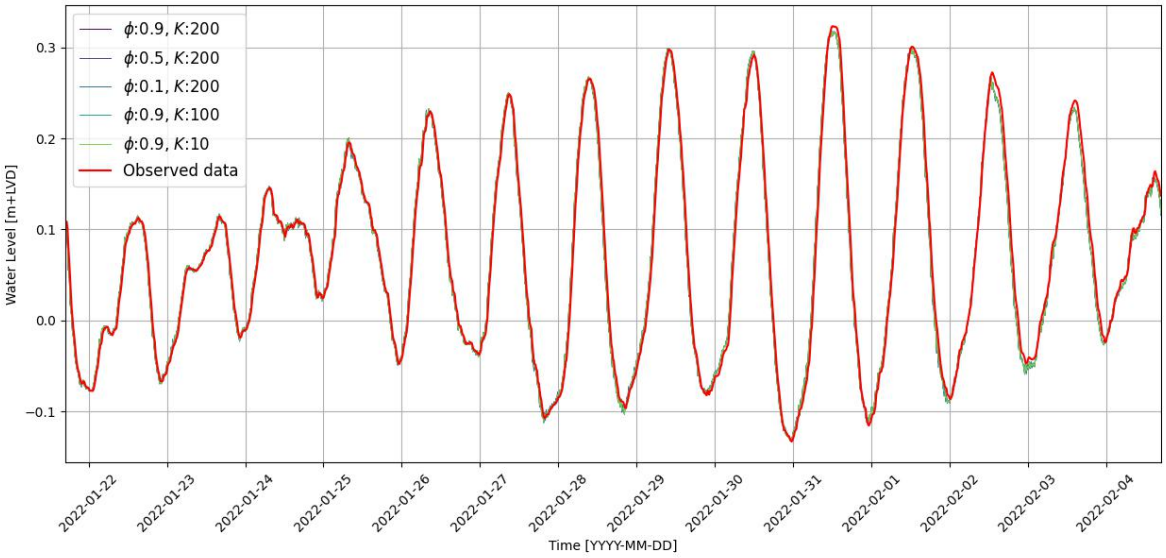

Figure H.1: Water level at the west fringe for the different porosity and hydraulic conductivity values in the porous layer compared with the observations (red line)

In Figure H.3, the velocities in the east creek can be seen when changing the porosity and hydraulic conductivity.

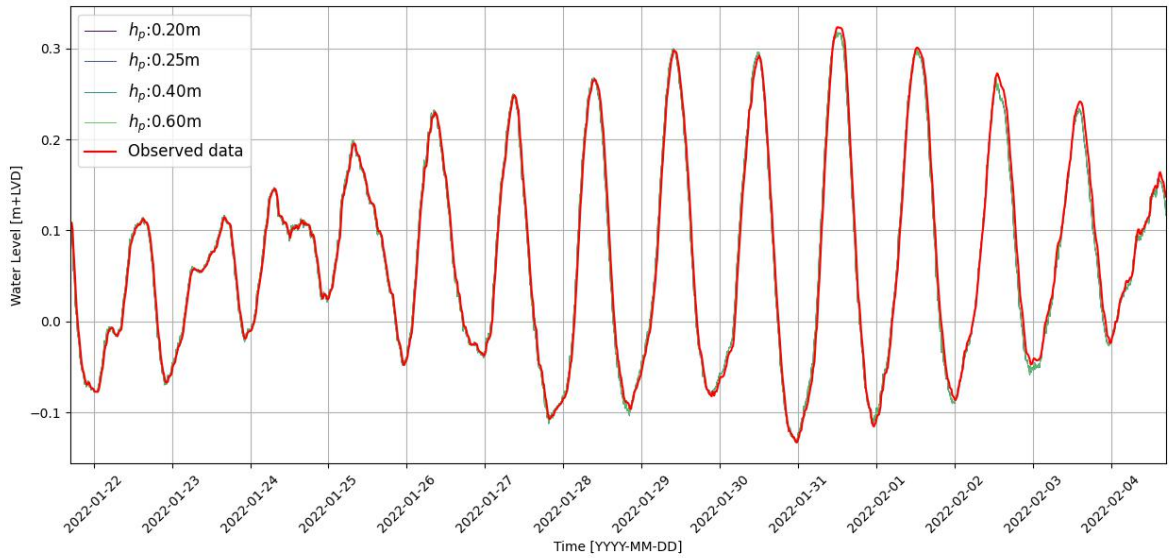

Figure H.2: Water level at the west fringe for the different porous layer heights compared with the observations (red line)

For all simulations, there is almost no flow through the creek, indicating that the porous layer might block the connection towards Awa di Lodo, preventing water flow. Changing these parameters in the porous layer shows no changes, suggesting that the parameters may not be calibrated in the correct range. While higher values might improve the simulation, they would contradict observations. This might indicate that using the porous layer for both types is not useful. Figure H.4 shows the flow velocity in the east creek when changing the porous layer height. Reducing the height creates a lower obstacle towards Awa di Lodo. This allows water to flow over the porous layer during spring tide, increasing the flow velocities through the creek. Lowering the layer shows much better results compared to the observations.

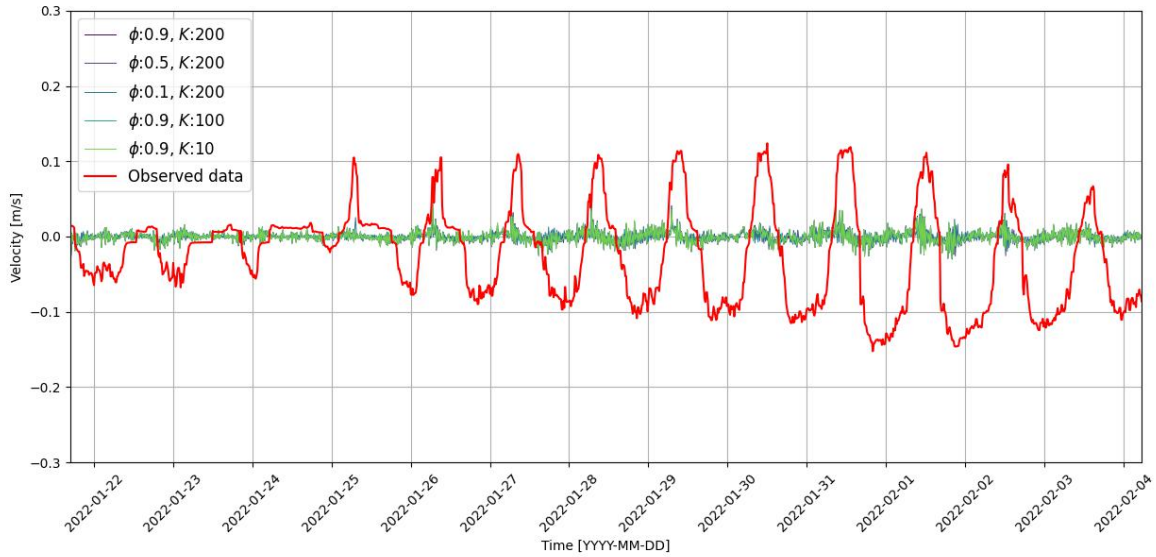

Figure H.3: The velocity in the east creek for changing the porosity and hydraulic conductivity in the porous layer. The observations are indicated with a red line to compare.

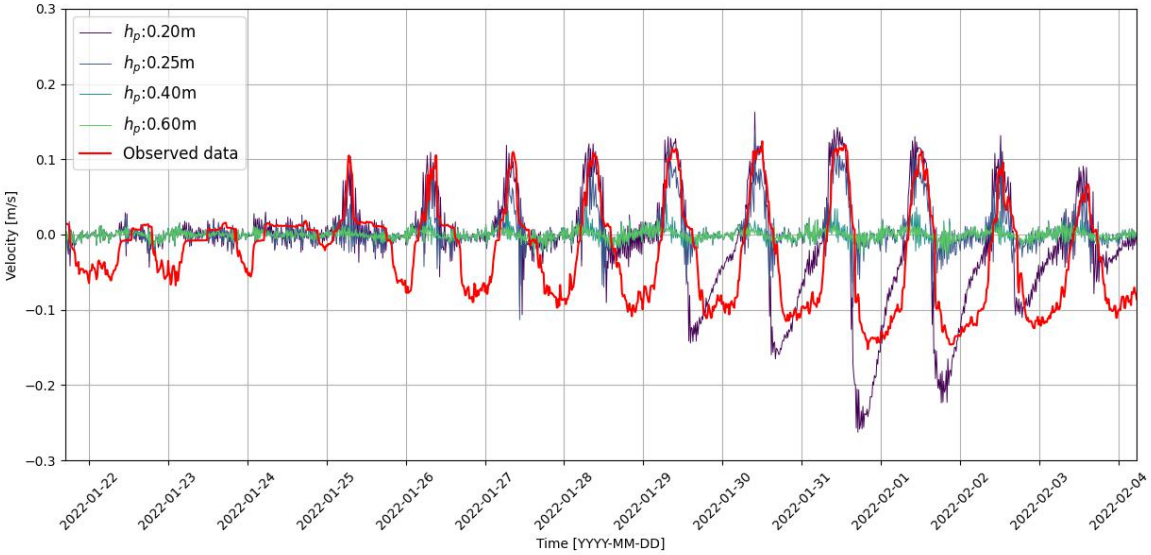

Figure H.4: The velocity in the east creek for the changing porous layer height. The observations are indicated with a red line to compare.

I Calibration Results for the Hybrid Model

Calibration Baptist

The calibration of the stem height for the black mangroves did not change a lot on the water level at Awa di Lodo, which is shown in Figure I.1. There were only slight changes in water level during the very high water levels. Similar results are also seen on the velocities in the east and west creek (Figure I.2). For all different vegetation heights the velocity does not change at all. This is because the black mangroves grow mainly at the back of the forest behind the measurement points. Adjusting the height does not change a lot on the vegetation drag which is already modelled, it only heightens the impact.

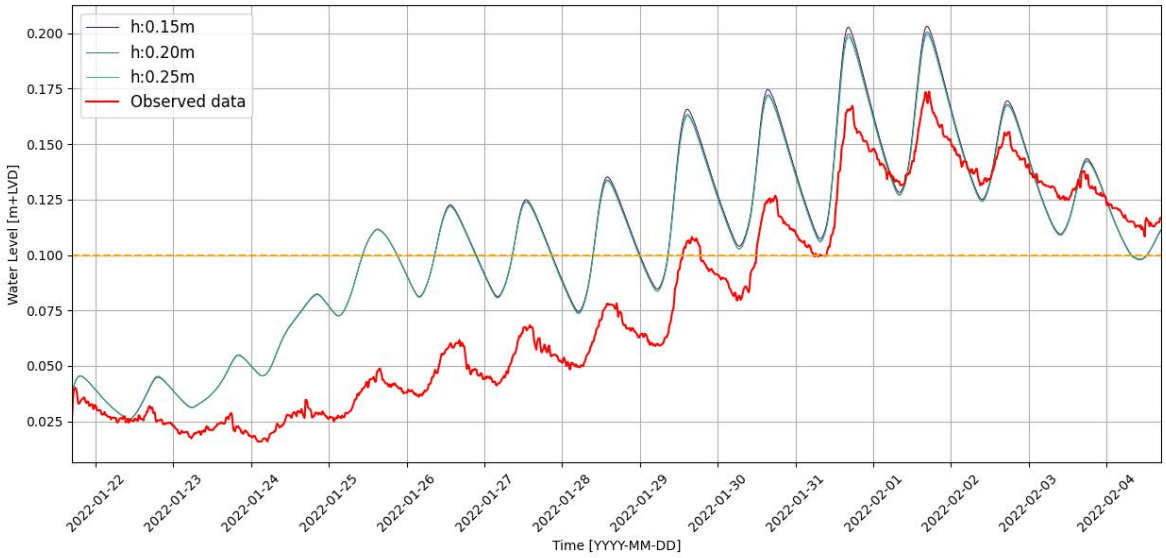

Figure I.1: The water level at Awa di Lodo with a changing vegetation height in Baptist. The observations are indicated with a red line.

Changing the drag coefficient has more impact on the low water levels, as it directly effects the vegetation drag.

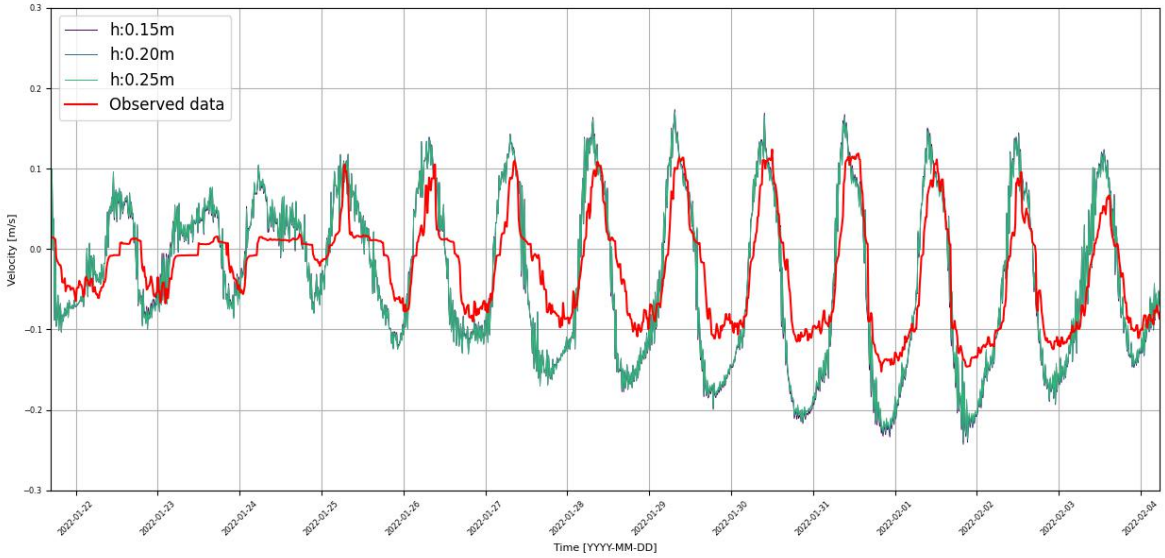

Figure I.2: The results of the flow velocities in east creek by changing the vegetation height for Baptist. The observations are indicated with a red line.

It increases the total resistance, which is seen in the east creek (Figure I.3). Higher drag coefficients increase the resistance and lower the flow velocities. This is especially noticeable in the ebb period. The reason for this is that during flood the flow feels the impact behind the measurement point and during ebb they feel the impact before the measurement point.

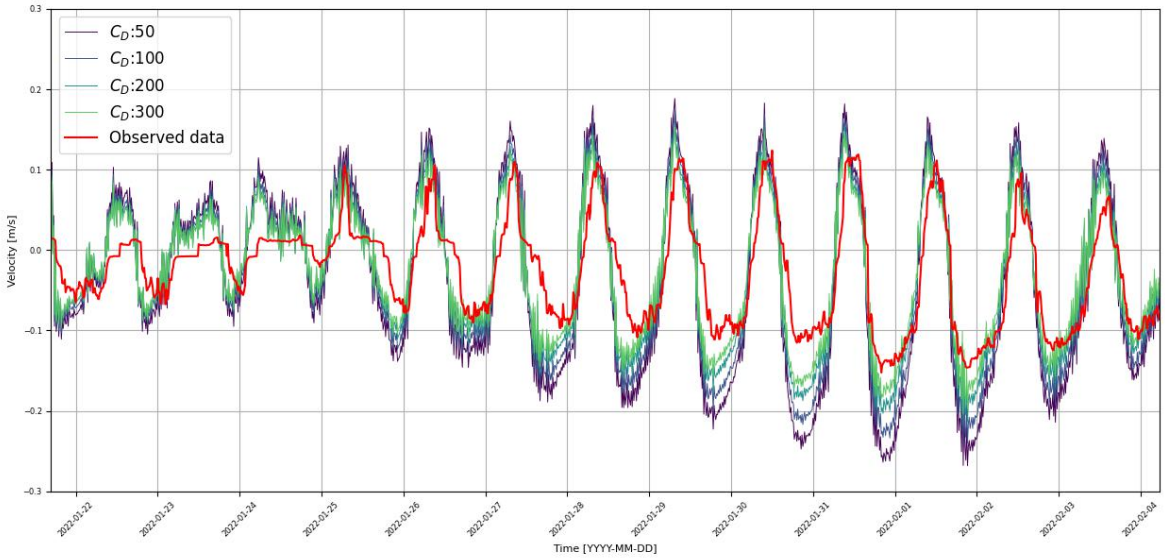

Figure I.3: The results of the flow velocities in the east creek by changing the drag coefficient for Baptist. The observations are indicated with a red line.

J Validation Result for the Hybrid Model

Figure J.1 shows the water levels at the fringe for the validation period. All individual models and the hybrid model show similar values as the observations. During the first spring-neap cycle, a slight shift can be seen, where the simulated water level is a bit higher. In the spring-neap cycle, the water levels are almost the same between observations and simulations. This proves that in front of the mangrove forest, the system is correctly simulated.

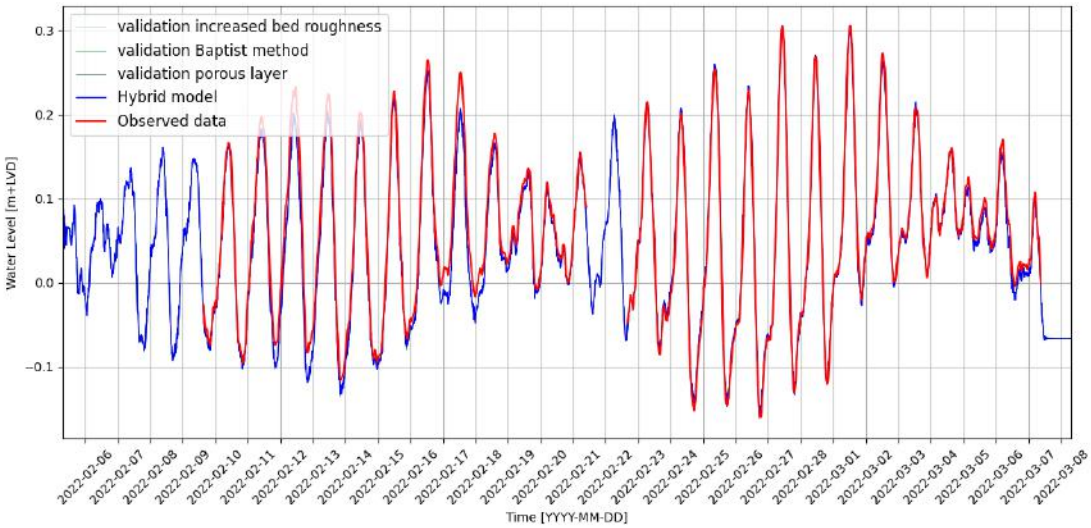

Figure J.1: The water level at the fringe for the validation data. The hybrid model is shown with a blue line. The individual models have green lines and the observations are indicated with a thick red line.

K Evaporation

The evaporation has large influences on the water level within the system. The question is whether it also has effect on the water level at the fringe. Figure K.1 shows the water level at the fringe, which shows that the tidal signal is very close to the observations. This means that evaporation mainly effect the water level inside the forest and at the backwater. The evaporation has only very little effect on the velocities within the east creek. It reduces the overall water volume, which reduces the pressure gradient reducing the velocity only a little bit, which is shown in Figure K.2. Using the evaporation improves the performance on the peaks and troughs at Awa di Lodo, however it compromises performance in velocities and overall system behaviour.

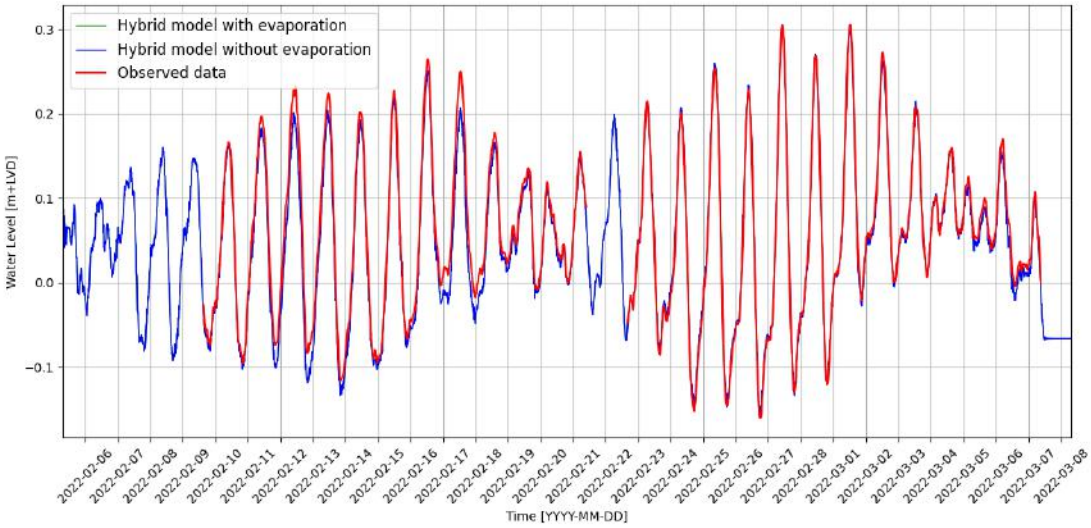

Figure K.1: The water level at the fringe shown for the validation period. The hybrid model is used without and with a global evaporation of 6mm/day. The observed data is used as comparison.

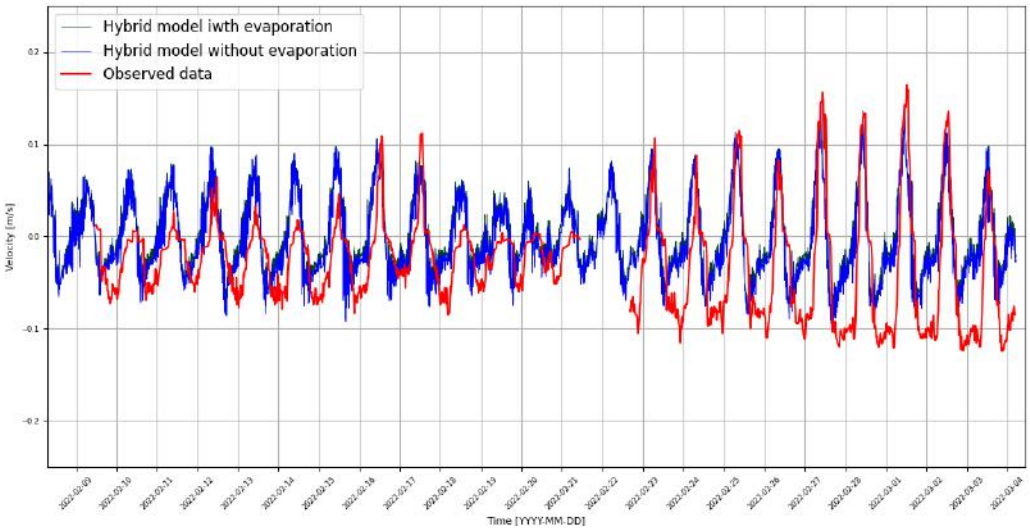

Figure K.2: The velocities in the east creek for a scenario with and without evaporation. The observe velocities are indicated with a red line in bot graphs